1 **DRMY1 promotes robust morphogenesis by sustaining translation of a hormone**
2 **signaling protein**

3

4 Shuyao Kong,[1,2, †] Mingyuan Zhu,[1,2,3,†] M. Regina Scarpin,[4] David Pan,[1,2] Longfei Jia,[5] Ryan E.
5 Martinez,[4] Simon Alamos,[6,7,8] Batthula Vijaya Lakshmi Vadde,[1,2] Hernan G. Garcia,[9,10,11,12,13] Shu-
6 Bing Qian,[5] Jacob O. Brunkard,[4] Adrienne H. K. Roeder [1,2,14,*]

7

8 [1] Weill Institute for Cell and Molecular Biology, Cornell University, Ithaca, NY 14853, USA
9 [2] Section of Plant Biology, School of Integrative Plant Science, Cornell University, Ithaca, NY 14853, USA
10 [3] Present address: Department of Biology, Duke University, Durham, NC 27708, USA
11 [4] Laboratory of Genetics, University of Wisconsin, Madison, WI 53706, USA
12 [5] Division of Nutritional Sciences, Cornell University, Ithaca, NY 14853, USA
13 [6] Environmental Genomics and Systems Biology Division, Lawrence Berkeley National Laboratory,
14 Berkeley, CA 94720, USA
15 [7] Feedstocks Division, Joint BioEnergy Institute, Emeryville, CA 94608, USA
16 [8] Department of Plant and Microbial Biology, University of California at Berkeley, Berkeley, CA 94720, USA
17 [9] Biophysics Graduate Group, University of California at Berkeley, Berkeley, CA 94720, USA
18 [10] Department of Physics, University of California at Berkeley, Berkeley, CA 94720, USA
19 [11] Institute for Quantitative Biosciences-QB3, University of California at Berkeley, Berkeley, CA 94720, USA
20 [12] Department of Molecular and Cell Biology, University of California at Berkeley, Berkeley, CA 94720, USA
21 [13] Chan Zuckerberg Biohub-San Francisco, San Francisco, CA 94158, USA
22 [14] Lead Contact
23 [†] These authors contributed equally
24 [*] Correspondence: ahr75@cornell.edu

25

26

27 **SUMMARY**

28

29 Robustness is the invariant development of phenotype despite environmental changes
30 and genetic perturbations. In the Arabidopsis flower bud, four sepals initiate at robust positions
31 and times and grow to equal size to enclose and protect the inner floral organs. We previously
32 characterized the mutant *development related myb-like1* (*drmy1*), where 3-5 sepals initiate at
33 irregular positions and variable times and grow to different sizes, compromising their protective
34 function. The molecular mechanism underlying this loss of robustness was unclear. Here, we
35 show that *drmy1* has reduced TARGET OF RAPAMYCIN (TOR) activity, ribosomal content, and
36 translation. Translation reduction decreases the protein level of ARABIDOPSIS RESPONSE
37 REGULATOR7 (ARR7), a rapidly synthesized and degraded cytokinin signaling inhibitor. The
38 resultant upregulation of cytokinin signaling disrupts the robust positioning of auxin signaling,
39 causing variable sepal initiation. Our work shows that the homeostasis of translation, a ubiquitous
40 cellular process, is crucial for the robust spatiotemporal patterning of organogenesis.

41

42 Keywords: Robustness, TOR, translation, cytokinin, auxin, ARR, ribosomopathy, Arabidopsis,
43 sepal, morphogenesis

44

45 **INTRODUCTION**

46

47   Robustness, or canalization, is the invariant, reproducible development of phenotype,
48   unchanged by environmental fluctuations, genetic perturbations, or gene expression noise[1–4].
49   Commonly, within an individual, a given number of organs develop at well-defined positions to a
50   robust final size and shape, which is crucial for fitness under stabilizing selection[2]. For example,
51   transplanted eyes, limbs, and kidneys in mammals grow to a mature size similar to their donor,
52   irrespective of the mature size of the same type of organ in the recipient[5–7]. The pairs of wings
53   and halteres in Drosophila develop to robust, precisely coordinated final size and shape, which
54   are required for flight[8–11]. The characteristic cruciform flower in *Brassicaceae* consists of four
55   petals[12], a trait that can contribute to pollinator attraction[13]. The robust positioning of leaves
56   around the shoot apical meristem in plants, or phyllotaxis, ensures optimal light capture[14–16]. While
57   these examples of developmental robustness have been documented for a long time, the
58   underlying molecular mechanisms have just begun to be unveiled.

59

60   Earlier studies looking for genes involved in maintaining robustness have found *HEAT*
61   *SHOCK PROTEIN 90* (*HSP90*). Mutations of *HSP90* cause a diverse array of phenotypic changes
62   in plants, fruit fly, zebrafish, worm, and humans[4,17,18]. Notably, the display and severity of these
63   changes vary between individuals and even between different parts of the same individual,
64   indicating that developmental robustness is disrupted[17,18]. *HSP90* encodes a protein chaperone
65   which has clients from nearly all developmental and signaling pathways[4]. *HSP90*, therefore, is a
66   hub gene that affects numerous other genes within the gene network[2]. Disruption of such a hub
67   gene would therefore trigger many defects in numerous developmental processes. Similarly,
68   genes involved in central cellular processes such as chromatin remodelling[19–21], transcription[19,20],
69   translation[22,23], and protein degradation[24,25] are also hub genes, and they have been found to be
70   important for developmental robustness in various systems including fungi, animals, and plants.
71   How these broadly acting hub genes contribute to the robustness of tissue-specific developmental
72   phenotypes is still largely unclear.

73

74   We have developed the *Arabidopsis* sepal as a system to elucidate the mechanisms
75   maintaining robustness in organ size and shape[26–28]. Sepals are the outermost floral organs
76   whose function is to enclose buds and protect the developing inner organs, i.e. petals, stamens,
77   and carpels, before the flower blooms. To fulfill this protective function, each flower robustly
78   develops four sepals of equal length, allowing them to close at the top (Figure 1A, middle left);
79   these four sepals are of equal width and positioned 90° from each other, leaving no gap on the
80   sides (Figure 1A, top left). This robustness in sepal size and shape stems from the robust initiation
81   of the four sepal primordia from the floral meristem with precisely coordinated spatiotemporal
82   patterns[26] (Figure 1A, bottom left). The initiated sepal primordia attain robust final size and shape
83   by spatiotemporal averaging of cellular growth variability during sepal elongation, and
84   synchronous progression of a whole-flower growth termination signal from tip to base[27]. In
85   addition, noise in gene expression must be kept low to ensure sepal size robustness[29]. We
86   previously characterized a mutant in *DEVELOPMENT RELATED MYB-LIKE 1* (*DRMY1*) that

87   develops flowers where the inner organs are exposed due to gaps between sepals[26]. The gaps
88   are caused by variability in sepal development. Specifically, some sepals are shorter than others,
89   leaving gaps on the top (Figure 1A, middle right); the arrangement of sepals around the flower
90   deviate from the canonical form such that parts of the flower are not covered by a sepal, leaving
91   gaps on the side (Figure 1A, top right). This variability in the size, number, and position of the
92   mature sepal originates from the earliest stages of floral development where the initiation of sepal
93   primordia is variable in spatiotemporal patterns (Figure 1A, bottom right). Variability in sepal
94   initiation, in turn, is driven by the loss of robust patterning of auxin and cytokinin[26], two plant
95   hormones critical for organ initiation and morphogenesis[30–32], in the floral meristem before sepal
96   initiation. However, the molecular mechanism through which DRMY1 maintains robust hormone
97   patterning is still unknown.
98

99   In this study, we elucidate a mechanism through which DRMY1 maintains robust hormone
100   patterning and thus robust sepal initiation. Specifically, we find that DRMY1 maintains proper
101   activity of TARGET OF RAPAMYCIN (TOR), a crucial regulator of ribosome biogenesis and
102   protein translation[33,34], and thereby sustains translation *in vivo*. When *DRMY1* is mutated, the
103   protein level of ARABIDOPSIS RESPONSE REGULATOR7 (ARR7), a rapidly synthesized and
104   degraded cytokinin signaling inhibitor, is reduced in the floral meristem. Consequently, cytokinin
105   signaling uniformly increases in the meristem periphery, causing variability in auxin patterning
106   and sepal initiation. We further propose that the increase in cytokinin signaling may be a survival
107   mechanism to alleviate the translation rate reduction when ribosomal content is limited. In
108   summary, our work shows that the hub processes of TOR signaling and translation, which occur
109   in every cell, have very specific roles in robust organ primordium initiation by sustaining the rapid
110   synthesis of a hormone signaling protein.
111
112

113 **RESULTS**
114
115 **The *drmy1* mutant has reduced TOR activity, ribosome content, and translation rate**
116

117   *DRMY1* encodes a MYB/SANT domain protein which may exert transcriptional
118   regulation[26]. To look for differentially expressed genes in *drmy1* which may be candidates
119   underlying variable sepal initiation, we performed RNA-sequencing (RNA-seq) in *drmy1* and wild
120   type (WT) of *apetala1* (*ap1*) *cauliflower* (*cal*) *AP1-GR* background[35,36]. The *ap1 cal AP1-GR*
121   inflorescence produces numerous tightly packed ball-shaped meristems, which, upon induction
122   of AP1-GR with dexamethasone, synchronously initiate sepal primordia, allowing us to collect
123   large quantities of floral meristems with sepal primordia initiating (Stage 3)[37] (Figure S1A). We
124   crossed *drmy1* into *ap1 cal AP1-GR* and performed RNA-seq on induced inflorescences of WT
125   and *drmy1* in this background. We detected transcripts from a total of 21,496 genes, of which
126   1,042 (4.8%) were differentially expressed in *drmy1* (Figure S1B; Supplemental Dataset 1). We
127   found that the 443 genes downregulated at the transcript level in *drmy1* were most enriched in
128   the gene ontology (GO) term "Translation", a fundamental and ubiquitous cellular process that

129   converts genetic information from transcript to protein. Within this term, genes encoding ribosomal
130   components were most downregulated (Figure S1C). The 443 downregulated genes were also
131   enriched in several other GO terms related to ribosome biogenesis and assembly (Figure 1B).
132   We therefore hypothesized that ribosome abundance and translation rate are lower in *drmy1*,
133   potentially altering the accumulation of proteins critical to developmental robustness.

134

135   To determine whether and how ribosome abundance and translation are affected in
136   *drmy1*, we performed polysome profiling in induced inflorescences of WT and *drmy1* in *ap1 cal*
137   *AP1-GR* background. Compared to WT, polysomal peaks are drastically reduced in *drmy1* (Figure
138   1D; Supplemental Dataset 2). To see whether this reduction in ribosomal content affected
139   translation rate (*de novo* protein synthesis) *in vivo*, we performed puromycin labeling. Samples
140   were incubated with puromycin, an amino acid-tRNA analog that is incorporated into nascent
141   polypeptide chains and can be detected using an anti-puromycin antibody to infer global
142   translation rate[38,39]. In both young seedlings and induced *ap1 cal AP1-GR* inflorescences, we
143   found that the puromycin level detected in *drmy1* mutant samples was much reduced compared
144   to WT (Figure 1E), indicating translation rate is reduced. We hypothesized that a reduction in
145   protein translation should likely result in a decrease in protein level. For this, we looked at a
146   ubiquitously expressed membrane marker *UBQ10::mCherry-RCI2A*, and found that it had a small
147   (~25%) but significant decrease in fluorescence intensity in the inflorescence meristem and young
148   floral buds of *drmy1* compared with WT. We also measured its fluorescence intensity in the
149   ribosomal mutant *ul4y* (*rpl4d*)[40] and we found that the decrease in fluorescence intensity in *drmy1*
150   is even greater than in *ul4y* (Figure S1G-J). These results validate our proteomics findings, and
151   show that ribosome content and translation are indeed reduced in the *drmy1* mutant.

152

153   To test how the global repression of translation in *drmy1* impacts its proteome, we
154   extracted total soluble protein from induced inflorescences of WT and *drmy1* in *ap1 cal AP-GR*
155   background and performed mass spectrometry. We identified a total of 5,077 proteins, of which
156   548 (10.8%) were differentially accumulated in *drmy1* (Figure S1B; Supplemental Dataset 1).
157   These differentially accumulated proteins were enriched in GO terms related to translation and
158   ribosomal assembly (Figure 1C). Despite the overall reduction in ribosomes (Figure 1D), relative
159   to other proteins, ribosomal components are more abundant in *drmy1* (Figure S1D; Supplemental
160   Dataset 1). This is not true for all proteins involved in translation; poly-A binding proteins and
161   tRNA synthetases, for example, are relatively less abundant in *drmy1* than in WT. Moreover, the
162   26S proteasome responsible for targeted protein degradation is much more abundant in *drmy1*
163   than in WT (Supplemental Dataset 1). In concert, these results demonstrate that the machinery
164   responsible for maintaining protein homeostasis is substantially dysregulated in *drmy1*.

165

166   A key signaling pathway that regulates protein homeostasis is TARGET OF RAPAMYCIN
167   (TOR)[41,42]. TOR is a hub that integrates information from light, sugars, nutrient availability, etc.,
168   to promote growth-related processes, including ribosome biogenesis and translation, and to
169   repress catabolic processes, including protein degradation by autophagy and the
170   proteasome[33,34,43–45]. We therefore hypothesize that the decrease in ribosomal content and protein

171 translation in *drmy1* may reflect altered TOR signaling. To test for signatures of transcriptomic
172 changes that have been well defined in seedlings under TOR inhibition[34,46,47], we performed RNA-
173 seq on seedlings of WT, *drmy1*, WT treated with AZD-8055 (a potent TOR inhibitor), and mock-
174 treated WT (Supplemental Dataset 3). We found that the *drmy1* mutation causes transcriptomic
175 changes similar to TOR inhibition (Figure 1F). A significant portion of genes differentially
176 expressed under TOR inhibition vs. mock were also differentially expressed in *drmy1* vs. WT
177 (466/2044 = 22.8%; hypergeometric test, p = 4.7×10^{-108}). Not only were these 466 genes
178 differentially expressed in both situations, but also most of them were coherently downregulated
179 or upregulated (439/466 = 94.2%, Chi-square test, p < 2.2×10^{-16}; Figure S1E). Genes coherently
180 downregulated in both situations were enriched in GO terms related to translation and ribosome
181 biogenesis, and, most strikingly, a quarter of them were under the GO term "translation" (Figure
182 1F, S1F). These similar transcriptomic changes support our hypothesis that TOR activity is
183 reduced in *drmy1*. To further test this hypothesis, we measured TOR activity in WT and *drmy1* by
184 assaying the phosphorylation of its direct substrate, RIBOSOMAL PROTEIN eS6 KINASE
185 (S6K)[48,49]. While the total protein level of S6K did not change in *drmy1*, we found that S6K
186 phosphorylation decreased by half, demonstrating reduced TOR activity (Figure 1G, 1H). Overall,
187 these results are consistent with the idea that *drmy1* has reduced TOR activity—a main pathway
188 controlling ribosome biogenesis and translation—which causes reduced ribosomal content and
189 translation rate.
190
191 **Defects in TOR activity, ribosome integrity, and translation disrupt robust sepal initiation**
192
193 We next asked whether defects in TOR activity, ribosome, or translation have any effects
194 on robust sepal initiation like the *drmy1* mutation does (Figure 2A vs 2B; also see Zhu et al.[26]). In
195 a WT bud, initiation is robust in that four sepal primordia of similar size form evenly spaced around
196 the periphery of the floral meristem (Figure 2A, 2H). Angles between them vary little, i.e., they are
197 all at around 90° angles from each other (Figure 2I, 2J). By contrast, in *drmy1* buds, three to five
198 sepal primordia initiate and grow to different sizes (Figure 2B, 2H; also see Zhu et al.[26]). The
199 *drmy1* sepal primordia are generally unevenly spaced, and angles between them have a high
200 coefficient of variation (CV) (Figure 2I, 2J). To determine whether defects in ribosomes can cause
201 the same sepal initiation defects, we imaged three ribosomal mutants, *ul4z* (*rpl4a*), *ul4y*, and *ul18z*
202 (*rpl5a*)[40], each mutated in a gene encoding a ribosomal component that is also downregulated in
203 *drmy1* at the transcript level (Figure S1C). The *ul4z* mutant bud shows reduced size of the inner
204 sepal primordia relative to the outer sepal primordia (Figure 2C), and slightly more variable spatial
205 distribution of sepal primordia (Figure 2J), although it always develops four sepal primordia
206 (Figure 2H). This is a weaker phenotype than *drmy1* but has similar characteristics. The *ul4y* and
207 *ul18z* mutants show great variability in the number and position of sepal primordia (Figure 2D,
208 2E, 2H, 2J), more similar to *drmy1*. We also crossed these ribosomal mutants with *drmy1* to study
209 sepal variability in the double mutants (Figure S2A-H). In *drmy1 ul4z*, *drmy1 ul4y*, and *drmy1*
210 *ul18z/+*, on average, sepal initiation was as variable as in the *drmy1* single mutant (Figure S2I,
211 SIJ). However, there were buds with no outgrowth in the adaxial or lateral regions of the bud
212 periphery (Figure S2B, S2E, S2G), buds with six sepal primordia (Figure S2C, S2F, S2H), and

213   buds with two outer sepal primordia (Figure S2D, S2H), which were not seen in the single mutants.
214   Note that we were unable to characterize the homozygous *drmy1 ul18z* double mutant because
215   they were embryo-lethal (Figure S2K), further supporting the idea that ribosomal mutations
216   enhance the phenotypic defects in *drmy1*.

218   We then imaged mutants with reduced TOR activity to determine whether sepal initiation
219   is also less robust. *lst8-1-1* is a T-DNA insertional mutant of the TOR complex component LST8-
220   1[50] and is weakly hypomorphic in TOR activity. We found that *lst8-1-1* shows variable sepal
221   initiation in a small proportion of buds (4/41, 9.8%) (Figure 2F, 2H, 2J). The *spaghetti-1* mutant
222   defective in TOR complex 1 (TORC1) assembly[51] showed a level of variability comparable to the
223   *drmy1* mutant and the ribosomal mutants *ul4y* and *ul18z* (Figure 2G, 2H, 2J). Mutants with more
224   severe disruption of TOR activity are embryo lethal and could not be analyzed[51,52]. These results
225   show that reduction in TOR activity can cause variability in sepal initiation, similar to *drmy1*.

227   To corroborate these findings, we directly inhibited translation by *in vitro* culture of
228   dissected WT inflorescences on 2 µM cycloheximide (CHX, a chemical inhibitor of translation) for
229   9-10 days. This is a low concentration that does not completely block translation, as
230   inflorescences were still alive after 10 days in this condition. Compared with mock, CHX-treated
231   inflorescences develop buds that have 2 to 6 sepal primordia of variable sizes that are unevenly
232   spaced around the bud periphery (Figure 2K, 2M, 2N). These phenotypes are stronger than
233   *drmy1*. Similarly, we directly inhibited TOR activity by continuous bi-daily application of 2 nmol
234   Torin2 to the growing shoot apex for 15 days, and we observed variable sepal initiation (Figure
235   2L, 2M, 2N). Overall, data reported above show that inhibition of TOR activity and translation can
236   disrupt the robustness of sepal initiation, in terms of sepal primordium number, position, and size.

238   We previously showed that the *drmy1* mutant bud develops sepals of different sizes
239   because some sepal primordia initiate much later than others[26]. The late-initiating primordia
240   remain smaller throughout development. They end up as smaller sepals relative to those that
241   initiated earlier, leaving gaps that expose the developing inner floral organs[26]. We asked whether
242   TOR or ribosomal defects disrupt the relative timing of sepal initiation just as the *drmy1* mutation
243   does. We live imaged WT and *ul4y* every six hours during sepal initiation and quantified the
244   amount of time the bud takes to initiate the inner and lateral sepals after it initiates the outer sepal.
245   In WT, after the initiation of the outer sepal, most buds initiate the inner sepal within 6 hours and
246   the lateral sepals within 12 hours (Figure 3A, 3C; also see Zhu et al.[26]). In *ul4y*, the initiation times
247   of the inner and lateral sepals are more variable and delayed relative to the outer sepal, with 7.5%
248   of the buds initiating the inner sepal 18 hours after the outer sepal, and 32.5% of the buds initiating
249   the lateral sepals 18 hours after the outer sepal (Figure 3B, 3C). Similarly, we compared the
250   relative timing of sepal initiation in Torin2 vs mock-treated WT buds. While in most mock-treated
251   buds, the inner and lateral sepals initiate within 12 hours after the outer sepal (Figure 3D, 3F), in
252   Torin2-treated buds they are much more variable and delayed (Figure 3E, 3F), to a similar extent
253   as previously observed in *drmy1*[26]. In some cases, the inner and lateral sepals initiate more than

254   30 hours after the outer sepal. These results show that TOR and ribosomal defects can disrupt
255   the precisely orchestrated initiation timing of sepal primordia.

256

257   Does the variability in initiation timing cause variable sizes and gaps in mature sepals, as
258   in *drmy1* (Figure S3A,B,G,H; also see Zhu et al. [26])? We imaged the mature sepals of the
259   ribosomal mutants *ul4z*, *ul4y*, *ul18z*, as well as the TOR component mutant *lst8-1-1*. Surprisingly,
260   unlike *drmy1*, the sepals in *ul4z*, *ul4y*, *ul18z* enclose the inner floral organs perfectly, leaving no
261   gaps, regardless of sepal number (Figure S3C-E). Small gaps still exist in buds of *lst8-1-1*,
262   although sepal size differences appear greatly reduced (Figure S3F). Further dissection shows
263   that in these mutants, sepals within the same flower are of similar sizes, although sepals from
264   different flowers can be of vastly different sizes, most conspicuously for *lst8-1-1* (Figure S3I-N).
265   This is unlike *drmy1*, where sepal size variability is equally high comparing sepals within the same
266   flower or from different flowers (Figure S3H, S3M-N). Upon closer examination, while sepals
267   initiating late in *drmy1* buds remain small, continuously leaving a gap in the sepal whorl (Figure
268   S3O-P), those in *ul4y* were able to catch up with the other sepals and close the gap (Figure S3Q).
269   Our results are consistent with the hypothesis that there exists a size-coordinating mechanism
270   independent of TOR or ribosome function that allows sepals within the same bud to reach the
271   same mature length, and that this mechanism is disrupted in *drmy1*. Such a mechanism requires
272   further investigation in future studies.

273

274   **Inhibition of TOR activity and translation increase cytokinin signaling and disrupts the**
275   **robust spatial pattern of auxin and cytokinin signaling**

276

277   Auxin and cytokinin are two important plant hormones critical to many aspects of plant
278   development[30–32], and there is accumulating evidence that they act synergistically in the shoot
279   apical meristem to promote lateral organ initiation[16,53,54]. We previously showed that, in a WT floral
280   meristem prior to sepal initiation, auxin and cytokinin signaling are concentrated at the four
281   incipient primordia, which is required for robust sepal initiation from these regions (Figure 4A,
282   S4A; Zhu et al.[26]). In the *drmy1* mutant, cytokinin signaling becomes stronger and diffuse around
283   the bud periphery (Figure 4A-B). Auxin signaling also becomes more diffuse, forming irregular
284   auxin maxima that are less focused than those in WT, except at the incipient outer sepal where it
285   remains robust (Figure 4A, S4B; Zhu et al.[26]). These changes in hormone signaling correlate with
286   variable sepal initiation (Figure S4B)[26]. We wondered whether ribosomal mutations have similar
287   effects on auxin and cytokinin signaling. To this end, we imaged the auxin signaling reporter
288   *DR5::3xVENUS-N7* and the cytokinin signaling reporter *TCS::GFP* in floral meristems of the
289   ribosomal mutant *ul4y*. Both reporters lose their robust spatial pattern except in the incipient outer
290   sepal (Figure 4A, S4C). The hormone signaling patterns were quantified by circular histogram
291   analysis (see Methods for details). For each of DR5 and TCS, WT buds showed four clear peaks
292   ~90 degrees apart from each other, with very little signal in between, whereas in *drmy1* and *ul4y*,
293   peaks were barely seen except at the incipient outer sepal (at 45 degrees), and there was greater
294   noise and variation all around the bud (Figure 4C-D). Diffuse bands of auxin signaling that typically
295   occurs in the adaxial or lateral periphery of *drmy1* and *ul4y* buds (Figure S4B and S4C, brackets)

296 can later resolve into several distinct auxin maxima of various intensity and at various positions,
297 correlated with the initiation of sepal primordia of various sizes at these same positions (Figure
298 S4B and S4C, red arrowheads).
299
300   We also tested whether drug treatments that inhibit TOR activity or translation can disrupt
301 the robust hormone patterning. Buds treated *in vitro* with the translation inhibitor CHX (2 μM) for
302 3 days showed a 50% increase in cytokinin signaling, and both auxin and cytokinin signaling
303 became diffuse around the bud periphery (Figure 4E-H). By day 6, cytokinin signaling was still
304 diffuse all around, and increased to more than two-fold relative to mock (Figure 4I, 4J, 4L). Auxin
305 signaling formed maxima of variable number at variable positions (Figure 4I arrowheads, 4K),
306 correlated with the variable initiation of sepal outgrowth at these positions (Figure S4D-E). Similar
307 changes occurred in buds treated *in vitro* with the TOR inhibitor AZD-8055 (2 μM) for 6 days
308 (Figure 4I-L). For both CHX and AZD-8055, the disruptions of hormone signaling are similar to
309 *drmy1*. *In vivo* treatment using another TOR inhibitor Torin2 for 15 days increased cytokinin
310 signaling by 70%, although it did not make auxin and cytokinin signaling more diffuse (Figure
311 S4F-I). Overall, these results show that defects in TOR activity and translation increase cytokinin
312 signaling, and disrupt the precise spatial patterning of cytokinin and auxin signaling required for
313 robust sepal initiation.
314
315 **An increase in cytokinin signaling is necessary and sufficient for variable auxin signaling**
316 **and sepal initiation under translation inhibition**
317
318   Auxin is a critical hormone in organogenesis[55,56]. As shown above, variable patterning of
319 auxin signaling correlates with variable sepal initiation during inhibition of TOR activity and
320 translation. We wondered what caused auxin to lose its robust patterning under such conditions.
321 It was previously reported that the ribosomal mutants *ul4y*, *ul18z*, and *el24y* have reduced protein
322 levels of AUXIN RESPONSE FACTOR (ARF) 3, 5, and 7[57–59], key transcription factors that
323 mediate the auxin signaling response[60]. The transcripts of these ARFs contain upstream open
324 reading frames (uORFs), requiring translation reinitiation to translate their main open reading
325 frames[61,62], a process defective in *ul4y*, *ul18z*, and *el24y*[57–59]. We therefore hypothesized that
326 *drmy1* loses robust auxin signaling pattern because of reduced translation of uORF-containing
327 transcripts, including those of certain ARFs. To begin, we utilized our transcriptomics and
328 proteomics data, and considered that the protein-transcript ratio of a gene should reflect both its
329 level of translation and stability. Therefore, following our hypothesis, genes containing uORFs
330 should, in general, have a lower protein-transcript ratio in *drmy1* than in WT. We calculated the
331 difference of this ratio between *drmy1* and WT for all 5,086 gene-protein pairs in our inflorescence
332 dataset, and compared the ratio against the number of uORFs in each transcript (Figure S5A;
333 uORF data from von Arnim et al.[62]). We found a small but significant decrease in the protein-
334 transcript ratio in *drmy1* for the 724 genes containing at least 2 uORFs in their transcripts,
335 supporting the hypothesis that *drmy1* has reduced translation reinitiation for uORF-containing
336 transcripts, just like the ribosomal mutants *ul4y*, *ul18z*, and *el24y*[57–59]. Then, we examined
337 whether the translation reinitiation of uORF-containing ARFs are indeed reduced in the *drmy1*

338   mutant. We selected *ARF3/ETTIN*, *ARF5/MONOPTEROS*, and *ARF6*, which have 2, 6, and 6
339   uORFs respectively, and as controls, *ARF8* and *ARF10* which do not contain uORFs. None of
340   these *ARF*s were differentially expressed in *drmy1* at the transcript level, except *ARF10* which
341   was slightly upregulated (Figure S5B). We utilized promoter-fluorescent protein fusion reporters
342   (Figure S5C) which have the same uORFs in the promoter region as the corresponding ARF
343   genes if the genes have them. These reporters reflect transcriptional and uORF-mediated
344   translational regulation. *pARF3::N3xGFP*, *pARF5::ER-EYFP-HDEL*, and *pARF6::N3xGFP*
345   contain uORFs and thus, following our hypothesis, are expected to drastically decrease in
346   fluorescence intensity in *drmy1* compared to WT. *pARF8::N3xGFP* and *pARF10::N3xGFP* do not
347   have uORFs and are thus expected to have comparable or higher fluorescence intensity in *drmy1*.
348   Surprisingly, we saw no correlation between the presence of uORFs and decrease in fluorescent
349   intensity in *drmy1* (Figure S5C). While it might arise from additional layers of regulation on these
350   ARFs, this result suggests that the decrease in translation reinitiation of uORF-containing ARFs
351   is not the main factor explaining the loss of robust auxin signaling pattern in *drmy1*.

352

353   It was previously reported that external application of cytokinin increases auxin
354   biosynthesis in actively growing tissue including the shoot apex, young leaves, and roots[63], and
355   cytokinin application also changes the expression and polarity of PIN-FORMED (PIN) polar auxin
356   transport carriers[64,65]. We previously noticed that external application of 6-benzylaminopurine
357   (BAP), a synthetic cytokinin, induced additional convergence points of PIN1 and increased
358   variability in auxin signaling, causing variability in sepal initiation (Zhu et al.[26], in this reference
359   see Fig. 4e, Extended Data Fig. 7e and 7f). Here, we confirmed this observation by circular
360   histogram analysis (Figure 5A-D). While the mock-treated WT buds showed four clear peaks of
361   DR5 signal with very little signal in between (Figure 5A-B), those treated with 5 µM BAP showed
362   a less robust spatial pattern, with less distinguishable peaks and larger variation all around the
363   bud (Figure 5C-D). Thus, excessive cytokinin is sufficient for the variable spatial pattern of auxin
364   signaling.

365

366   We then wondered whether an increase in cytokinin signaling (Figure 4) is the cause of
367   variable pattern of auxin signaling under translation-limited conditions such as *drmy1*. To test this
368   hypothesis, we crossed *drmy1* containing the DR5 reporter with a triple mutant of *ARABIDOPSIS*
369   *RESPONSE REGULATOR* (*ARR*) *1*, *10*, and *12*, the three most highly expressed B-type ARRs
370   in our RNA-seq (Supplementary Dataset 1) which are crucial for the activation of cytokinin-
371   responsive genes[66]. While buds of *arr1,10,12* did not show apparent phenotypic differences from
372   WT, the quadruple mutant *drmy1 arr1,10,12* largely rescued the *drmy1* phenotype, with much
373   less variability in sepal number and position (Figure 5E-G). While mature buds of *drmy1* have
374   sepals of variable sizes, leaving gaps and exposing the inner floral organs (Figure S6D vs. S6A),
375   those of *drmy1 arr1,10,12* have sepals of robust sizes that are able to close (Figure S6E).
376   Likewise, mutation in a cytokinin receptor *WOODEN LEG* (*WOL*)/*ARABIDOPSIS HISTIDINE*
377   *KINASE 4* (*AHK4*) showed a similar rescue of the *drmy1* sepal phenotype (Figure 5E-G, S6F).
378   While the auxin signaling reporter DR5 was diffuse and variable in *drmy1* except in the incipient
379   outer sepal (Figure 5H-I), in *drmy1 arr1,10,12*, it was focused in all the four incipient sepals that

380 were robustly positioned, although the signal intensity in the incipient outer sepal was much higher
381 than others (Figure 5J-K). These results indicate that cytokinin signaling is required for the
382 variability in auxin signaling pattern and sepal initiation in *drmy1*.

384 Furthermore, we wanted to test whether cytokinin signaling is required for variability in
385 more general conditions where translation is inhibited. The translation inhibitor CHX disrupted
386 robustness in auxin signaling and sepal initiation in WT (Figure 2K, 4E, 4I), and we tested whether
387 these effects are still present in *arr1,10,12* and *wol* mutants. We found that, unlike WT, sepal
388 initiation remained mostly robust in *arr1,10,12* and *wol* after ten days of 2 μM CHX treatment
389 (Figure 5L-N). While DR5 in WT became diffuse and occurred in variable positions after three
390 days of CHX treatment (Figure 5O-P, arrow), DR5 in *arr1,10,12* remained robust and
391 concentrated at the four incipient sepal primordia (Figure 5Q-R). These results suggest that
392 elevated cytokinin signaling level is the primary cause for variability in auxin patterning under
393 translation-inhibited conditions. Thus, in WT, maintaining a low level and focused cytokinin
394 signaling is crucial for robust auxin patterning and sepal initiation.

Upregulation of cytokinin signaling is required to sustain translation and fitness in *drmy1*

398 Why does the plant upregulate cytokinin signaling at the cost of robust morphogenesis
399 under translation-inhibited conditions? Early studies revealed that cytokinin signaling can
400 stimulate translation[67–71], by increasing transcription or protein abundance of ribosomal
401 components or biogenesis factors[72–74] and modification of initiation and elongation factors[75]. We
402 therefore hypothesized that an increase in cytokinin signaling under translation-inhibited
403 conditions such as in *drmy1* serves to sustain a survivable rate of translation in a feedback loop.
404 We first validated that, under our growth conditions, an increase in cytokinin signaling (*arr1*
405 *35S::ARR1*) increases translation rate (Figure 6A; also see Karunadasa et al.[67]) in 14-day-old
406 seedlings. We then tested whether cytokinin signaling is required to sustain translation, especially
407 in *drmy1* (Figure 6B-C). The cytokinin receptor single mutant *wol* does not differ from WT in
408 translation rate 8 days after germination but shows a reduced translation rate at day 14.
409 Conversely, at day 8, *drmy1* seedlings showed a drastically reduced translation rate compared to
410 WT, but by day 14, translation rate in *drmy1* increased and matched WT. In the *drmy1 wol* double
411 mutant, however, translation rate was unable to recover at day 14 and remained lower than either
412 single mutant. Our data suggests that cytokinin signaling is required to sustain translation in
413 *drmy1*, despite reduced ribosomal content (Figure 1D).

415 We then examined whether removal of cytokinin signaling and consequent failure to
416 sustain translation in *drmy1* affects plant vitality and reproduction. As expected, at day 14, the
417 *drmy1 wol* double mutant plants were extremely small, with tiny and chlorotic cotyledons and true
418 leaves (Figure 6D). These plants typically produced tiny rosettes and short inflorescences with a
419 few chlorotic buds that develop into small, short siliques (Figure 6E, S6F). Similarly, the *drmy1*
420 *arr1,10,12* quadruple mutant plants are slightly chlorotic and accumulate anthocyanins in the
421 rosette leaves (Figure 6F). They produced a tiny inflorescence composed of very few buds (Figure

422 6F, S6E) and, in the end, siliques in which all seeds had aborted (Figure 6G). Overall, these
423 results show that the growth defects in *drmy1* are exaggerated by downregulation of cytokinin
424 signaling. While it is possible that *drmy1* can be particularly sensitive to other defects caused by
425 cytokinin downregulation, our results are consistent with the hypothesis that the upregulation of
426 protein synthesis by increased cytokinin signaling promotes the survival of mutants with reduced
427 ribosomal content such as *drmy1*.

428

429 **Translation inhibition decreases the level of ARR7, a cytokinin signaling inhibitor protein**

430

431 What causes cytokinin signaling to increase in plants with reduced TOR activity and
432 translation (Figure 4)? It was previously known that *cis*-type cytokinins can be synthesized from
433 tRNAs by the tRNA isopentenyltransferases (IPTs), IPT2 and IPT9[76]. We hypothesized that the
434 decrease in translation rate may increase the availability of tRNAs as substrates for cytokinin
435 biosynthesis, increasing the level of cytokinins. To test this idea, we extracted cytokinins from
436 induced inflorescences of WT and *drmy1* in *ap1 cal AP1-GR* background (Figure S1A). We
437 measured the level of three cytokinin bases, *trans*-Zeatin (tZ), *cis*-Zeatin (cZ), and
438 isopentenyladenine (iP), and their corresponding nucleosides (tZR, cZR, and iPR), using liquid
439 chromatography-mass spectrometry. Surprisingly, we found no significant difference in their
440 levels between WT and *drmy1*, and notably, the amount of *cis*-Zeatin was barely detectable in all
441 samples (Figure S7A). This suggests that the increase in *cis*-type cytokinin synthesis is not the
442 mechanism underlying the increase in cytokinin signaling under our translation-inhibited
443 conditions.

444

445 We then considered the effects that a decrease in translation rate might have on the
446 protein components of the cytokinin signaling pathway. A-type ARR proteins are inhibitors of
447 cytokinin signaling[77–79]. They are rapidly induced upon cytokinin application and serve to dampen
448 cytokinin response in the tissue[80–82]. These proteins also have a fast turnover rate, being rapidly
449 depleted upon blocking translation with a half-life ranging from 60 to 180 min[83]. The rapid
450 synthesis and degradation of these proteins may be crucial for maintaining homeostasis of
451 cytokinin signaling during developmental processes. We therefore hypothesized that, during
452 sepal initiation, translation defects in *drmy1* cause reduced synthesis of A-type ARR proteins,
453 decreasing them to a level insufficient to repress cytokinin signaling (Figure 7A).

454

455 We set out to test whether the level of A-type ARR proteins are reduced in *drmy1*. We
456 were unable to detect fluorescence in the inflorescence of a published GFP-tagged A-type ARR
457 line under the endogenous promoter (*pARR4::ARR4-GFP*)[84]. We reasoned that this was because
458 A-type ARRs have low protein levels in the inflorescence (none was detected in our proteomics
459 dataset) and fast turnover rates[83]. We therefore employed LlamaTagging, a recently developed
460 method to visualize the abundance of nuclear-localized proteins with short half-lives[85]. Rapidly
461 degraded proteins cannot be visualized through fusion with standard fluorescent proteins,
462 because fluorescent proteins take time to fold and mature before they fluoresce, and the protein
463 of interest is degraded before the maturation of the fluorescent protein. On the other hand, the

464　　LlamaTag folds immediately. A LlamaTag with a high affinity for GFP can be encoded as a
465　　translational fusion with a nuclear-localized protein of interest. In this case, soon after translation,
466　　the fusion immediately binds GFP in the cytosol and translocates the GFP with the protein to the
467　　nucleus. Thus, increased GFP fluorescence in the nucleus indicates higher abundance of the
468　　protein of interest. We decided to focus on ARR7, the A-type ARR that is most highly expressed
469　　in our RNA-seq dataset and not differentially expressed in *drmy1* (Figure 7B; Supplemental
470　　Dataset 1). We designed a construct with ARR7 fused with GFP-specific LlamaTag by a short
471　　linker, driven by the ARR7 native promoter (*pARR7::ARR7-linker-llama-ARR7ter*; *ARR7-llama* for
472　　short). This construct was co-transformed with cytosol-localized GFP containing a nuclear
473　　exclusion signal (*pUBQ10::sfGFP-nes-UBQ3ter*; *GFP-nes* for short; Figure 7C). When ARR7-
474　　llama is produced in the cytosol, LlamaTag binds to cytosolic GFP. ARR7 then localizes to the
475　　nucleus, guided by its C-terminal nuclear localization signal[86,87], dragging GFP into the nucleus.
476　　Thus, when ARR7-llama is present at a low level, GFP is predominantly cytosol-localized; at an
477　　intermediate level, GFP may be nearly equally localized in the cytosol and nucleus; at a high level,
478　　most GFP are transported by ARR7-llama into the nucleus, and thus GFP signal is mainly seen
479　　in the nucleus (Figure 7D).
480
481　　　　As a proof of concept, we treated this reporter in WT background with 200 μM BAP. We
482　　found that GFP signal became more nuclear-localized within 5 hours of the treatment (Figure
483　　S7B), agreeing with an increased expression and stability of A-type ARR proteins upon cytokinin
484　　application as previously reported[83,88].
485
486　　　　We then compared the localization of GFP signal in floral meristems of WT and *drmy1*
487　　before sepal initiation. Following our hypothesis, if the increase in cytokinin signaling in *drmy1* is
488　　caused by reduced translation of A-type ARR proteins, there should be a decrease in ARR7 level,
489　　and thus an increase in cytosolic GFP signal, in *drmy1* vs WT. On the other hand, if the increase
490　　in cytokinin signaling in *drmy1* is caused by any other mechanism, we should see an increase in
491　　ARR7 level and nuclear GFP signal because cytokinin signaling increases the gene expression
492　　and protein stability of A-type ARRs[81,83,89]. We found that WT buds had slightly more nuclear-
493　　localized GFP signal than cytosol-localized GFP signal, with brighter spots corresponding to the
494　　nucleus surrounded by darker grooves in between corresponding to the cytosol (Figure 7E-F). In
495　　contrast, in the periphery of *drmy1* buds, GFP signal localizes more to the cytosol than to the
496　　nucleus, with darker spots surrounded by brighter grooves (Figure 7E-F). More nuclear GFP was
497　　present near the center of *drmy1* buds. This result indicates nuclear ARR7 protein concentration
498　　is reduced in the *drmy1* mutant, particularly in the zone where sepals initiate. To see whether this
499　　conclusion holds in other translation-inhibited conditions, we treated WT plants carrying the
500　　*ARR7-llama* and *GFP-nes* reporters with the translation inhibitor CHX and the TOR inhibitor AZD-
501　　8055. 2 μM CHX treatment for 24 hours drastically reduced the nuclear localization of the GFP
502　　signal and increased its cytosolic localization (Figure 7G). 2 μM AZD-8055 treatment for 72 hours
503　　had a milder but similar effect (Figure 7H). These treatments did not affect the localization of the
504　　GFP signal in plants without *ARR7-llama* (Figure S7C-D). These results show that conditions that
505　　decrease translation rate generally decrease the nuclear level of ARR7 protein. Further, these

506 results are consistent with our hypothesis that disruption of protein translation upregulates
507 cytokinin signaling in the floral meristem due to depletion of A-type ARR proteins. This suggests
508 that the rapid synthesis of A-type ARR proteins is crucial for maintaining homeostasis of cytokinin
509 signaling during sepal initiation.
510
511 Given that the level of nuclear ARR7 was reduced in *drmy1*, we next asked whether
512 increasing the level of ARR7 would restore robustness in *drmy1*. We found that while WT buds
513 carrying the *ARR7-llama* and *GFP-nes* constructs do not phenotypically differ from WT without
514 these constructs (Figure 7I-J, S7E-F), *drmy1* plants with these constructs show a partial
515 restoration of sepal initiation robustness, particularly in terms of sepal primordium position (Figure
516 7K-N, S7G-H). In stage 9-12 buds, some buds have robustly sized sepals that are able to close
517 properly, while others still have variably sized sepals that leave gaps just like in *drmy1* (Figure
518 S7H). Thus, increasing ARR7 level by adding an extra functional transgene of *ARR7-llama* to the
519 genome can partially restore robustness in both sepal initiation and mature sepal size in *drmy1*.
520 This indicates that the decrease in ARR7 protein level in *drmy1* is at least partially responsible for
521 its variability in these aspects.
522
523 We also considered other protein components of auxin and cytokinin signaling that are
524 being rapidly synthesized and degraded during developmental processes, and therefore, may be
525 depleted under translation defects. AUXIN/INDOLE-3-ACETIC ACID INDUCIBLE (Aux/IAA)
526 proteins are auxin signaling inhibitors that are rapidly induced by auxin[90,91]. In the presence of
527 auxin, they are rapidly degraded, mediated by the ubiquitin E3 ligase SKP1, CUL1, F-BOX
528 PROTEIN (SCF) complex involving TRANSPORT INHIBITOR RESPONSE1/AUXIN SIGNALING
529 F-BOX (TIR1/AFB)[92–95]. Degradation is dependent on the Short Linear Motif (SLiM) degron
530 contained within Domain II (DII)[94–96]. We hypothesized that the level of DII-containing proteins
531 including Aux/IAAs would be drastically decreased in *drmy1* because they are unable to be rapidly
532 synthesized to keep up with their degradation. To test this, we used the R2D2 reporter[97], which
533 contains a DII fused with 3xVENUS (*pUS7Y::DII-n3xVENUS*), and as a control, a mutated non-
534 degraded DII fused with tdTomato (*pUS7Y::mDII-ntdTomato*). We compared this reporter in
535 *drmy1* vs. WT. The ratio of *VENUS* to *tdTomato* was not reduced in *drmy1*, but instead slightly
536 but significantly elevated (Figure S7I-J). In addition, *drmy1* has stochastic patches of DII-VENUS
537 degradation, consistent with its often mislocalized auxin maxima (Figure 4A, S4B), unlike WT
538 which had four patches of degradation corresponding to the four incipient sepal primordia where
539 auxin maxima robustly form (Figure 4A, S4A). Overall, these results suggest that the level of DII-
540 containing Aux/IAA proteins is not reduced in *drmy1*, despite the high requirement for synthesis
541 due to their rapid turnover. They also indicate that not all proteins that are rapidly synthesized and
542 depleted in response to hormone signaling are equally affected by translation inhibition, which
543 may result in different changes in hormone signaling output under such condition.
544
545

546 **DISCUSSION**
547

13

548   Robustness, the strikingly reproducible development of phenotype, has fascinated
549   biologists for decades[2]. The Arabidopsis flower robustly develops four sepals of equal size. This
550   stems from the robust initiation of four sepal primordia from the floral meristem, which is in turn
551   dictated by the robust patterning of auxin and cytokinin controlled by DRMY1[26]. Here we
552   elucidated how DRMY1 controls robust hormone patterning and thus robust sepal initiation. We
553   show that DRMY1 sustains TOR activity, ribosomal content, and translation. We further show that
554   inhibition of TOR activity or translation is sufficient to cause variability in the timing, position, and
555   number of sepal primordia, mimicking the *drmy1* phenotype. Our findings are in concert with
556   previous studies that have shown robustness is often maintained by genes involved in central
557   cellular processes[2]. In our case, the rate of translation in wild type maintains a proper level of
558   ARR7, which needs to be rapidly synthesized to dampen cytokinin signaling. ARR7 in turn
559   ensures a normal level and spatial pattern of cytokinin signaling and indirectly auxin signaling,
560   and thus robust sepal initiation (Figure 7O, top). In the *drmy1* mutant, the reduced TOR activity,
561   ribosomal content, and translation rate causes inability to rapidly synthesize ARR7, which are
562   short-lived proteins that are easily depleted[83]. Consequently, cytokinin signaling is elevated,
563   disrupting the robust spatial distribution of both cytokinin and auxin, leading to variable sepal
564   initiation (Figure 7O, bottom). Blocking cytokinin signaling in *drmy1* is sufficient to restore robust
565   initiation of four sepal primordia, but has severe consequences on the overall fitness of the plant.
566   Our results reveal how defects in hub cellular processes such as TOR signaling and translation
567   can have very tissue-specific phenotypic effects.
568
569   It was discovered long ago that extrinsic cytokinin application to plant tissue or cell-free
570   extracts can promote mRNA translation[68–71]. Recent studies further confirmed that the up-
571   regulation of translation by cytokinin is at least in part mediated by the cytokinin signaling
572   pathway[67,75]. Here, we show that cytokinin signaling in floral buds is upregulated in translation-
573   inhibited conditions, such as *drmy1*, AZD-8055 treatment, or CHX treatment (Figure 4; also see
574   Zhu et al.[26]), through reduced level of ARR7 (Figure 7). The enhanced cytokinin signaling
575   maintains translation rate at a level necessary for the survival and reproduction of the plant (Figure
576   6). We propose that there is a homeostasis mechanism where plants leverage increased cytokinin
577   signaling to rescue the translation rate reduction caused by deficient TOR activity and ribosomal
578   content (Figure 7O, bottom). It remains to be tested how widely this mechanism is applicable to
579   other mutants with ribosomal defects, or whether parallel mechanisms operate in other species
580   across kingdoms.
581
582   While translation-inhibited plants likely upregulate cytokinin signaling to maintain protein
583   synthesis, this upregulation negatively affects developmental robustness. We have previously
584   shown that exogenous cytokinin application to the WT floral meristem increases variability in PIN1
585   convergence and auxin signaling patterns, and consequently, in sepal initiation. Mutation of a
586   cytokinin signaling inhibitor *AHP6* causes similar variability in sepal initiation. These effects are
587   more pronounced in the *drmy1* mutant, which by itself has increased and diffuse cytokinin
588   signaling[26]. Here, we provide additional evidence that increased and diffuse cytokinin signaling is
589   necessary for such variability. While *drmy1* and CHX-treated WT floral meristems are variable in

14

590   auxin signaling pattern and sepal initiation (Figure 2, 4), mutations in *wol* and *arr1,10,12*, which
591   decreases cytokinin signaling, largely restore robustness (Figure 5). Robustness is also restored
592   in the mature sepals of *drmy1 wol* and *drmy1 arr1,10,12*, enabling sepal closure (Figure S6).
593   Similar effects in restoring robustness are seen when an extra functional transgene of *ARR7*
594   (*pARR7::ARR7-llama*) is introduced to the *drmy1* mutant (Figure 7, S7). Our results suggest that
595   cytokinin upregulation is necessary and sufficient for variability in auxin patterning and sepal
596   initiation, indicating that the cytokinin signaling changes are primary defects in *drmy1*, and the
597   auxin signaling changes are secondary. Our results suggest a mechanism different from that
598   previously reported in *ul4y*, *ul18z*, and *el24y*, where ribosomal mutations affect auxin signaling
599   through reduced translation reinitiation of uORF-containing mRNAs, including those of AUXIN
600   RESPONSE FACTOR (ARF) 3, 5, and 7[57–59]. While we found that uORF-containing mRNAs
601   generally have reduced protein-transcript ratio in *drmy1* suggestive of reduced translation, we did
602   not see a consensus reduction in the level of uORF-containing promoter reporters of ARFs (Figure
603   S5). This suggests that the variable auxin signaling pattern in *drmy1* is unlikely to result from
604   changes in uORF-mediated translational regulation of ARFs. Overall, our results suggest that
605   homeostasis in cytokinin signaling is crucial for maintaining robust patterns of auxin signaling and
606   robust morphogenesis in the floral meristem.

607

608   Mutations affecting ribosome biogenesis or translation have long attracted interest due to
609   the surprisingly tissue-specific phenotypes they cause[98]. In humans, these mutations have been
610   associated with diseases collectively known as ribosomopathies, where patients show various
611   abnormalities in blood, skeleton, hair, teeth, and pancreas, as well as intellectual disability and
612   increased risk of cancer[99–104]. Ribosomal protein mutants have been characterized in numerous
613   other species with similarly diverse impacts. They display a range of specific phenotypic changes,
614   such as altered pigmentation and skeletal structure in mouse[105–107] and zebrafish[108], shorter
615   bristles and notched wing margins in fruit fly[22,109], abnormal gonad development in worm[110], and
616   pointed leaves and abnormal vascular patterning in Arabidopsis[57,58,111–113]. Here, we show that
617   the Arabidopsis mutant *drmy1* has reduced TOR activity, ribosomal content, and translation rate,
618   causing variable sepal initiation which phenocopies the ribosomal mutants *ul4y* and *ul18z* and the
619   TORC1 assembly mutant *spaghetti-1* (Figure 2, 3). We therefore propose that *drmy1* is an
620   Arabidopsis ribosomopathy mutant like those previously characterized[112].

621

622   Several mechanisms have been proposed to explain why ribosomopathies do not usually
623   cause a general reduction in growth, but rather affect development in tissue-specific ways. These
624   include extra-ribosomal functions of certain ribosomal proteins[114–118], altered translation behavior
625   of ribosomal variants on certain mRNAs[119], different competitiveness of mRNAs for scarce
626   ribosomes[57–59,120–123], and high translation rate requirement for certain proteins[124,125]. For example,
627   neurotransmitter release in animals relies on constant synthesis of the synaptic vesicle protein
628   Syt1[126]. A Drosophila *Minute* mutant, *uS15/+,* shows reduced synthesis of Syt1, which in turn
629   reduces ecdysone secretion in 5-HT neurons, causing delayed larval-to-pupal transition[124].
630   Similarly, the human apoptosis inhibitor Mcl-1 has a half-life of ~30 min and thus requires a high
631   translation rate to maintain its proper level. Under translation inhibition, Mcl-1 is rapidly degraded,

15

632 causing apoptosis[125]. Here, we show that the level of ARR7, another rapidly synthesized and
633 degraded protein[83], is drastically reduced under translation inhibition, which underlies the
634 upregulation of cytokinin signaling and loss of robustness in auxin signaling and morphogenesis
635 (Figure 7). This mechanism parallels those previously found in animal systems[124,125], and
636 highlights how defects in translation, which occurs in every cell, can have tissue-specific effects
637 on how cells robustly arrange into organs. Outside the floral meristem, the *drmy1* mutant shows
638 other phenotypic changes such as enlarged shoot apical meristem, reduced apical dominance,
639 phyllotaxy defects, and reduced root system, all of which are related to altered cytokinin/auxin
640 signaling activity[26].

641

642 In addition, we note that not all proteins that are rapidly synthesized and depleted in
643 response to hormone signaling are equally affected under broad translation inhibition. Our data
644 suggest that DII-containing proteins, including auxin signaling inhibitors Aux/IAAs, are not present
645 at a lower level in *drmy1* (Figure S7H-I). Aux/IAAs are degraded by the proteasome in an auxin-
646 dependent manner[96], while A-type ARRs can also be degraded by selective autophagy when
647 phosphorylated, in addition to proteasomal degradation[84]. In addition, the transcription of *Aux/IAA*
648 genes can be induced under translation inhibition, possibly as a feedback mechanism to maintain
649 Aux/IAA protein homeostasis[90]. Therefore, distinct turnover mechanisms and/or transcriptional
650 regulation may shape distinct effects of translational inhibition on the level of these hormone
651 signaling proteins.

652

653

654 **ACKNOWLEDGEMENTS**

682

683

AUTHOR CONTRIBUTIONS

685   S.K.: Conceptualization, Investigation, Formal Analysis, Visualization, Writing - Original Draft,
686   Writing - Review & Editing. M.Z.: Conceptualization, Investigation, Formal Analysis, Writing -
687   Review & Editing. M.R.S: Investigation, Visualization. D.P.: Investigation, Formal Analysis,
688   Visualization. L.J.: Investigation. R.E.M.: Investigation, Formal Analysis. S.A.: Methodology,
689   Resources. B.V.L.V.: Methodology, Resources, Writing - Review & Editing. H.G.: Methodology,
690   Resources, Writing - Review & Editing, Supervision. S.B.Q: Writing - Review & Editing,
691   Supervision. J.O.B.: Resources, Writing - Review & Editing, Supervision. A.H.K.R:
692   Conceptualization, Writing - Review & Editing, Supervision, Project administration, Funding
693   acquisition.

694

695

DECLARATION OF INTERESTS

697   The authors declare no competing interests.

FIGURE TITLES AND LEGENDS

Figure 1. *drmy1* has reduced ribosome abundance, translation rate, and TOR activity.

(A) Top row, stage 12 buds of WT (left) and *drmy1* (right) viewed from the top. Arrowheads point to sepals. Note that the *drmy1* bud has 5 sepals of unequal size and unevenly spaced, exposing the stamens and carpels. Middle row, stage 12 buds of WT (left) and *drmy1* (right) viewed from the side. Asterisk shows the gap between sepals with petals and carpels exposed. Bottom row, stage 5 buds of WT (left) and *drmy1* (right) containing *35S::mCitrine-RCI2A* (plasma membrane marker). Arrowheads point to sepal primordia. Note that the *drmy1* bud has 5 sepal primordia of different sizes. Scale bars are 0.5 mm for stage 12 bud images and 25 μm for stage 5 bud images.

(B-C) Gene ontology (GO) enrichment of downregulated genes **(B)** and differentially accumulated proteins **(C)** in *drmy1* compared to WT, in the *ap1 cal AP1-GR* background. Shown are the top 8 GO terms and their enrichment p-values. A complete list can be found in Supplemental Dataset 1. Arrowheads highlight terms related to ribosome biogenesis or translation.

(D) Ribosome profiles of WT (blue) and *drmy1* (red) in the *ap1 cal AP1-GR* background, representative of 3 biological replicates each. Polysomal peaks are highlighted. All replicates can be found in Supplemental Dataset 2.

(E) Puromycin labeling of WT vs *drmy1*. Left, puromycin labeling in WT and *drmy1* seedlings. From left to right: WT pre-treated with CHX, two biological replicates of WT pre-treated with mock, and two biological replicates of *drmy1* pre-treated with mock. All groups were then treated with puromycin. For seedlings to match in size, WT seedlings were 8 days old and *drmy1* seedlings were 10 days old. Right, puromycin labeling in WT and *drmy1* inflorescences of induced *ap1 cal AP1-GR* background. From left to right: WT co-treated with puromycin and CHX, three biological replicates of WT treated with puromycin, and three biological replicates of *drmy1* treated with puromycin. In both experiments, RuBisCO large subunit on Ponceau S-stained membrane is shown as a loading control (bottom).

(F) Coherent alteration of gene expression by *drmy1* and AZD-8055 TOR inhibitor treatment. Shown here is a scatterplot of RNA log 2 fold change in *drmy1* vs WT (x-axis), and WT+AZD vs WT+Mock (y-axis), in 7-day-old seedlings. Genes are color-coded based on the following categories: genes in "Structural constituents of the ribosome" (GO:0003735) and its offspring terms (magenta); all other genes in "Translation" (GO:0006412) and its offspring terms (orange); all other genes (gray). Blue line shows a linear regression of all points (R^2 = 0.1446, p < 2.2x10^{-16}). Note that the axes were trimmed to (-3,3) for ease of display.

(G-H) Phosphorylation of the direct TOR substrate, S6K-pT449, in WT and *drmy1*. Representative images are shown in **(G)**. Top, Western blot against S6K-pT449. Middle, Western blot against total S6K protein. Bottom, Ponceau S staining as a loading control. **(H)** Quantification of the intensity of S6K-pT449 over Ponceau normalized by WT, in three experiments, shows that TOR activity decreased by half in *drmy1*. (mean ± SD; *, p<0.05).

Figure 2. Defects in TOR activity, ribosome integrity, and translation cause variable sepal initiation.

(A-G) Representative images of stage 5 buds in WT (A), *drmy1* (B), *ul4z* (C), *ul4y* (D), *ul18z* (E), *lst8-1-1* (F), and *spaghetti-1* (G). Tissue morphology is visualized by either propidium iodide (a cell wall-staining dye) or a plasma membrane marker. Arrowheads indicate sepal primordia that are variable in number, position, and size. Note that *ul4z* flowers always develop four sepal primordia, although of different sizes; *lst8-1-1* occasionally (4/41, 9.8%) develops buds with more than four sepal primordia. Scale bars, 25 μm.

(H) Quantification of sepal primordium number, comparing *ul4z* (n = 52 buds), *ul4y* (n = 53 buds), *ul18z* (n = 52 buds), *lst8-1-1* (n = 41 buds), and *spaghetti-1* (n = 84 buds) with WT (n = 51 buds). Asterisks indicate statistically significant ($p < 0.05$) differences from WT in Fisher's contingency table tests.

(I) Illustration of robust versus variable positioning of sepal primordia. Primordia are considered robustly positioned if they are evenly distributed around the edge of the bud. Within each bud, angles between adjacent primordia with respect to the center of the bud are measured, and coefficient of variation (CV) is calculated. A bud with robustly positioned primordia would have similar angular values and a low CV value. A bud with variably positioned primordia would have very different angular values and a high CV value.

(J) Quantification of variability in primordium positioning (CV) in the same buds as in (H), following illustration in (I). Asterisks indicate statistically significant ($p < 0.05$) differences from WT in Wilcoxon's rank sum tests.

(K) Representative images of buds from *in vitro*-cultured WT inflorescences treated with mock or 2 μM CHX for 9 days (see Material and Methods). Arrowheads indicate sepal primordia that are variable in number, position, and size. Scale bars, 25 μm.

(L) Representative images of buds from WT plants treated with mock or 2 nmol Torin2 for 15 days (see Material and Methods). Arrowheads indicate sepal primordia that are variable in number, position, and size. Scale bars, 25 μm.

(M-N) Quantification of variability in primordium number (M) and positional variability (N) similar to (H,J), comparing CHX-treated (n = 31 buds), CHX-mock (n = 42 buds), Torin2-treated (n = 51 buds) and Torin2-mock buds (n = 56 buds).

768 **Figure 3. TOR and ribosomal defects cause variability in the timing of sepal initiation.**

769 **(A-C)** 6h-interval live imaging of the sepal initiation process in WT (A) and *ul4y* (B), which is
770 quantified in (C). n = 48 buds for WT; n = 40 buds for *ul4y*.

771 **(D-F)** 6h-interval live imaging of the sepal initiation process in buds from WT plants treated with
772 mock or 2 nmol Torin2 bi-daily for 15 days, which is quantified in (F). n = 31 buds for mock; n =
773 15 buds for Torin2.

774 In **(A,B,D,E)**, top rows show the *35S::mCitrine-RCI2A* membrane marker, and bottom rows show
775 Gaussian curvature heatmaps calculated from the same image stacks. Asterisks indicate sepal
776 initiation events, defined as a dark red band (primordium with positive curvature) separated from
777 the floral meristem by a dark blue band (boundary with negative curvature) in the Gaussian
778 curvature heatmap. Scale bars, 25 µm.

779 In **(C,F)**, the amount of time between outer and inner sepal initiation (left) and between outer and
780 lateral sepal initiation (right) were calculated for each bud, and summarized over all the buds.
781 Asterisks indicate statistically significant ($p < 0.05$) differences in the distribution of relative
782 initiation timing in Fisher's contingency table tests.

783

784 **Figure 4. Defects in TOR activity, ribosome integrity, and translation cause variability in**
785 **auxin and cytokinin signaling.**
786 **(A-D)** The ribosomal mutant *ul4y* loses robustness in auxin and cytokinin signaling. (A)
787 Representative images of late stage 2 buds of WT, *drmy1*, and *ul4y*, showing the auxin signaling
788 reporter *DR5::3xVENUS-N7* in yellow, the cytokinin signaling reporter *TCS::GFP* in cyan, and
789 both merged with Chlorophyll (in WT) or *UBQ10::mCherry-RCI2A* (in *drmy1* and *ul4y*) in magenta.
790 (B) Quantification of TCS intensity (integrated density divided by area) from maximum intensity
791 projection images, normalized to mean of WT. Shown are mean ± SD. Asterisks show statistically
792 significant differences from WT in two-tailed Student's t-tests (*drmy1*, $p = 2.1 \times 10^{-6}$; *ul4y*, $p =$
793 3.4×10^{-5}). (C) Circular histogram of DR5 distribution around the bud. Each bud was divided into
794 360 sectors of 1° each. Within each sector, DR5 signal measured in pixel intensity units (0-255
795 range) was summed. This sum was plotted along the x-axis starting from the sector at 1:30
796 position (between the incipient outer sepal and incipient lateral sepal on the right) going
797 counterclockwise. I.e. in WT, the outer sepal is near 45°, the inner sepal near 225°, and the lateral
798 sepals near 45° and 135° (vertical dotted lines). The mean was plotted as a solid line, and mean
799 ± SD was plotted as a shaded area. (D) Circular histogram of TCS distribution around the bud.
800 Sample size for (A-D): WT, n = 12 buds; *drmy1*, n = 15 buds; *ul4y*, n = 10 buds.
801 **(E-H)** 3 days of translation inhibition causes increased and diffuse cytokinin signaling, and diffuse
802 auxin signaling. (E) Representative images of late stage 2 buds from dissected and cultured WT
803 inflorescences treated with mock or 2 μM CHX for 3 days. Shown are *DR5::3xVENUS-N7* in
804 yellow, *TCS::GFP* in cyan, and both merged with Chlorophyll in magenta. (F) Quantification of
805 TCS intensity from maximum intensity projection images, normalized to mean of WT mock day 3.
806 Shown are mean ± SD. Asterisk shows statistically significant difference in a two-tailed Student's
807 t-test ($p = 2.0 \times 10^{-4}$). (G) Circular histogram of DR5 distribution around the bud. (H) Circular
808 histogram of TCS distribution around the bud. Sample size for (E-H): WT mock day 3, n = 10
809 buds; WT CHX day 3, n = 12 buds.
810 **(I-L)** 6 days of TOR or translation inhibition causes increased and diffuse cytokinin signaling, and
811 randomly positioned auxin signaling maxima. (I) Representative images of late stage 2 buds from
812 dissected and cultured WT inflorescences treated with mock, 2 μM CHX, or 2 μM AZD for 6 days.
813 Shown are *DR5::3xVENUS-N7* in yellow, *TCS::GFP* in cyan, and both merged with Chlorophyll
814 in magenta. Arrowheads point to randomly positioned auxin maxima in buds of the CHX or AZD
815 group. (J) Quantification of TCS intensity from maximum intensity projection images, normalized
816 to mean of WT mock day 6. Shown are mean ± SD. Asterisks show statistically significant
817 differences from mock in two-tailed Student's t-tests (CHX, $p = 1.0 \times 10^{-3}$; AZD, $p = 1.2 \times 10^{-4}$). (K)
818 Circular histogram of DR5 distribution around the bud. (L) Circular histogram of TCS distribution
819 around the bud. Sample size for (I-L): WT mock day 6, n = 12 buds; WT CHX day 6, n = 11 buds;
820 WT AZD day 6, n = 10 buds. Scale bars in (A,E,I) represent 25 μm.
821

822 **Figure 5. Cytokinin signaling is required for variability in auxin signaling and sepal**
823 **initiation under translation inhibition.**
824 **(A-D)** Cytokinin treatment makes auxin signaling diffuse. Shown are late stage 2 WT buds under
825 mock (A,B) or 5 µM cytokinin (BAP) treatment (C,D) for 4 days. (A,C) Representative images of
826 the auxin signaling reporter *DR5::3xVENUS-N7* in yellow, and *DR5* merged with Chlorophyll in
827 magenta. (B,D) Circular histograms of the *DR5::3xVENUS-N7* signal, showing mean (solid line)
828 and mean ± SD (shaded area). Arrows point to DR5 signal in variable positions. Sample size: WT
829 Mock n = 10, WT BAP n = 10. Also see Zhu et al. (2020), Extended Data Figure 7e.
830 **(E-G)** Cytokinin signaling is required for variable sepal initiation in *drmy1*. (E) Representative
831 images of stage 5 buds in WT, *drmy1*, *arr1,10,12*, *drmy1 arr1,10,12*, *wol*, and *drmy1 wol*.
832 Arrowheads indicate initiated sepal primordia that are variable in number, position, and size. (F,G)
833 Quantification of sepal primordium number (F) and positional variability (G), comparing WT (n =
834 58) with *drmy1* (n = 31), *arr1,10,12* (n = 24) with *drmy1 arr1,10,12* (n = 20), and *wol* (n = 36) with
835 *drmy1 wol* (n = 39). Asterisks indicate statistically significant (p < 0.05) differences in Fisher's
836 contingency table tests (F) and Wilcoxon's rank sum tests (G) respectively. ns indicates no
837 significant difference.
838 **(H-K)** Cytokinin signaling is required for variable patterning of auxin signaling in *drmy1*. Shown
839 are late stage 2 buds of WT vs *drmy1* (H,I), and *arr1,10,12* vs *drmy1 arr1,10,12* (J,K). (H,J)
840 Representative images of the auxin signaling reporter *DR5::3xVENUS-N7* in yellow, and *DR5*
841 merged with propidium iodide in magenta. Arrows point to diffuse DR5 signal in variable positions
842 in the *drmy1* bud. Arrowheads show four robust DR5 maxima in *drmy1 arr1,10,12*. (I,K) Circular
843 histograms of the *DR5::3xVENUS-N7* signal, showing mean (solid line) and mean ± SD (shaded
844 area). For ease of visualization, circular histograms of *drmy1* and *drmy1 arr1,10,12* between 90
845 and 360 degrees are enlarged and shown as insets (y-axis range 0-0.4). Sample size: WT n =
846 19, *drmy1* n = 16, *arr1,10,12* n = 13, *drmy1 arr1,10,12* n = 9.
847 **(L-N)** Cytokinin signaling is required for variable sepal initiation under translation inhibition. (L)
848 Representative images of stage 6 buds in WT, *arr1,10,12*, and *wol*, treated with Mock or 2 µM
849 CHX for 10 days. Arrowheads indicate variable initiation of sepal primordia. (M,N) Quantification
850 of sepal primordium number (M) and positional variability (N), comparing Mock and CHX within
851 each genotype. Sample size: WT Mock n = 29, WT CHX n = 19, *arr1,10,12* Mock n = 18,
852 *arr1,10,12* CHX n = 19, *wol* Mock n = 15, *wol* CHX n = 19. Asterisks indicate statistically significant
853 (p < 0.05) differences in Fisher's contingency table tests (M) and Wilcoxon's rank sum tests (N)
854 respectively. ns indicates no significant difference.
855 **(O-R)** Cytokinin signaling is required for diffuse auxin signaling under translation inhibition. Shown
856 are late stage 2 buds of WT (O,P) and *arr1,10,12* (Q,R), treated with Mock or 2 µM CHX for 3
857 days. (O,Q) Representative images of the auxin signaling reporter *DR5::3xVENUS-N7* in yellow,
858 and *DR5* merged with Chlorophyll in magenta. Arrows point to diffuse DR5 signal in variable
859 positions in CHX-treated WT. Arrowheads show four robust DR5 maxima in CHX-treated
860 *arr1,10,12*. (P,R) Circular histograms of the *DR5::3xVENUS-N7* signal, showing mean (solid line)
861 and mean ± SD (shaded area). Sample size: WT Mock n = 17, WT CHX n = 18, *arr1,10,12* Mock
862 n = 7, *arr1,10,12* CHX n = 7. Scale bars in (A,C,E,H,J,L,O,Q) represent 25 µm.
863

864 **Figure 6. Upregulation of cytokinin signaling is required to maintain translation and**
865 **fitness in *drmy1*.**
866 **(A)** Puromycin labeling of WT seedlings with 4 h CHX pre-treatment (control), and three biological
867 replicates each of WT and *arr1 35S::ARR1* seedlings with 4 h mock pre-treatment. All seedlings
868 are 14 days old. RuBisCO large subunit in Ponceau S-stained membrane is shown as a loading
869 control. Also see Karunadasa et al. (2020).
870 **(B,C)** Puromycin labeling of WT seedlings with 4 h CHX pre-treatment (control), and two biological
871 replicates of WT, *drmy1*, *wol*, and *drmy1 wol* seedlings with 4 h mock pre-treatment. Seedlings
872 are 8 days old in (B) and 14 days old in (C). RuBisCO large subunit in Ponceau S-stained
873 membrane is shown as a loading control.
874 **(D)** Representative 14 days old seedling images of WT, *drmy1*, *wol*, and *drmy1 wol* used in (C).
875 Notice that *drmy1 wol* is very small and pale. Scale bars, 5 mm.
876 **(E)** Representative aerial part images of 42 days old plants of WT, *drmy1*, *wol*, and *drmy1 wol*.
877 Inset shows enlarged *drmy1 wol* plant; notice that it has a tiny rosette and inflorescence. Scale
878 bars, 5 cm. See also Supplemental Figure 6F.
879 **(F)** Representative aerial part images of 74 days old plants of WT, *drmy1*, *arr1,10,12*, and *drmy1*
880 *arr1,10,12*. Inset shows enlarged *drmy1 arr1,10,12* plant; notice its pale leaves accumulating
881 anthocyanin, and short inflorescence. Scale bars, 5 cm. See also Supplemental Figure 6E.
882 **(G)** Dissected siliques of *arr1,10,12* (left) and *drmy1 arr1,10,12* (right) showing developing seeds.
883 Notice that while *arr1,10,12* occasionally have aborted seeds, all seeds in the *drmy1 arr1,10,12*
884 silique were aborted. Scale bars, 0.2 mm.
885

886 **Figure 7. A-type ARR protein levels are sensitive to TOR and translation inhibition.**
887 **(A)** The hypothesis. A-type ARRs are rapidly synthesized and degraded to dampen cytokinin
888 signaling. Translation inhibition causes inability to rapidly synthesize these proteins in response
889 to cytokinin signaling, resulting in an upregulation of cytokinin signaling.
890 **(B)** Expression of A-type ARR genes in WT vs *drmy1* inflorescences (*ap1 cal AP1-GR*) measured
891 in RNA-seq. Shown are the five A-type ARR genes with the highest expression, ranked by mean
892 expression level in WT. Asterisk indicates statistically significant difference, while ns means no
893 significant difference. P-values: ARR7, p = 0.807; ARR4, p = 0.611; ARR15, p = 0.532; ARR8, p
894 = 0.0115; ARR9, p = 0.0416.
895 **(C)** A GFP-channel image of a stage 2 bud of GFP-nes (*pUBQ10::sfGFP-nes-UBQ3ter*). For this
896 panel and (E-H), each image was brightened to reveal GFP distribution patterns. A square region
897 taken from the image containing 5-10 cells is enlarged and shown on the top right. Within the
898 enlargement, GFP intensity was quantified along the dotted line and plotted on the bottom right.
899 X-axis, pixels (range 0-238). Y-axis, GFP intensity in gray value (smoothened by taking the
900 average intensity of 11-pixel neighborhoods; range 90-210). Scale bars, 25 μm.
901 **(D)** Illustration of the Llama Tag system used in this study. Plants were co-transformed with *ARR7-*
902 *llama* (*pARR7::ARR7-linker-llama-ARR7ter*) and *GFP-nes* (*pUBQ10::sfGFP-nes-UBQ3ter*).
903 Without ARR7-llama, the GFP is localized in the cytosol. ARR7-llama is produced in the cytosol
904 and translocates into the nucleus. When this happens, the Llama Tag capable of binding GFP
905 drags GFP into the nucleus (note that from our observation it is excluded from the nucleolus).
906 Therefore, at low ARR7-llama levels, GFP signal is mainly seen in the cytosol. At intermediate
907 ARR7-llama levels, GFP is at comparable intensities between the cytosol and the nucleus, and
908 no clear pattern can be seen. At high ARR7-llama levels, GFP is mainly seen in the nucleus.
909 **(E,F)** GFP channel images of stage 2 buds from two independent transgenic lines of *ARR7-llama*
910 *GFP-nes*, 7-4 (E) and 7-6 (F), in WT (top) vs *drmy1* (bottom). Images are representative of n =
911 17 (line 7-4, WT), n = 40 (line 7-4, *drmy1*), n = 9 (line 7-6, WT), and n = 6 (line 7-6, *drmy1*) buds.
912 **(G)** GFP channel images of WT *ARR7-llama GFP-nes* buds treated with mock (top) or 2 μM CHX
913 (bottom) for 24 hours. The mock image is representative of n = 20 buds (12 from line 7-4, 5 from
914 line 7-6, and 3 from line 7-12). The CHX image is representative of n = 19 buds (11 from line 7-
915 4, 5 from line 7-6, and 3 from line 7-12).
916 **(H)** GFP channel images of WT *ARR7-llama GFP-nes* buds treated with mock (top) or 2 μM AZD-
917 8055 (bottom) for 72 hours. The mock image is representative of n = 13 buds (8 from line 7-4 and
918 5 from line 7-6). The AZD-8055 image is representative of n = 11 buds (8 from line 7-4 and 3 from
919 line 7-6).
920 **(I-N)** *ARR7-llama* partially restores robustness in *drmy1* sepal primordia. (I-L) Representative
921 stage 5 or 6 buds from WT (I), WT with the *ARR7-llama* and *GFP-nes* constructs (J), *drmy1* (K),
922 and *drmy1* with these constructs (L). (M) Quantification of sepal primordium number. ns indicates
923 no significance difference in a Fisher's exact test (WT vs *ARR7-llama*, p = 1; *drmy1* vs *drmy1*
924 *ARR7-llama*, p = 0.44). (N) Quantification of variability in sepal primordium position. Asterisk
925 indicates statistically significant difference (p = 5.7×10^{-6}), while ns indicates no statistically
926 significant difference (p = 0.91). Data for WT and *drmy1* were reused from Figure 2H, 2J. Data
927 for *ARR7-llama GFP-nes* and *drmy1 ARR7-llama GFP-nes* were pooled from line 7-4 and 7-6.

928   Sample size: WT n = 51, *ARR7-llama GFP-nes* n = 16, *drmy1* n = 67, *drmy1 ARR7-llama GFP-*
929   *nes* n = 20. Scale bars, 25 µm.

930   **(O)** Working model. In WT, DRMY1 maintains TOR activity and translation, which sustains the
931   rapid translation of A-type ARRs in response to cytokinin signaling. This suppresses excessive
932   cytokinin signaling, allowing auxin and cytokinin signaling to interact and form robust spatial
933   patterns. Robust patterning of auxin and cytokinin signaling gives rise to robustly numbered,
934   positioned, and sized sepal primordia. In *drmy1*, A-type ARR protein levels are reduced due to
935   insufficient TOR activity, ribosome content, and translation rate. Cytokinin signaling is
936   upregulated, which rescues the translation rate reduction in a homeostatic mechanism. This
937   upregulation of cytokinin signaling disrupts the robust spatial pattern of both cytokinin and auxin
938   signaling, which in turn causes variable sepal initiation.

939

940 **MATERIALS AND METHODS**
941
942 **Plant material**
943   Most Arabidopsis plants were in Col-0 background (WT). *ap1 cal 35S::AP1-GR* was in Ler
944 background. *drmy1* (Col-0) was backcrossed to Ler twice and then crossed with *ap1 cal*
945 *35S::AP1-GR* to obtain *drmy1 ap1 cal 35S::AP1-GR*. R2D2 was originally in Col-Utrecht
946 background and was backcrossed twice into WT (Col-0) and *drmy1* (Col-0). The following mutants
947 and reporters were previously described: *drmy1-2*[26], *wol-1*[127], *spaghetti-1* (*tpr5-1*)[128], *ap1 cal*
948 *35S::AP1-GR* (Ler)[35,36], *arr1-1 35S::ARR1*[67], *DR5::3xVENUS-N7*[129], *TCS::GFP*[130], *pARF5::ER-*
949 *EYFP-HDEL*[131], *pUS7Y-mDII-NtdTomato-pUS7Y-DII-N3xVENUS* (R2D2)[97], *35S::mCirtine-*
950 *RCI2A*[26], *UBQ10::mCherry-RCI2A*[26]. The following mutants and reporter lines were obtained from
951 Arabidopsis Biological Resource Center (ABRC): *ul4z* (SALK_130595), *ul4y* (SALK_029203),
952 *ul18z* (SALK_089798), *arr1-3 arr10-5 arr12-1*[132] (CS39992), *lst8-1-1* (SALK_002459),
953 *pARF3::N3xGFP*[133] (CS67072), *pARF6::N3xGFP*[133] (CS67078), *pARF8::N3xGFP*[133] (CS67082),
954 *pARF10::N3xGFP*[133] (CS67086).
955
956 **Llama-tagged ARR7 construct**
957   For the LlamaTag system, we first generated plasmid *pVV13* containing linker-llama. We
958 amplified the LlamaTag (from a plasmid containing vhhGFP4[134]) and added a linker sequence of
959 tccggagcagctgcggctgccgctgcggcagcggccactagt at its 5' end by two rounds of overlap PCRs.
960 Primers for the first round were oVV64 and oVV53, and primers for the second round were oVV35
961 and oVV53. After the second round, we A-tailed the PCR product according to the Promega
962 manufacturer's protocol. A-tailed product was ligated to the pGEMTeasy vector according to the
963 Promega ligation protocol, to create the plasmid *pVV13*.
964   To make *pARR7::ARR7-llama*, a genomic fragment of *pARR7::ARR7* minus the stop
965 codon and terminator was amplified from the Arabidopsis (Col-0) genome using the primers
966 oSK197 and oSK198. The linker-llama fragment was PCR-amplified from *pVV13* using the
967 primers oSK199 and oSK200. The *ARR7* stop codon, 3' UTR, and terminator was amplified from
968 the Arabidopsis (Col-0) genome using the primers oSK201 and oSK202. *pMLBART* backbone
969 was digested with NotI, and all fragments were assembled into *pMLBART* using NEBuilder
970 according to the manufacturer's protocol.
971   To make *pUBQ10::sfGFP-NES:UBQ3ter*, sfGFP sequence was amplified from the *35S-*
972 *sfGFP-nosT* plasmid[135] (Addgene # 80129) using primers UsfGM-F1 and UsfGnes-R1. The
973 UBQ10 promoter was amplified from the *UPG* plasmid[136] (Addgene # 161003) using primers
974 OutALFd and UsfGM-R1. The UBQ3 terminator was amplified from the *UPG* plasmid[136] (Addgene
975 # 161003) using primers UsfGnes-F1 and OutALRb. Primer overhangs spanning the junction
976 between sfGFP and the UBQ3 terminator contain the sequence of the mouse PKIα NES.
977 *pCambia1300* backbone was digested with BamHI and KpnI, and all fragments were Gibson-
978 assembled into the backbone. Sequences of primers, *pARR7::ARR7-llama*, and *pUBQ10::sfGFP-*
979 *NES:UBQ3ter* can be found in Supplemental Dataset 5.
980   Col-0 plants were co-transformed with *pARR7::ARR7-llama* and *pUBQ10::sfGFP-*
981 *NES:UBQ3ter*, and selected with Basta (for *pARR7::ARR7-llama*) + Hygromycin (for

982 *pUBQ10::sfGFP-NES:UBQ3ter*). Surviving T1 plants were screened for clear nuclear signal in the
983 inflorescence, and 5 independent T1 plants were selected and crossed into *drmy1*. F2 plants from
984 each line were again selected with Basta + Hygromycin and genotyped. One line showed co-
985 segregation with the *DRMY1* locus. Two lines showed severe silencing in the F2 and could not
986 be used. Two lines (7-4 and 7-6), though with minor silencing in F2, were used for imaging and
987 image analysis. F3 plants of 7-4 and 7-6 had severe silencing, and therefore only F2 were imaged.
988

Plant growth conditions

990 For most experiments, seeds were sown in wetted Lamber Mix LM-111 soil and stratified
991 at 4°C for 3-5 days. For experiments including *drmy1 wol* and *drmy1 arr1,10,12*, all seeds were
992 sown onto ½ MS plates with 0.05% (w/v) MES, 1% (w/v) sucrose, 1.2% (w/v) agar, pH 5.7, and
993 stratified at 4°C for a week. They were grown for 7-10 days before being transplanted to soil (for
994 imaging of inflorescence or aerial part of the plant) or left on the plates until desired time of the
995 experiment (for seedling imaging or puromycin labeling).
996 Most plants were grown under 16 h – 8 h light-dark cycles (fluorescent light, ~100 µmol
997 m^{-1} s^{-1}) at 22°C in a Percival walk-in growth chamber. We found that the *drmy1* phenotype is more
998 pronounced in this condition than under continuous light. The *ap1 cal 35S::AP1-GR* and *drmy1*
999 *ap1 cal 35S::AP1-GR* plants were grown in soil under continuous light at 16°C to prevent
1000 premature floral induction.
1001

Flower staging

1003 Flower buds were staged as previously described[37]. Briefly, stage 1 is when the floral
1004 meristem emerges, but not yet separated, from the inflorescence meristem. Stage 2 is when the
1005 floral meristem separates from the inflorescence meristem but with no floral organs initiated.
1006 Stage 3 is when sepal primordia initiate. Stage 4 is when sepal primordia bend to cover part of
1007 the floral meristem. Stage 5 is when stamen primordia initiate. Stage 6 is when sepal primordia
1008 completely cover the floral meristem.
1009

RNA-seq data collection and analysis

1011 For RNA-seq in the inflorescence, bolting *ap1 cal 35S::AP1-GR* and *drmy1 ap1 cal*
1012 *35S::AP1-GR* plants were induced daily with an aqueous solution containing 10 µM
1013 dexamethasone (Sigma-Aldrich), 0.01% (v/v) ethanol, and 0.015% (v/v) Silwet L-77
1014 (Rosecare.com). When sepals initiated from the floral meristems, usually on the fourth day after
1015 three daily inductions, three inflorescence samples per genotype (including inflorescence
1016 meristems and buds under stage 6) were collected and immediately put into liquid nitrogen. RNA
1017 extraction, library preparation, RNA-seq, and data analysis for inflorescence samples were done
1018 as previously described[26] with a few changes. After read mapping, genes with at least two raw
1019 reads in at least two biological replicates in either WT or *drmy1* were kept for downstream
1020 analysis. For differentially expressed genes, we set a log2 fold change threshold of ±1 and a BH-
1021 adjusted p-value threshold of 0.05. For GO term enrichment, gene-GO mapping data was
1022 obtained from TAIR (https://www.arabidopsis.org
1023 /download_files/GO_and_PO_Annotations/Gene_Ontology_Annotations/ATH_GO_GOSLIM.txt)

1024   . The R package "topGO"[137] (version 2.38.1) was used for the enrichment, with statistic "fisher",
1025   algorithm "weight01", annotation function "annFUN.gene2GO", and minimum node size 10. The
1026   results were ranked by their p-value, and the first 8 terms were plotted.
1027   For RNA-seq in seedlings, WT and *drmy1* seedlings were grown to quiescence (7 days)
1028   in ½ MS liquid media as previously described[34]. After 7 days, the media was replaced with ½ MS
1029   liquid media containing 15 mM glucose and incubated for 24 hours to activate TOR. Seedlings
1030   were then incubated with or without AZD-8055 in addition to 15 mM glucose in ½ MS liquid media
1031   for 2 hours before collecting tissue. RNA was extracted from 100 mg pooled seedlings using the
1032   Spectrum Plant Total RNA Kit (Sigma). This RNA was used as a template for RNA-Seq library
1033   synthesis and sequencing, which was performed by Novogene. RNA-seq data for AZD-8055
1034   treated WT and *drmy1* seedlings were preprocessed with fastp (v. 0.22.0) using default
1035   parameters. Preprocessed reads were then mapped to the TAIR10 reference genome using
1036   STAR (v. 2.7.10z_alpha_220314). Following alignment, BAM output files from STAR were used
1037   to generate feature counts for transcripts using subread-featureCounts (v. 2.0.3) and the
1038   Araport11 transcriptome. TPMs were generated using TPMCalculator (v. 0.0.3). Differential
1039   expression analysis was performed using feature count data and DESeq2 (v. 1.36.0).
1040   A list of genes with uORFs based on gene models of the TAIR10 Arabidopsis genome
1041   assembly were downloaded from von Arnim et al.[62]. For each gene, within each genotype, protein-
1042   transcript ratio was calculated as the ratio between mean protein abundance and mean transcript
1043   TPM across all bio-reps in our proteomics and RNA-seq datasets, respectively. This was log2-
1044   transformed, and the difference between *drmy1* and WT was calculated. This was used as an
1045   indicator of translation rate difference between *drmy1* and WT, although we acknowledge that
1046   other factors such as protein stability may affect this number. This was plotted against the number
1047   of uORFs in each gene model (0, 1, or ≥ 2).
1048
1049   **Proteomics**
1050   Five induced inflorescence samples of WT and *drmy1* in *ap1 cal AP1-GR* background
1051   were collected as described above. Samples were ground in liquid nitrogen. Total soluble proteins
1052   were extracted in ice-cold extraction buffer (50 mM PBS-HCl (pH 8.0) buffer with 150 mM NaCl,
1053   2% NP-40, 1 mM PMSF, 1x Roche cOmplete protease inhibitor cocktail (Sigma 11697498001),
1054   and 1x Halt TM Phosphatase inhibitor cocktail (ThermoFisher 78420)) and filtered through
1055   Pierce™ Micro-Spin Columns (30 μm pore size; Thermo Scientific 89879). Extracts were
1056   RuBisCO-depleted using Seppro Bubisco Kit (Sigma SEP070-1KT), concentrated, denatured,
1057   reduced, cysteine blocked, trypsin-digested, and TMT 10-plex labeled. Then, mass spectrometry
1058   was done using an UltiMate 3000 RSLCnano / Orbitrap Fusion system (Thermo Scientific). Raw
1059   data was searched against the NCBI protein database using PD 2.3 (Thermo Scientific) with
1060   Sequest HT searching engine. Precursor-based protein identification and relative quantification
1061   was done using the standard processing workflow in PD 2.3, with an additional node of Minora
1062   Feature Detector. Proteins with at least 2 supporting peptides were kept for downstream analysis.
1063   For each protein, data was fit with an ANOVA model and a p-value was calculated. Proteins with
1064   a p-value < 0.05 were considered differentially accumulated in *drmy1*. GO term enrichment was
1065   done as above, using genes corresponding to the differentially accumulated proteins.

1066

Polysome extraction and profiling

1068 Three induced inflorescence samples of WT and *drmy1* in *ap1 cal AP1-GR* background
1069 were collected as described above, and polysomes were extracted as previously described[138].
1070 Briefly, samples were ground in liquid nitrogen, mixed with an extraction buffer (0.2 M Tris pH 9.0,
1071 0.2 M KCl, 0.025 M EGTA, 0.035 M MgCl$_2$, 1% (w/v) Brij-35, 1% (v/v) Triton X-100, 1% (v/v) Igepal
1072 CA-630, 1% (v/v) Tween-20, 1% (w/v) Sodium deoxycholate, 1% (v/v) Polyoxyethylene 10 tridecyl
1073 ether, 5 mM Dithiothreitol, 1 mM Phenylmethylsulfonyl fluoride, 100 µg/ml cycloheximide, 100
1074 µg/ml chloramphenicol, 40 U/ml RNasin, 0.5 mg/ml Heparin), and let sit on ice for 10 min. Samples
1075 were centrifuged at 4°C 4,000 g for 5 min, supernatant was transferred to a new tube, centrifuged
1076 at 4°C 16,000 g for 15 min, and supernatant was filtered through Miracloth.

1077 Polysome extracts were profiled as previously described[139]. Briefly, samples were loaded
1078 onto 15%-45% sucrose density gradients and centrifuged at 4°C 38,000 rpm in a SW41 rotor.
1079 Separated samples were fractionated at a rate of 0.375 mL/min in an Isco fractionation system,
1080 and absorbance at 254 nm was recorded.

1081

Puromycin labeling

1083 Puromycin labeling was done as previously described[39], with slight modifications.
1084 In seedlings, when comparing WT and *drmy1*, in order to control for plant size, WT
1085 seedlings were grown for 8 days and *drmy1* seedlings were grown for 10 days (Figure 1E). When
1086 comparing WT, *drmy1*, *wol*, and *drmy1 wol*, we were unable to control for plant size because
1087 *drmy1 wol* seedlings were too small. We therefore controlled for plant age, and seedlings were
1088 grown to specified age (8 days for Figure 6B and 14 days for Figure 6C). Seedlings were
1089 harvested from plates and incubated with an incubation buffer (½ MS, 0.05% (w/v) MES, 1% (w/v)
1090 sucrose, 0.1% (v/v) Tween-20, 0.1% (v/v) DMSO, 1x Gamborg vitamin mix, pH 5.7), with or
1091 without 50 µM CHX, for 4 hours in an illuminated growth chamber. Then, the buffer was replaced
1092 with a fresh incubation buffer (which is same as above, but contains 50 µM puromycin (GoldBio
1093 P-600-100)), and incubation continued for another 45 min.
1094 In inflorescences of WT and *drmy1* in *ap1 cal AP1-GR* background, inflorescences were
1095 DEX-induced as described above. Inflorescence samples were collected and put in an incubation
1096 buffer (½ MS, 1% (w/v) sucrose, 0.02% (v/v) Silwet L-77, 0.1% (v/v) DMSO, 50 µM puromycin,
1097 1x Gamborg vitamin mix, pH 5.7), with or without 100 µM CHX. Samples were vacuum infiltrated
1098 for 15 minutes and then put on a rocking shaker in an illuminated growth chamber for 45 minutes.
1099 In both cases, at the end of the incubation, samples were washed three times with water,
1100 blot dry, weighed, and frozen in liquid nitrogen. Soluble proteins were extracted as described
1101 above. Puromycin incorporated into the proteins were detected in a Western blot using a mouse-
1102 origin anti-puromycin monoclonal antibody (12D10, Sigma MABE343, lot # 3484967) and a goat-
1103 anti-mouse HRP-conjugated secondary antibody (Abcam ab6789, lot # 3436981). RuBisCO large
1104 subunit in Ponceau S-stained membrane was used as a loading control.

1105

TOR activity assay

1107   WT and *drmy1* seedlings were grown in a six-well plate containing ½ MS liquid media.
1108   After seven days, the media were replaced with half-strength MS liquid media plus 15 mM glucose
1109   and incubated for 24 hours. At least 120 quiescent seedlings per sample were collected and
1110   frozen in liquid nitrogen. Protein was then extracted from the plant tissue in 100 mM MOPS (pH
1111   7.6), 100 mM NaCl, 5% SDS, 0.5% b-mercaptoethanol, 10% glycerin, 2 mM PMSF, and 1x
1112   PhosSTOP phosphatase inhibitor (Sigma). S6K-pT449 was detected by Western blot using a
1113   phosphospecific antibody (Abcam ab207399) and an HRP-conjugated goat anti-rabbit IgG
1114   secondary antibody (Jackson Immuno Research 111-035-003). Total S6K was detected using a
1115   custom monoclonal antibody described by Busche et al.[140]. Total protein visualized in Ponceau
1116   S-stained membrane was used as a loading control.
1117
1118   **Confocal microscopy**
1119   Confocal imaging of reporter lines in the inflorescence were done as previously
1120   described[26]. Briefly, main inflorescences (not side branches) were cut and dissected with a
1121   Dumont tweezer (Electron Microscopy Sciences, style 5, no. 72701-D) to remove buds older than
1122   stage 9 or 10. The inflorescences were then inserted upright into a small petri dish (VWR, 60 x
1123   15 mm) containing inflorescence culture medium (1/2 MS, 1% (w/v) sucrose, 1x Gamborg vitamin
1124   mixture, 0.1% (v/v) plant preservative mixture (Plant Cell Technology) 1% (w/v) agarose, pH 5.8),
1125   leaving most of the stem inside the medium and the buds outside. They were then further
1126   dissected to reveal stage 6 and younger buds, immersed with water, and imaged under a
1127   Zeiss710 upright confocal microscope with a 20x Plan-Apochromat water-dipping lens (1.0 NA).
1128   For live imaging experiments, inflorescence samples were put in a continuous-light growth
1129   chamber between time points. To prevent bacterial growth, samples were transferred onto fresh
1130   media every 2 to 3 days, and for live imaging experiments lasting longer than 6 days, once in the
1131   middle, plants were incubated with an aqueous solution of 100 µg/ml Carbenicillin (GoldBio, C-
1132   103-5, lot # 0129.091814A) for 30 minutes.
1133   To visualize tissue morphology of inflorescence samples without a reporter, samples were
1134   stained for 5 minutes with an aqueous solution of 0.1 mg/ml propidium iodide (PI) and 0.1% (v/v)
1135   Tween-20, washed three times with water, and imaged.
1136   The following laser and wavelength were used in confocal imaging. Chlorophyll, excitation
1137   488 nm, emission 647-721 nm. PI, excitation 514 nm, emission 566-659 nm. mCherry, excitation
1138   594 nm, emission 600-659 nm. tdTomato, excitation 561 nm, emission 566-595 nm. For
1139   EYFP/VENUS/mCitrine, in *35S::mCirtine-RCI2A*, excitation 514 nm, emission 519-580 nm; in
1140   *DR5::3xVENUS-N7*, excitation 514 nm, emission 519-569 nm; in *pARF5::ER-EYFP-HDEL*,
1141   excitation 514 nm, emission 519-550 nm; in *R2D2*, excitation 488 nm, emission 493-551 nm. For
1142   GFP/sfGFP, in *pARR7::ARR7-llama UBQ10::sfGFP-NES*, excitation 488 nm, emission 493-569
1143   nm; in *pARF3::N3xGFP*, *pARF6::*N3xGFP, *pARF8::N3xGFP*, and *pARF10::N3xGFP*, excitation
1144   488 nm, emission 493-564 nm; in *TCS::GFP*, excitation 488 nm, emission 493-513 nm.
1145
1146   **Visualization of tissue morphology**
1147   For single-channel image stacks intended for the visualization of tissue morphology
1148   (*35S::mCitrine-RCI2A* or PI), stacks were 3D-rendered using the ZEN confocal software

1149   (Processing -> 3D). Parameters were set to best visualize tissue morphology, typically, minimum
1150   5-10, ramp 60-80, maximum 100. Buds were rotated to desired orientation, and screenshots were
1151   taken using the "Create Image" button. For fluorophores that are dimmer, less sharp, or have a
1152   noisy background (*UBQ10::mCherry-RCI2A* or Chlorophyll), stacks were converted from LSM to
1153   TIF using ImageJ[141,142], loaded into MorphoGraphX[143], and screenshots were taken using the
1154   built-in screenshot function in MorphoGraphX.

1155   To aid visualizing tissue morphology and determine the timing of sepal initiation, each
1156   stack was fitted with a surface, and a Gaussian curvature heatmap was calculated from the
1157   surface (see below). We consider a sepal primordium as initiated when we see a dark red band
1158   of positive Gaussian curvature (primordium) separated from the center of the floral meristem by
1159   a dark blue band of negative Gaussian curvature (boundary)[26].

1160   Gaussian curvature heatmaps were calculated as previously described[26], with slight
1161   modifications. Briefly, stacks underwent the following processes in MorphoGraphX: Gaussian blur
1162   (3 times; X/Y/Z sigma = 1 µm for the first 2 times, and 2 µm for the third time), edge detection
1163   (threshold = 2000-8000 depending on the brightness of the stack, multiplier = 2.0, adapt factor =
1164   0.3, fill value = 30000), marching cube surface (cube size = 8 µm, threshold = 20000), subdivide
1165   mesh, smooth mesh (passes = 5), subdivide mesh, smooth mesh (passes = 5), project mesh
1166   curvature (type = Gaussian, neighborhood = 10 µm, autoscale = no, min curv = -0.0015, max curv
1167   = 0.0015). For ease of visualization, the lookup table "jet" was applied to the mesh.
1168

1169   **Quantification of sepal initiation robustness**
1170   For sepal primordium number, screenshots were taken of stage 3-6 buds of indicated
1171   genotypes, in either ZEN or MorphoGraphX. The number of sepal primordia initiated were
1172   counted from these screenshots.

1173   For variability in sepal primordium positioning, within each bud, an angular distance was
1174   measured between each pair of adjacent sepal primordia (with vertex at the center of the bud),
1175   using ImageJ. Note that the last pair was not measured – the angular distance was calculated as
1176   the sum of all other angular distances subtracted from 360°. A CV value (standard deviation
1177   divided by mean) was calculated from all the measured or calculated angular distances. Buds
1178   with sepal primordia evenly distributed around the bud periphery should have a small CV value,
1179   i.e. all angles are around 90° for four-sepal buds (or 72° for five-sepal buds, etc.). Buds whose
1180   sepal primordia distributed variably or randomly around the bud periphery will have widely varying
1181   angular distances between adjacent sepal primordia, and thus large CV values.

1182   Relative sepal initiation timing was quantified as previously described[26]. Briefly, dissected
1183   inflorescence samples were live-imaged every 6 hours. A Gaussian curvature heatmap was
1184   generated for each sample at each time point and was used to determine the time point at which
1185   a sepal primordium initiates. A sepal primordium is considered initiated at time point Tn if it is
1186   absent at time point T(n-1) but becomes present at time point Tn. Within the same bud, we
1187   counted the number of time points between outer and inner sepal initiation, and between outer
1188   and lateral sepal initiation, and multiplied them by 6 hours to get the relative initiation timing of
1189   these sepals.
1190

1191 **Quantification of fluorescent reporters**

1192   For *TCS::GFP*, *pARF3::N3xGFP*, *pARF5::ER-YFP-HDEL*, *pARF6::N3xGFP*,
1193 *pARF8::N3xGFP*, *pARF10::N3xGFP*, *pUS7Y::mDII-NtdTomato, pUS7Y::DII-N3xVENUS*, and
1194 *UBQ10::mCherry-RCI2A*, total signal (integrated density) was quantified from maximum intensity
1195 projection images using ImageJ[141,142]. Fluorescence intensity was measured in pixel intensity
1196 units (0-255 range). Signal intensity was calculated as total signal divided by area.

1197   For both *TCS::GFP* and *DR5:3xVENUS-N7*, circular histogram analysis was done as
1198 previously described[26]. Briefly, individual buds were cropped out of image stacks, channels were
1199 split using FIJI and saved in TIF format, and TIF stacks were imported into MorphoGraphX. Signal
1200 from outside the buds (e.g. inflorescence meristem, parts of other buds within the same image)
1201 was manually removed using the Voxel Edit function. Buds were positioned so that the incipient
1202 sepal primordia are in the XY plane: the incipient outer sepal is at 45°, the incipient inner sepal
1203 and the inflorescence meristem are at 225°, and the incipient lateral sepals are at 135° and 315°,
1204 respectively. Fluorescence intensity was measured in pixel intensity units (0-255 range). A circular
1205 histogram of bin width 1° centered around the Z axis was exported for each replicate expressing
1206 DR5 and/or TCS. Multiple circular histograms of the same reporter and genotype were pooled
1207 and mean ± SD were plotted.

1208   For GFP signal in plants carrying *pUBQ10::sfGFP-nes-UBQ3ter* and *pARR7::ARR7-*
1209 *linker-llama-ARR7ter* reporters, screenshots were taken in MorphoGraphX as described above.
1210 Screenshots were subtracted of a background determined using blank regions with no tissue, and
1211 brightened to the same level to reveal differences in GFP distribution patterns. A square region
1212 containing 5-10 cells were taken from each screenshot, and GFP intensity (in gray value ranging
1213 from 0 to 255) along a straight line of 239 pixels in length was quantified using ImageJ[141,142]
1214 (Analyze -> Plot profile). For ease of visualization, the curves were smoothed by taking the
1215 average of the gray value of 11 neighboring pixels (including itself) as the value of each pixel.

1216

1217 ***In vitro* drug treatments on inflorescence samples**

1218   For cycloheximide (CHX) treatment, a stock solution of 10 mM CHX was made from
1219 powder (Sigma C1988) in pH 4.0 water. The stock solution was filter-sterilized and stored in -
1220 20°C and replaced every six months to prevent degradation. The stock solution was added to an
1221 autoclaved and cooled (but not solidified) inflorescence culture medium (see above) to a final
1222 concentration of 2 µM. The medium was not pH-buffered. The medium was made at the beginning
1223 of each experiment and was stored at 4°C. After each imaging session (at day 3 and day 6), new
1224 medium was taken out of 4°C, warmed to room temperature, and inflorescence samples were
1225 transferred onto the new medium.

1226   For AZD-8055 treatment, a stock solution of 16 mM AZD-8055 was prepared from powder
1227 (Cayman Chemical 16978) in DMSO within days of use, and stored in -80°C. The stock was serial-
1228 diluted with water to 2 mM, and added to autoclaved and cooled (but not solidified) inflorescence
1229 culture medium (see above) to a final concentration of 2 µM. For the mock medium, DMSO was
1230 added to the inflorescence culture medium to a final concentration of 0.0125% (v/v).

1231   For 6-benzylaminopurine (BAP) treatment, a stock solution of 50 mM BAP was prepared
1232 from powder (Alfa Aesar A14678) in DMSO, and stored in -80°C. The stock was added to an

1233   autoclaved and cooled (but not solidified) inflorescence culture medium (see above) to a final
1234   concentration of 5 µM. For the mock medium, DMSO was added to the inflorescence culture
1235   medium to a final concentration of 0.01% (v/v).

1236   Inflorescences were dissected and inserted into regular inflorescence culture medium
1237   without drugs, and pre-treatment image stacks were captured. Then, they were transferred into
1238   specified treatment or mock media, and imaged at the specified time points.

1239

1240   ***In vivo* Torin2 treatment**

1241   Starting at 14 days after germination, twice each day for 15 days, 2 nmol of Torin2
1242   (Cayman Chemical 14185) in 20 µl of aqueous solution containing 0.5% DMSO and 0.5% Tween-
1243   20 was applied to the center of the rosette using a pipette. For mock, 20 µl aqueous solution
1244   containing 0.5% DMSO and 0.5% Tween-20 was applied. At the end of the 15-day treatment
1245   period, inflorescences were dissected and put in the inflorescence culture medium for imaging.

1246   To prevent Torin2 degradation, throughout the duration of this experiment, the Torin2
1247   stock solution in DMSO was kept in -80°C and replaced each week, and the treatment and mock
1248   solutions were kept in 4°C and replaced each day.

1249

1250   **Imaging of whole plant, whole inflorescence, silique, and mature sepals**

1251   For whole-plant imaging, aerial parts of the plants were removed from the pots, flattened,
1252   put on a dark cloth, and imaged with a cell phone (iPhone 12, iOS 16.2).

1253   For whole-inflorescence imaging, inflorescences consisting of open flowers and unopened
1254   buds were removed from the plant and held with forceps. Images were taken under a Zeiss Stemi
1255   2000-C Stereo Microscope with a cell phone (iPhone 12, iOS 16.2).

1256   For silique imaging, siliques on inflorescences sufficiently distant from the shoot apex that
1257   were developed and started to ripen were picked with forceps, opened with a razor blade, and
1258   imaged under a Zeiss Stemi 2000-C Stereo Microscope with a cell phone (iPhone 12, iOS 16.2).

1259   Mature sepal imaging was done as previously described[26,27]. Briefly, mature sepals from
1260   stage 15 flowers (10th to 25th flower on the inflorescence) were dissected and sandwiched
1261   between two slides to flatten. Images were taken using a Canon Powershot A640 camera
1262   attached to a Zeiss Stemi 2000-C Stereo Microscope. Minor damages were manually fixed, and
1263   undesired objects such as pollen grains were manually removed from these images. Sepals with
1264   major damages were discarded. Then, a contour was extracted from each sepal using custom
1265   python scripts[27]. This gave us measurements such as length, width, area, etc. of each sepal. To
1266   measure between-flower variability of length, within each genotype and for each of outer, inner,
1267   and lateral positions, a CV (standard deviation divided by mean) of all sepals was calculated (for
1268   example, a CV of length of all outer sepals in WT). To determine statistical significance, genotypes
1269   were compared pairwise using permutation tests. To measure within-flower variability of length,
1270   a CV was calculated for all sepals within each flower (for example, a CV of length of outer, inner,
1271   and two lateral sepals in WT bud #10). For accurate calculation of CV, flowers with length data of
1272   at least four sepals were included in the analysis. To determine statistical significance, genotypes
1273   were compared pairwise using Wilcoxon rank sum tests.

1274

Translation and developmental robustness

Cytokinin extraction and measurement

Cytokinin extraction was based on a previously published protocol[144] with modifications. Briefly, five inflorescence samples of induced *ap1 cal 35S::AP1-GR*, and six inflorescence samples of induced *drmy1 ap1 cal 35S::AP1-GR* were collected as described above. Samples were ground in liquid nitrogen and twice extracted in methanol : water : formic acid (15:4:1). 200 pg of BAP per sample was added as an internal control. Extracts were centrifuged at 14,650 rpm in -4°C for 30 min, and supernatant was evaporated of methanol and reconstituted in 1% (v/v) acetic acid. Samples were passed through an Oasis MCX SPE column (Waters 186000252), washed with 1% acetic acid, washed with methanol, and eluted with 0.35 M ammonia in 70% methanol. Eluents were evaporated to complete dryness, reconstituted in 5% acetonitrile, and sent for LC-MS.

LC-MS was done as previously described[145], with modifications. Briefly, 1 µl of each sample was injected into a Thermo Fisher Scientific Vanquish Horizon UHPLC System coupled with a Thermo Q Exactive HF hybrid quadropole-orbitrap high-resolution mass spectrometer equipped with a HESI ion source. Samples were separated on a C18 ODS column (AQUITY UPLC BEH C18, 1.7 µm, 2.1 × 100 mm, Waters), at a flow rate of 0.3 ml/min, with linear gradients of solvent A (0.1% formic acid) and solvent B (0.1% formic acid in methanol) according to the following profile: 0 min, 99.0% A + 1.0% B; 4.0 min, 55.0% A + 45.0% B; 7 min, 30.0% A + 70.0% B; and then with isocratic conditions: 8 min, 1.0% A + 99.0% B; 12 min, 99.0% A + 1.0% B. Cytokinins were detected using the positive ion mode.

For tZ, tZR, iP, iPR, and the internal control BAP, peaks were identified from an external standard mix composed of 0.1 µg/ml each of BAP (Alfa Aesar A14678), tZ (Sigma Z0876), tZR (Sigma Z3541), iP (Cayman Chemical 17906), and iPR (Cayman chemical 20522) in 5% acetonitrile. For cZ and cZR, peaks were identified based on previously reported precursor m/z and retention time[146]. Using Xcalibur (Thermo Scientific), peak area was quantified for each cytokinin in each sample, normalized against the peak area of BAP (internal control) and sample fresh weight, and then normalized against the average abundance of tZ in WT samples.

Software

Image processing was done in ImageJ (version 2.9.0/1.53t, build a33148d777)[141,142] and MorphoGraphX (version 2.0, revision 1-294, CUDA version 11.40)[143].

Data processing was done in RStudio (R version 4.0.5 "Shake and Throw" (2021-03-31))[147]. Graphs were made using the package ggplot2 (version 3.3.3)[148]. Fisher's contingency table tests were done using the function fisher.test in R. Wilcoxon rank sum tests were done using the function wilcox.test in R. Hypergeometric tests were done using the function phyper in R. Data fitting with ANOVA was done using the function aov in R.

Figures were assembled in Adobe Illustrator (version 25.4.1). An RGB color profile "Image P3" was used for all the figures.

1314 **SUPPLEMENTAL INFORMATION TITLES AND LEGENDS**

1315

1316 **Supplemental Figure 1. Evidence that the *drmy1* mutant has ribosomal and translation**
1317 **defects, associated with Figure 1.**

1318 **(A)** The *drmy1* phenotype is reproduced in the *ap1 cal AP1-GR* system (Ler background). Shown
1319 are representative buds of *ap1 cal AP1-GR* (top row) *and drmy1 ap1 cal AP1-GR* (bottom row) at
1320 day 0 (before DEX induction), day 3 (after 3 DEX inductions, when tissue is collected for RNA,
1321 protein, or cytokinin extraction), and day 5 (after 5 DEX inductions). Arrowheads show sepal
1322 primordia that are of variable number, position, and sizes. Asterisks indicate periphery of the floral
1323 meristem that has limited or no sepal outgrowth in *drmy1 ap1 cal AP1-GR* compared with *ap1 cal*
1324 *AP1-GR*. Scale bars, 25 μm.

1325 **(B)** Summary of the inflorescence RNA-seq and proteomics datasets. Shown are numbers of
1326 genes in each category. Down, downregulated in *drmy1*; NS, not significantly changed between
1327 *drmy1* and WT; Up, upregulated in *drmy1*; NA, not available. Note that in the combined dataset
1328 (gene-protein pairs), different genes encoding for the same protein were separately counted, so
1329 were different proteins encoded by the same gene. See also Supplemental Dataset 1.

1330 **(C)** Violin and box plots of log2 fold change in RNA between *drmy1* and WT in induced *ap1 cal*
1331 *AP1-GR* inflorescence, for genes encoding ribosomal components ("Structural constituents of the
1332 ribosome" GO:0003735, and its offspring terms) and all other genes involved in translation
1333 ("Translation" GO:0006412, and its offspring terms). The following genes are labeled on the
1334 graph: *UL4Z* (AT3G09630), log2FC = -0.492; *UL4Y* (AT5G02870), log2FC = -0.509; *UL18Z*
1335 (AT3G25520), log2FC = -0.459. Note that the x-axis was trimmed to (-2,2) for ease of display.

1336 **(D)** Violin and box plots of log2 fold change in protein level between *drmy1* and WT in induced
1337 *ap1 cal AP1-GR* inflorescence, for genes in the same categories as in (C). The following genes
1338 are labeled on the graph: *UL4Z* (AT3G09630), log2FC = 0.352; *UL4Y* (AT5G02870), log2FC =
1339 0.811; *UL18Z* (AT3G25520), log2FC = 0.742.

1340 **(E)** Coherent regulation of gene expression by *drmy1* and AZD-8055. Shown is a contingency
1341 table of genes downregulated (Down), not significantly changed (NS), and upregulated (Up) in
1342 *drmy1* vs WT (columns), and in AZD-8055-treated WT vs mock-treated WT (rows). Bold font
1343 shows the number of genes in each category, and gray font shows the expected number of genes
1344 if there were no correlation between two conditions (calculated as row margin × column margin /
1345 total number of genes). Categories where the number of genes is above expectation are
1346 highlighted blue, and categories where the number of genes is below expectation are highlighted
1347 red. Chi-square test $p < 2.2 \times 10^{-16}$.

1348 **(F)** Gene ontology enrichment of genes coherently downregulated by both *drmy1* and AZD-8055.
1349 Shown are the top 8 terms and their enrichment p-values. A complete list can be found in
1350 Supplementary Dataset 3.

1351 **(G-J)** Fluorescence of a constitutively expressed marker supports the hypothesis that *drmy1* has
1352 reduced translation rate. (G-I) are representative confocal images of *UBQ10::mCherry-RCI2A* in
1353 dissected inflorescences of WT (G), *drmy1* (H), and *ul4y* (I). Numbers show how the signal is
1354 divided based on the stage of floral meristem when quantified (IM+1, inflorescence meristem plus
1355 stage 1; 2, stage 2; 3, stage 3). Scale bars, 25μm. (J) shows quantification of signal intensity (i.e.

1356   integrated density divided by area) in all images divided as in (G-I). Mean $\pm$ SD are shown. Data

1357   was fit using a two-way ANOVA model with genotype and stage as two additive factors. Asterisks

1358   show statistically significant pairwise contrasts between WT and *drmy1* ($p < 2\text{x}10^{-16}$) and between

1359   WT and *ul4y* ($p = 2.1\text{x}10^{-15}$). Sample sizes: WT IM+1, n = 30; *drmy1* IM+1, n = 22; *ul4y* IM+1, n =

1360   18; WT stage 2, n = 99; *drmy1* stage 2, n = 100; *ul4y* stage 2, n = 52; WT stage 3, n = 39; *drmy1*

1361   stage 3, n = 27; *ul4y* stage 3, n = 26.

1362

1363 **Supplemental Figure 2. Ribosomal mutations enhance the *drmy1* phenotype, associated**
1364 **with Figure 2.**
1365 **(A-H)** Examples of stage 5 buds from *drmy1* (A), *drmy1 ul4z* (B-D), *drmy1 ul4y* (E-F), and *drmy1*
1366 *ul18z/+* (G-H). In (B,E,G) sepal primordia within each bud have bigger size differences than typical
1367 *drmy1* single mutant buds; asterisks show giant outer sepal primordia and brackets show bud
1368 peripheral regions with little or no primordium outgrowth. In (C,F,H), arrowheads show 6 sepal
1369 primordia within each bud, which does not occur in *drmy1*. In (D,H), asterisks show the presence
1370 of two outer sepal primordia within a bud, instead of one in *drmy1*. Scale bars, 25µm.
1371 **(I-J)** Quantification of sepal primordium number (I) and positional variability (J), comparing each
1372 of *drmy1 ul4z* (n = 60), *drmy1 ul4y* (n = 61), and *drmy1 ul18z/+* (n = 69) with *drmy1* (n = 67). "ns"
1373 indicates no significant difference in Fisher's contingency table tests (I) and Wilcoxon's rank sum
1374 tests (J) respectively. Data of *drmy1* is reproduced from the same dataset presented in Figure 2.
1375 **(K)** Dissected young silique of *drmy1 ul18z/+* mother plant. Arrowheads point to aborted ovules.
1376 Scale bar, 200 µm.
1377

1378 **Supplemental Figure 3. Sepal primordia in ribosome and TOR mutants catch up in growth**
1379 **to form uniformly sized mature sepals within the bud, associated with Figure 3.**
1380 **(A-F)** Representative inflorescences images (left) of WT (A), *drmy1* (B), *ul4z* (C), *ul4y* (D), *ul18z*
1381 (E), and *lst8-1-1* (F), with boxed regions enlarged (right). Blue arrowheads show sepals of regular
1382 length, and red arrowheads show sepals shorter than others. Note that sepals in *drmy1* were
1383 unable to close due to unequal lengths, while sepals in *ul4z*, *ul4y*, and *ul18z*, and close like in
1384 WT. Sepals in *lst8-1-1* were unable to close although there is no apparent variation in length.
1385 Scale bars, 0.5 mm.
1386 **(G-L)** Dissected sepals from a representative bud of WT (G), *drmy1* (H), *ul4z* (I), *ul4y* (J), *ul18z*
1387 (K), and two buds of *lst8-1-1* (L). Note that sepals in the *drmy1* bud are of different sizes. Sepals
1388 within each bud of *ul4z*, *ul4y*, *ul18z*, and *lst8-1-1* are of similar sizes, although there can be
1389 variation between different buds of the same genotype. O, outer sepal. I, inner sepal. L, lateral
1390 sepal. Scale bars, 200 μm.
1391 **(M)** Quantification of between-flower variability of sepal length. Length was measured from all
1392 imaged outer sepals of each genotype, and coefficient of variation (CV) was calculated. A two-
1393 sided permutation test (100,000 permutations) for CV difference not equating to zero was done
1394 for each pair of genotypes, and results were represented by letters (left). Similar analysis was
1395 done for the inner sepal (middle), and the lateral sepal (right). Sample size: Outer sepal, WT n =
1396 35, *drmy1* n = 43, *ul4z* n = 37, *ul4y* n = 42, *ul18z* n = 39, *lst8-1-1* n = 43. Inner sepal, WT n = 34,
1397 *drmy1* n = 46, *ul4z* n = 38, *ul4y* n = 44, *ul18z* n = 37, *lst8-1-1* n = 44. Lateral sepal, WT n = 65,
1398 *drmy1* n = 84, *ul4z* n = 81, *ul4y* n = 89, *ul18z* n = 76, *lst8-1-1* n = 82.
1399 **(N)** Quantification of within-flower variability of length. Flowers with length data from at least four
1400 sepals were analyzed. A CV of length from all sepals within each flower was calculated, and mean
1401 ± SD was plotted, grouped by genotype. A Wilcoxon rank sum test was done for each pair of
1402 genotypes, and results were represented by letters. Sample size: WT n = 31 buds, *drmy1* n = 38
1403 buds, *ul4z* n = 33 buds, *ul4y* n = 36 buds, *ul18z* n = 32 buds, *lst8-1-1* n = 39 buds.
1404 **(O-Q)** Live imaging of sepal development from stage 3 to 6 in a bud each of WT, *drmy1*, and *ul4y*,
1405 showing chlorophyll or propidium iodide channel, and Gaussian curvature calculated from the
1406 surface. Note that both *drmy1* and *ul4y* have inner sepals that initiate late (day 2, asterisk). The
1407 *drmy1* inner sepal develops slowly, and leaves the bud open at day 3 (red arrowhead). The *ul4y*
1408 inner sepal catches up with the rest of the sepals and closes the bud (blue arrowhead). Scale
1409 bars, 25 μm.
1410

1411 **Supplemental Figure 4. Inhibition of TOR activity and translation causes auxin maxima**
1412 **formation at variable positions, correlated with variable positions of sepal primordia,**
1413 **associated with Figure 4.**
1414 **(A-E)** Variable patterning of auxin signaling in *drmy1*, *ul4y*, and CHX-treated WT buds
1415 corresponds to variable sepal initiation. Shown are a representative bud each of the labeled
1416 genotype or treatment live-imaged over three or four days. In all but the last time point, in the top
1417 row is *DR5::3xVENUS-N7* (yellow), in the middle row is a composite of *DR5::3xVENUS-N7*
1418 (yellow) and Chlorophyll (magenta), and in the bottom row is Gaussian curvature calculated from
1419 a surface extracted from the Chlorophyll channel. In the last time point, propidium iodide is shown
1420 on the top, and Gaussian curvature calculated from a surface extracted from the propidium iodide
1421 channel is shown on the bottom. (A) In WT, four robustly positioned auxin maxima at day 1
1422 correlates with four robustly positioned sepal primordia at day 4 (blue arrowheads). (B) In *drmy1*,
1423 at day 1 there are three robustly positioned auxin maxima (blue arrowheads). At day 2, a diffuse
1424 band of auxin signaling occurs in the adaxial periphery of the bud, joining with one of the lateral
1425 auxin maxima (red bracket). At day 3, this diffuse band splits into three auxin maxima (red
1426 arrowheads), making a total of 5. The maxima correlate with the five sepal primordia at day 4,
1427 three at robust positions (blue arrowheads) and two at irregular positions (red arrowheads). (C)
1428 In *ul4y*, at day 1 there are two auxin maxima at robust positions (blue arrowheads), one at robust
1429 lateral position but much weaker (red arrowhead), and a band of weak auxin signaling in the
1430 adaxial periphery of the bud (red bracket). At day 2, the weak auxin maxima at lateral position got
1431 stronger, and the weak band split into two auxin maxima on the adaxial side (red arrowheads).
1432 These five auxin maxima correspond to the five sepal primordia at day 3, three in robust positions
1433 (blue arrowheads) and two in irregular positions (red arrowheads). (D) In the WT bud treated with
1434 Mock, four robust auxin maxima at day 6 of the treatment corresponds to four robust sepal
1435 primordia seen at day 9 (blue arrowheads). (E) In the WT bud treated with CHX, at day 6 there
1436 are three stronger auxin maxima (blue arrowheads) and two weaker ones (red arrowheads),
1437 corresponding to three bigger primordium outgrowth regions (blue arrowheads) and two smaller
1438 ones (red arrowheads) at day 9. For ease of display, the DR5 channel in CHX-treated WT was
1439 brightened three times relative to mock. Scale bars, 25 µm.
1440 **(F-I)** TOR inhibition using Torin2 causes increased cytokinin signaling, and occasional variability
1441 in both auxin and cytokinin signaling. (F) Representative images of late stage 2 buds from WT
1442 plants treated with mock or 2 nmol Torin2 for 15 days. Shown are *DR5::3xVENUS-N7* in yellow,
1443 *TCS::GFP* in cyan, and both merged with propidium iodide in magenta. Note that 3/16 (19%) buds
1444 had variable number and position of DR5 and TCS maxima, and 13/16 (81%) had robust DR5
1445 and TCS maxima, although TCS intensity is higher in both cases compared with mock-treated
1446 buds. Scale bars, 25 µm. (G) Quantification of TCS intensity from maximum intensity projection
1447 images, normalized to the mean of WT mock. Shown are mean ± SD. Asterisk shows statistical
1448 significance in a two-tailed Student's t-test compared with WT mock ($p = 1.2 \times 10^{-4}$). (H) Circular
1449 histograms of DR5 distribution around the bud (mean ± SD). (I) Circular histograms of TCS
1450 distribution around the bud (mean ± SD). For calculation of circular histograms, please see Figure
1451 4 legends and Materials and Methods. Sample size: WT mock, n = 11 buds; WT Torin2, n = 16
1452 buds.

Supplemental Figure 5. Translation of uORF-containing ARFs is not universally downregulated in *drmy1*, associated with Figure 5.

(A) *drmy1* has a lower protein-transcript ratio than WT for genes with at least 2 uORFs. 5,086 transcript-protein pairs in our dataset were grouped according to the maximum number of uORFs in all transcript isoforms (0, n = 3,485; 1, n = 874; ≥ 2, n = 724)[62]. For each pair, protein-transcript ratio was calculated, log-transformed, and the difference between *drmy1* and WT was plotted. A negative value means this gene has less protein per transcript in *drmy1* than WT, and could indicate reduced translation or protein stability. Medians for each group: 0 uORF, -0.00367; 1 uORF, -0.00808; ≥ 2 uORFs, -0.0243. Asterisk show statistically significant difference from Group 0 in a Wilcoxon rank sum test (p = 3.167×10^{-4}), while ns means no significant difference from Group 0 (p = 0.167).

(B-D) There is no universal decrease in the expression of uORF-containing ARF reporters. (B) Transcript level of three activator *ARF*s (*ARF5*, *ARF6*, *ARF8*) and two repressor *ARF*s (*ARF3*, *ARF10*) in RNA-seq (n = 3 per genotype). Note that *ARF3*, *ARF5*, and *ARF6* contain uORFs before the main ORF, and *ARF8* and *ARF10* do not. Asterisks show statistically significant differences between WT and *drmy1*, and ns means no significance difference. p values: *ARF3*, p = 0.583; *ARF5*, p = 0.497; *ARF6*, p = 0.603; *ARF8*, p = 0.058; *ARF10* p = 0.019. (C) Transcriptional reporters for these ARFs (*pARF3::n3xGFP*, *pARF5::erYFP*, *pARF6::n3xGFP*, *pARF8::n3xGFP* and *pARF10::n3xGFP*) were imaged in WT and *drmy1*, and representative late stage 2 buds were shown (cyan, GFP or YFP; magenta, propidium iodide). Note that the *pARF3*, *pARF5*, and *pARF6* reporters contain the same uORFs as the genes, reflecting a combination of transcriptional and uORF regulations. Scale bars, 20 μm. (D) Quantification of GFP intensity. Sample size: *pARF3* WT, n = 22; *pARF3 drmy1*, n = 25; *pARF5* WT, n = 22; *pARF5 drmy1*, n = 22; *pARF6* WT, n = 19; *pARF6 drmy1*, n = 28; *pARF8* WT, n = 25; *pARF8 drmy1*, n = 31; *pARF10* WT, n = 20; *pARF10 drmy1*, n = 29. Asterisks show statistically significant differences between WT and *drmy1* in Wilcoxon rank sum tests, and ns means no significance difference. p values: *pARF3*, p = 0.3797; *pARF5*, p = 6.22×10^{-5}; *pARF6*, p = 2.868×10^{-13}; *pARF8*, p = 0.5127; *pARF10* p = 7.073×10^{-14}.

1482 **Supplemental Figure 6. Cytokinin signaling causes variability in mature sepal number and**
1483 **size in *drmy1*, associated with Figure 5.**
1484 Shown are top-view inflorescence images of WT (A), *arr1,10,12* (B), *wol* (C), *drmy1* (D), *drmy1*
1485 *arr1,10,12* (E), and *drmy1 wol* (F), with boxed areas of individual buds enlarged and shown on
1486 the right. In the enlarged views, blue arrowheads point to sepals of regular size, and red
1487 arrowheads point to sepals that are much smaller. Scale bars, 0.5 mm.
1488

Supplemental Figure 7. ARR7-llama partially restores robustness in mature sepal number and size, associated with Figure 7.

(A) Cytokinin abundance does not significantly change in *drmy1*. Shown is mean ± SD of levels of trans-zeatin (tZ), cis-Zeatin (cZ), N^6-(Δ^2-Isopentenyl)adenine (iP), trans-Zeatin riboside (tZR), cis-Zeatin riboside (cZR), and N^6-(Δ^2-Isopentenyl)adenosine (iPR) quantified by LC-MS in induced WT and *drmy1* inflorescences of *ap1 cal AP1-GR* background. Levels are normalized to the mean tZ level in WT. Sample size: n = 5 for WT; n = 6 for *drmy1*. ns means no significant difference between WT and *drmy1* in a two-sided Wilcoxon rank sum test. P-values: tZ, p = 0.2468; cZ, p = 0.7922; iP, p = 0.2468; tZR, p = 0.1775; cZR, p = 0.6623; iPR, p = 0.6623.

(B) The *ARR7-llama* reporter responds to externally applied cytokinin. Shown are GFP channel images of stage 2 buds from *ARR7-llama GFP-nes* line 7-4 in WT, before (top) or after (bottom) 5 hours of 200 µM BAP treatment. Images are representative of n = 6 buds from line 7-4 and n = 3 buds from line 7-6.

(C) CHX treatment does not change the localization of GFP-nes. Shown are GFP channel images of stage 2 buds from *GFP-nes* in WT, treated with mock (top) or 2 µM CHX (bottom) for 24 hours. Images are representative of n = 10 buds (mock) and n = 9 buds (CHX).

(D) AZD-8055 treatment does not change the localization of GFP-nes. Shown are GFP channel images of stage 2 buds from *GFP-nes* in WT, treated with mock (top) or 2 µM AZD-8055 (bottom) for 72 hours. Images are representative of n = 10 buds (mock) and n = 11 buds (AZD-8055). For (B-D), each image was brightened to reveal patterns of GFP distribution. A square region taken from the image containing 5-10 cells is enlarged and shown on the top right. Within the enlargement, GFP intensity was quantified along the dotted line and plotted on the bottom right. X-axis, pixels (range 0-238). Y-axis, GFP intensity in gray value (smoothened by taking the average intensity of 11-pixel neighborhoods; range 90-175). Scale bars, 25 µm.

(E-H) The ARR7-llama construct partially rescues the mature sepal variability in *drmy1*. Shown are inflorescence images of WT (E), *ARR7-llama GFP-nes* (F), *drmy1* (G), and *drmy1 ARR7-llama GFP-nes* (H). The boxed regions were enlarged and shown on the right of each panel. Note that while *drmy1* buds have normal-sized (blue arrowheads) and smaller (red arrowheads) sepals, some buds in *drmy1 ARR7-llama GFP-nes* have robustly sized sepals (H, middle) while others still show variability (H, right). Scale bars, 0.5 mm.

(I-J) *drmy1* has decreased and disrupted pattern of DII degradation. (I) Representative late stage 2 buds of WT and *drmy1* showing *DII-n3xVENUS* (cyan), *mDII-ntdTomato* (magenta), and merge. For ease of display, the *VENUS* channel was brightened 3 times relative to the *tdTomato* channel. Scale bars, 25 µm. (J) Quantification of VENUS/tdTomato ratio using ImageJ. Note that a universal background of 6 gray value per pixel (determined in blank regions without tissue) were subtracted from each image before quantification. Sample size: WT, n = 8 buds; *drmy1*, n = 19 buds. Asterisk shows statistically significant difference in a Wilcoxon rank sum test (p = 0.01335).

1527 **Supplemental Dataset 1. Inflorescence RNA-seq and proteomics.**

1528

1529 **Supplemental Dataset 2. Unprocessed ribosome profiles.**

1530

1531 **Supplemental Dataset 3. Seedling RNA-seq.**

1532

1533 **Supplemental Dataset 4. Data used in graphs.**

1534

1535 **Supplemental Dataset 5. DNA sequences.**

1536

REFERENCES

1. Kaneko, K. (2007). Evolution of robustness to noise and mutation in gene expression dynamics. PLoS One *2*, e434. 10.1371/journal.pone.0000434.

2. Lachowiec, J., Queitsch, C., and Kliebenstein, D.J. (2016). Molecular mechanisms governing differential robustness of development and environmental responses in plants. Ann. Bot. *117*, 795–809. 10.1093/aob/mcv151.

3. Waddington, C.H. (1942). Canalization of Development and the Inheritance of Acquired Characters. Nature *150*, 563–656.

4. Zabinsky, R.A., Mason, G.A., Queitsch, C., and Jarosz, D.F. (2019). It's not magic – Hsp90 and its effects on genetic and epigenetic variation. Semin. Cell Dev. Biol. *88*, 21–35. 10.1016/j.semcdb.2018.05.015.

5. Twitty, V.C., and Schwind, J.L. (1931). The growth of eyes and limbs transplanted heteroplastically between two species of <i>Amblystoma. J. Exp. Zool. *59*, 61–86. 10.1002/jez.1400590105.

6. Silber, S.J. (1976). Growth of Baby Kidneys Transplanted Into Adults. Arch. Surg. *111*, 75–77. 10.1001/archsurg.1976.01360190077014.

7. Summerbell, D., and Lewis, J.H. (1975). Time, place and positional value in the chick limb bud. J. Embryol. Exp. Morphol. *33*, 621–643. 10.1242/dev.33.3.621.

8. Parker, J., and Struhl, G. (2020). Control of *Drosophila* wing size by morphogen range and hormonal gating. Proc. Natl. Acad. Sci. U. S. A. *117*, 31935–31944. 10.1073/pnas.2018196117.

9. Garelli, A., Gontijo, A.M., Miguela, V., Caparros, E., and Dominguez, M. (2012). Imaginal discs secrete insulin-like peptide 8 to mediate plasticity of growth and maturation. Science *336*, 579–582. 10.1126/science.1216735.

10. Crickmore, M.A., and Mann, R.S. (2006). Hox control of organ size by regulation of morphogen production and mobility. Science *313*, 63–68. 10.1126/science.1128650.

11. Recasens-Alvarez, C., Ferreira, A., and Milán, M. (2017). JAK/STAT controls organ size and fate specification by regulating morphogen production and signalling. Nat. Commun. *8*, 10–12. 10.1038/ncomms13815.

12. Irish, V.F. (2008). The Arabidopsis petal: a model for plant organogenesis. Trends Plant Sci. *13*, 430–436. 10.1016/j.tplants.2008.05.006.

13. Fenster, C.B., Armbruster, W.S., Wilson, P., Dudash, M.R., and Thomson, J.D. (2004). Pollination syndromes and floral specialization. Annu. Rev. Ecol. Evol. Syst. *35*, 375–403. 10.1146/annurev.ecolsys.34.011802.132347.

14. King, S., Beck, F., and Lüttge, U. (2004). On the mystery of the golden angle in phyllotaxis. Plant, Cell Environ. *27*, 685–695. 10.1111/j.1365-3040.2004.01185.x.

15. Smith, R.S., Guyomarc'h, S., Mandel, T., Reinhardt, D., Kuhlemeier, C., and Prusinkiewicz, P. (2006). A plausible model of phyllotaxis. Proc. Natl. Acad. Sci. U. S. A. *103*, 1301–1306. 10.1073/pnas.0510457103.

16. Besnard, F., Refahi, Y., Morin, V., Marteaux, B., Brunoud, G., Chambrier, P., Rozier, F., Mirabet, V., Legrand, J., Lainé, S., et al. (2014). Cytokinin signalling inhibitory fields provide robustness to phyllotaxis. Nature *505*, 417–421. 10.1038/nature12791.

17. Queitsch, C., Sangster, T.A., and Lindquist, S. (2002). Hsp90 as a capacitor of phenotypic variation. Nature *417*, 618–624. 10.1038/nature749.

18. Rutherford, S.L., and Lindquist, S. (1998). Hsp90 as a capacitor for morphological evolution. Nature *396*, 336–342. 10.1038/24550.

19. Lehner, B., Crombie, C., Tischler, J., Fortunato, A., and Fraser, A.G. (2006). Systematic mapping of genetic interactions in *Caenorhabditis elegans* identifies common modifiers of diverse signaling pathways. Nat. Genet. *38*, 896–903. 10.1038/ng1844.

20. Levy, S.F., and Siegal, M.L. (2008). Network hubs buffer environmental variation in

1587		*Saccharomyces cerevisiae*. PLoS Biol. *6*, 2588–2604. 10.1371/journal.pbio.0060264.
1588	21.	Folta, A., Severing, E.I., Krauskopf, J., van de Geest, H., Verver, J., Nap, J.P., and
1589		Mlynarova, L. (2014). Over-expression of Arabidopsis AtCHR23 chromatin remodeling
1590		ATPase results in increased variability of growth and gene expression. BMC Plant Biol.
1591		*14*, 76. 10.1186/1471-2229-14-76.
1592	22.	Marygold, S.J., Roote, J., Reuter, G., Lambertsson, A., Ashburner, M., Millburn, G.H.,
1593		Harrison, P.M., Yu, Z., Kenmochi, N., Kaufman, T.C., et al. (2007). The ribosomal protein
1594		genes and Minute loci of *Drosophila melanogaster*. Genome Biol. *8*, R216. 10.1186/gb-
1595		2007-8-10-r216.
1596	23.	Hintze, M., Katsanos, D., Shahrezaei, V., and Barkoulas, M. (2021). Phenotypic
1597		Robustness of Epidermal Stem Cell Number in C. elegans Is Modulated by the Activity of
1598		the Conserved N-acetyltransferase nath-10/NAT10. Front. Cell Dev. Biol. *9*, 640856.
1599		10.3389/fcell.2021.640856.
1600	24.	Wang, S., Kurepa, J., and Smalle, J.A. (2009). The *Arabidopsis* 26S proteasome subunit
1601		RPN1a is required for optimal plant growth and stress responses. Plant Cell Physiol. *50*,
1602		1721–1725. 10.1093/pcp/pcp105.
1603	25.	Gallois, J.L., Guyon-Debast, A., Lecureuil, A., Vezon, D., Carpentier, V., Bonhomme, S.,
1604		and Guerche, P. (2009). The *Arabidopsis* proteasome RPT5 subunits are essential for
1605		gametophyte development and show accession-dependent redundancy. Plant Cell *21*,
1606		442–459. 10.1105/tpc.108.062372.
1607	26.	Zhu, M., Chen, W., Mirabet, V., Hong, L., Bovio, S., Strauss, S., Schwarz, E.M.,
1608		Tsugawa, S., Wang, Z., Smith, R.S., et al. (2020). Robust organ size requires robust
1609		timing of initiation orchestrated by focused auxin and cytokinin signalling. Nat. Plants *6*,
1610		686–698. 10.1038/s41477-020-0666-7.
1611	27.	Hong, L., Dumond, M., Tsugawa, S., Sapala, A., Routier-Kierzkowska, A.L., Zhou, Y.,
1612		Chen, C., Kiss, A., Zhu, M., Hamant, O., et al. (2016). Variable Cell Growth Yields
1613		Reproducible Organ Development through Spatiotemporal Averaging. Dev. Cell *38*, 15–
1614		32. 10.1016/j.devcel.2016.06.016.
1615	28.	Roeder, A.H.K. (2021). Arabidopsis sepals: A model system for the emergent process of
1616		morphogenesis. Quant. Plant Biol. *2*. 10.1017/qpb.2021.12.
1617	29.	Trinh, D.-C., Martin, M., Bald, L., Maizel, A., Trehin, C., and Hamant, O. (2022). Paf1C
1618		denoises transcription and growth patterns to achieve organ shape reproducibility.
1619		bioRxiv, 2022.03.25.485770.
1620	30.	Jing, H., and Strader, L.C. (2019). Interplay of auxin and cytokinin in lateral root
1621		development. Int. J. Mol. Sci. *20*, 486. 10.3390/ijms20030486.
1622	31.	Hussain, S., Nanda, S., Zhang, J., Rehmani, M.I.A., Suleman, M., Li, G., and Hou, H.
1623		(2021). Auxin and Cytokinin Interplay during Leaf Morphogenesis and Phyllotaxy. Plants
1624		*10*, 1732. 10.3390/plants10081732.
1625	32.	Schaller, G.E., Bishopp, A., and Kieber, J.J. (2015). The yin-yang of hormones: Cytokinin
1626		and auxin interactions in plant development. Plant Cell *27*, 44–63.
1627		10.1105/tpc.114.133595.
1628	33.	Ingargiola, C., Duarte, G.T., Robaglia, C., Leprince, A.S., and Meyer, C. (2020). The plant
1629		target of rapamycin: A conduc TOR of nutrition and metabolism in photosynthetic
1630		organisms. Genes (Basel). *11*, 1285. 10.3390/genes11111285.
1631	34.	Scarpin, M.R., Leiboff, S., and Brunkard, J.O. (2020). Parallel global profiling of plant tor
1632		dynamics reveals a conserved role for LARP1 in translation. eLife *9*, e58795.
1633		10.7554/eLife.58795.
1634	35.	Yu, H., Ito, T., Wellmer, F., and Meyerowitz, E.M. (2004). Repression of AGAMOUS-LIKE
1635		24 is a crucial step in promoting flower development. Nat. Genet. *36*, 157–161.
1636		10.1038/ng1286.
1637	36.	Wellmer, F., Alves-Ferreira, M., Dubois, A., Riechmann, J.L., and Meyerowitz, E.M.

45

1638   (2006). Genome-wide analysis of gene expression during early *Arabidopsis* flower
1639   development. PLoS Genet. *2*, 1012–1024. 10.1371/journal.pgen.0020117.
1640   37.   Smyth, D.R., Bowman, J.L., and Meyerowitz, E.M. (1990). Early flower development in
1641   Arabidopsis. Plant Cell *2*, 755–767. 10.1105/tpc.2.8.755.
1642   38.   Goodman, C.A., and Hornberger, T.A. (2013). Measuring protein synthesis with SUnSET:
1643   A valid alternative to traditional techniques? Exerc. Sport Sci. Rev. *41*, 107–115.
1644   10.1097/JES.0b013e3182798a95.
1645   39.   Van Hoewyk, D. (2016). Use of the non-radioactive SUnSET method to detect decreased
1646   protein synthesis in proteasome inhibited Arabidopsis roots. Plant Methods *12*, 20.
1647   10.1186/S13007-016-0120-Z.
1648   40.   Scarpin, M.R., Busche, M., Martinez, R.E., Harper, L.C., Reiser, L., Szakonyi, D.,
1649   Merchante, C., Lan, T., Xiong, W., Mo, B., et al. (2023). An updated nomenclature for
1650   plant ribosomal protein genes. Plant Cell *35*, 640–643. 10.1093/plcell/koac333.
1651   41.   Schepetilnikov, M., and Ryabova, L.A. (2018). Recent discoveries on the role of tor
1652   (Target of rapamycin) signaling in translation in plants. Plant Physiol. *176*, 1095–1105.
1653   10.1104/pp.17.01243.
1654   42.   Scarpin, M.R., Simmons, C.H., and Brunkard, J.O. (2022). Translating across kingdoms:
1655   target of rapamycin promotes protein synthesis through conserved and divergent
1656   pathways in plants. J. Exp. Bot. *73*, 7016–7025. 10.1093/jxb/erac267.
1657   43.   Brunkard, J.O. (2020). Exaptive Evolution of Target of Rapamycin Signaling in
1658   Multicellular Eukaryotes. Dev. Cell *54*, 142–155. 10.1016/j.devcel.2020.06.022.
1659   44.   Battaglioni, S., Benjamin, D., Wälchli, M., Maier, T., and Hall, M.N. (2022). mTOR
1660   substrate phosphorylation in growth control. Cell *185*, 1814–1836.
1661   10.1016/j.cell.2022.04.013.
1662   45.   Valvezan, A.J., and Manning, B.D. (2019). Molecular logic of mTORC1 signalling as a
1663   metabolic rheostat. Nat. Metab. *1*, 321–333. 10.1038/s42255-019-0038-7.
1664   46.   Xiong, Y., McCormack, M., Li, L., Hall, Q., Xiang, C., and Sheen, J. (2013). Glucose-TOR
1665   signalling reprograms the transcriptome and activates meristems. Nature *496*, 181–186.
1666   10.1038/nature12030.
1667   47.   Riegler, S., Servi, L., Scarpin, M.R., Godoy Herz, M.A., Kubaczka, M.G., Venhuizen, P.,
1668   Meyer, C., Brunkard, J.O., Kalyna, M., Barta, A., et al. (2021). Light regulates alternative
1669   splicing outcomes via the TOR kinase pathway. Cell Rep. *36*, 109676.
1670   10.1016/j.celrep.2021.109676.
1671   48.   Obomighie, I., Lapenas, K., Murphy, B.E., Bowles, A.M.C., Bechtold, U., and Prischi, F.
1672   (2021). The Role of Ribosomal Protein S6 Kinases in Plant Homeostasis. Front. Mol.
1673   Biosci. *8*, 636560. 10.3389/fmolb.2021.636560.
1674   49.   Xiong, Y., and Sheen, J. (2012). Rapamycin and glucose-target of rapamycin (TOR)
1675   protein signaling in plants. J. Biol. Chem. *287*, 2836–2842. 10.1074/jbc.M111.300749.
1676   50.   Moreau, M., Azzopardi, M., Clé ment, G., Dobrenel, T., Marchive, C., Renne, C., Martin-
1677   Magniette, M.L., Taconnat, L., Renou, J.P., Robaglia, C., et al. (2012). Mutations in the
1678   *Arabidopsis* homolog of LST8/GβL, a partner of the target of Rapamycin kinase, impair
1679   plant growth, flowering, and metabolic adaptation to long days. Plant Cell *24*, 463–481.
1680   10.1105/tpc.111.091306.
1681   51.   Brunkard, J.O., Xu, M., Regina Scarpin, M., Chatterjee, S., Shemyakina, E.A., Goodman,
1682   H.M., and Zambryski, P. (2020). TOR dynamically regulates plant cell-cell transport. Proc.
1683   Natl. Acad. Sci. U. S. A. *117*, 5049–5058. 10.1073/pnas.1919196117.
1684   52.   Menand, B., Desnos, T., Nussaume, L., Bergert, F., Bouchez, D., Meyer, C., and
1685   Robaglia, C. (2002). Expression and disruption of the *Arabidopsis TOR* (target of
1686   rapamycin) gene. Proc. Natl. Acad. Sci. U. S. A. *99*, 6422–6427.
1687   10.1073/pnas.092141899.
1688   53.   Zhao, Z., Andersen, S.U., Ljung, K., Dolezal, K., Miotk, A., Schultheiss, S.J., and

Lohmann, J.U. (2010). Hormonal control of the shoot stem-cell niche. Nature *465*, 1089–1092. 10.1038/nature09126.

54. Yoshida, S., Mandel, T., and Kuhlemeier, C. (2011). Stem cell activation by light guides plant organogenesis. Genes Dev. *25*, 1439–1450. 10.1101/gad.631211.

55. Du, F., Guan, C., and Jiao, Y. (2018). Molecular Mechanisms of Leaf Morphogenesis. Mol. Plant *11*, 1117–1134. 10.1016/j.molp.2018.06.006.

56. Taylor-Teeples, M., Lanctot, A., and Nemhauser, J.L. (2016). As above, so below: Auxin's role in lateral organ development. Dev. Biol. *419*, 156–164. 10.1016/j.ydbio.2016.03.020.

57. Rosado, A., Li, R., Van De Ven, W., Hsu, E., and Raikhel, N. V. (2012). *Arabidopsis* ribosomal proteins control developmental programs through translational regulation of auxin response factors. Proc. Natl. Acad. Sci. U. S. A. *109*, 19537–19544. 10.1073/pnas.1214774109.

58. Nishimura, T., Wada, T., Yamamoto, K.T., and Okada, K. (2005). The *Arabidopsis* STV1 protein, responsible for translation reinitiation, is required for auxin-mediated gynoecium patterning. Plant Cell *17*, 2940–2953. 10.1105/tpc.105.036533.

59. Zhou, F., Roy, B., and von Arnim, A.G. (2010). Translation reinitiation and development are compromised in similar ways by mutations in translation initiation factor eIF3h and the ribosomal protein RPL24. BMC Plant Biol. *10*, 193. 10.1186/1471-2229-10-193.

60. Cancé, C., Martin-Arevalillo, R., Boubekeur, K., and Dumas, R. (2022). Auxin response factors are keys to the many auxin doors. New Phytol. *235*, 402–419. 10.1111/nph.18159.

61. Kim, B.H., Cai, X., Vaughn, J.N., and Von Arnim, A.G. (2007). On the functions of the h subunit of eukaryotic initiation factor 3 in late stages of translation initiation. Genome Biol. *8*, R60. 10.1186/gb-2007-8-4-r60.

62. Von Arnim, A.G., Jia, Q., and Vaughn, J.N. (2014). Regulation of plant translation by upstream open reading frames. Plant Sci. *214*, 1–12. 10.1016/j.plantsci.2013.09.006.

63. Jones, B., Ljung, K., Gunnerås, S.A., Petersson, S. V., Tarkowski, P., Graham, N., May, S., Dolezal, K., and Sandberg, G. (2010). Cytokinin regulation of auxin synthesis in Arabidopsis involves a homeostatic feedback loop regulated via auxin and cytokinin signal transduction. Plant Cell *22*, 2956–2969. 10.1105/tpc.110.074856.

64. Marhavý, P., Duclercq, J., Weller, B., Feraru, E., Bielach, A., Offringa, R., Friml, J., Schwechheimer, C., Murphy, A., and Benková, E. (2014). Cytokinin controls polarity of PIN1-dependent Auxin transport during lateral root organogenesis. Curr. Biol. *24*, 1031–1037. 10.1016/j.cub.2014.04.002.

65. Růžička, K., Šimášková, M., Duclercq, J., Petrášek, J., Zažímalová, E., Simon, S., Friml, J., Van Montagu, M.C.E., and Benková, E. (2009). Cytokinin regulates root meristem activity via modulation of the polar auxin transport. Proc. Natl. Acad. Sci. U. S. A. *106*, 4284–4289. 10.1073/pnas.0900060106.

66. Müller, B., and Sheen, J. (2007). Advances in cytokinin signaling. Science *318*, 68–69. 10.1126/science.1145461.

67. Karunadasa, S.S., Kurepa, J., Shull, T.E., and Smalle, J.A. (2020). Cytokinin-induced protein synthesis suppresses growth and osmotic stress tolerance. New Phytol. *227*, 50–64. 10.1111/nph.16519.

68. Szweykowska, A., Gwoidi, E., and Spychala, M. (1980). The Cytokinin Control of Protein Synthesis in Plants. In Metabolism and Molecular Activities of Cytokinins, J. Guern and C. Peaud-Lenoel, eds. (Springer-Verlag Berlin Heidelberg), pp. 212–217. 10.1007/978-3-642-68035-9.

69. Woźny, A., and Gwóźdź, E.A. (1980). The effect of cytokinin on the polyribosome formation in cucumber cotyledons. Biochem. und Physiol. der Pflanz. *175*, 476–480. 10.1016/s0015-3796(80)80032-1.

70. Klyachko, N.L., Yakovleva, L.A., Shakirova, F.M., and Kulaeva, O.N. (1982). Cell-free translation of polyribosomes from detached pumpkin cotyledons: Effects of starvation and cytokinin. Biol. Plant. *24*, 374–380. 10.1007/BF02909106.

71. Short, K.C., Tepfer, D.A., and Fosket, D.E. (1974). Regulation of polyribosome formation and cell division in cultured soybean cells by cytokinin. J. Cell Sci. *15*, 75–87.

72. Brenner, W.G., and Schmülling, T. (2012). Transcript profiling of cytokinin action in *Arabidopsis* roots and shoots discovers largely similar but also organ-specific responses. BMC Plant Biol. *12*, 112. 10.1186/1471-2229-12-112.

73. Kiba, T., Naitou, T., Koizumi, N., Yamashino, T., Sakakibara, H., and Mizuno, T. (2005). Combinatorial microarray analysis revealing Arabidopsis genes implicated in cytokinin responses through the His→Asp phosphorelay circuitry. Plant Cell Physiol. *46*, 339–355. 10.1093/pcp/pci033.

74. Černý, M., Kuklová, A., Hoehenwarter, W., Fragner, L., Novák, O., Rotková, G., Jedelský, P.L., Žáková, K., Šmehilová, M., Strnad, M., et al. (2013). Proteome and metabolome profiling of cytokinin action in Arabidopsis identifying both distinct and similar responses to cytokinin down- and up-regulation. J. Exp. Bot. *64*, 4193–4206. 10.1093/jxb/ert227.

75. Cerný, M., Dycka, F., Bobál'Ová, J., and Brzobohatý, B. (2011). Early cytokinin response proteins and phosphoproteins of Arabidopsis thaliana identified by proteome and phosphoproteome profiling. J. Exp. Bot. *62*, 921–937. 10.1093/jxb/erq322.

76. Miyawaki, K., Tarkowski, P., Matsumoto-Kitano, M., Kato, T., Sato, S., Tarkowska, D., Tabata, S., Sandberg, G., and Kakimoto, T. (2006). Roles of Arabidopsis ATP/ADP isopentenyltransferases and tRNA isopentenyltransferases in cytokinin biosynthesis. Proc. Natl. Acad. Sci. U. S. A. *103*, 16598–16603. 10.1073/pnas.0603522103.

77. Ren, B., Liang, Y., Deng, Y., Chen, Q., Zhang, J., Yang, X., and Zuo, J. (2009). Genome-wide comparative analysis of type-A Arabidopsis response regulator genes by overexpression studies reveals their diverse roles and regulatory mechanisms in cytokinin signaling. Cell Res. *19*, 1178–1190. 10.1038/cr.2009.88.

78. Ferreira, F.J., and Kieber, J.J. (2005). Cytokinin signaling. Curr. Opin. Plant Biol. *8*, 518–525. 10.1016/j.pbi.2005.07.013.

79. Kakimoto, T. (2003). Perception and Signal Transduction of Cytokinins. Annu. Rev. Plant Biol. *54*, 605–627. 10.1146/annurev.arplant.54.031902.134802.

80. Jain, M., Tyagi, A.K., and Khurana, J.P. (2006). Molecular characterization and differential expression of cytokinin-responsive type-A response regulators in rice (*Oryza sativa*). BMC Plant Biol. *6*, 1. 10.1186/1471-2229-6-1.

81. To, J.P.C., Haberer, G., Ferreira, F.J., Deruère, J., Mason, M.G., Schaller, G.E., Alonso, J.M., Ecker, J.R., and Kieber, J.J. (2004). Type-A Arabidopsis response regulators are partially redundant negative regulators of cytokinin signaling. Plant Cell *16*, 658–671. 10.1105/tpc.018978.

82. Kiba, T., Yamada, H., Sato, S., Kato, T., Tabata, S., Yamashino, T., and Mizuno, T. (2003). The type-A response regulator, ARR15, acts as a negative regulator in the cytokinin-mediated signal transduction in *Arabidopsis thaliana*. Plant Cell Physiol. *44*, 868–874. 10.1093/pcp/pcg108.

83. To, J.P.C., Deruère, J., Maxwell, B.B., Morris, V.F., Hutchison, C.E., Ferreira, F.J., Schaller, G.E., and Kieber, J.J. (2007). Cytokinin regulates type-A Arabidopsis response regulator activity and protein stability via two-component phosphorelay. Plant Cell *19*, 3901–3914. 10.1105/tpc.107.052662.

84. Acheampong, A.K., Shanks, C., Cheng, C.Y., Eric Schaller, G., Dagdas, Y., and Kieber, J.J. (2020). EXO70D isoforms mediate selective autophagic degradation of type-A ARR proteins to regulate cytokinin sensitivity. Proc. Natl. Acad. Sci. U. S. A. *117*, 27034–27043. 10.1073/pnas.2013161117.

85. Bothma, J.P., Norstad, M.R., Alamos, S., and Garcia, H.G. (2018). LlamaTags: A

Versatile Tool to Image Transcription Factor Dynamics in Live Embryos. Cell *173*, 1810–1822.e16. 10.1016/j.cell.2018.03.069.

86. Imamura, A., Yoshino, Y., and Mizuno, T. (2001). Cellular Localization of the Signaling Components of Arabidopsis His-to-Asp Phosphorelay. Biosci. Biotechnol. Biochem. *65*, 2113–2117. 10.1271/bbb.65.2113.

87. Lee, D.J., Kim, S., Ha, Y.M., and Kim, J. (2008). Phosphorylation of Arabidopsis response regulator 7 (ARR7) at the putative phospho-accepting site is required for ARR7 to act as a negative regulator of cytokinin signaling. Planta *227*, 577–587. 10.1007/s00425-007-0640-x.

88. Buechel, S., Leibfried, A., To, J.P.C., Zhao, Z., Andersen, S.U., Kieber, J.J., and Lohmann, J.U. (2010). Role of A-type Arabidopsis Response Regulators in meristem maintenance and regeneration. Eur. J. Cell Biol. *89*, 279–284. 10.1016/j.ejcb.2009.11.016.

89. Xie, M., Chen, H., Huang, L., O'Neil, R.C., Shokhirev, M.N., and Ecker, J.R. (2018). A B-ARR-mediated cytokinin transcriptional network directs hormone cross-regulation and shoot development. Nat. Commun. *9*, 1604. 10.1038/s41467-018-03921-6.

90. Abel, S., Nguyen, M.D., and Theologis, A. (1995). The *PS-IAA4/5-like* Family of Early Auxin-inducible mRNAs in *Arabidopsis thaliana*. J. Mol. Biol. *251*, 533–549. 10.1006/jmbi.1995.0454.

91. Park, J.Y., Kim, H.J., and Kim, J. (2002). Mutation in domain II of IAA1 confers diverse auxin-related phenotypes and represses auxin-activated expression of Aux/IAA genes in steroid regulator-inducible system. Plant J. *32*, 669–683. 10.1046/j.1365-313X.2002.01459.x.

92. Abel, S., Oeller, P.W., and Theologis, A. (1994). Early auxin-induced genes encode short-lived nuclear proteins. Proc. Natl. Acad. Sci. U. S. A. *91*, 326–330. 10.1073/pnas.91.1.326.

93. Zenser, N., Ellsmore, A., Leasure, C., and Callis, J. (2001). Auxin modulates the degradation rate of Aux/IAA proteins. Proc. Natl. Acad. Sci. U. S. A. *98*, 11795–11800. 10.1073/pnas.211312798.

94. Worley, C.K., Zenser, N., Ramos, J., Rouse, D., Leyser, O., Theologis, A., and Callis, J. (2000). Degradation of Aux/IAA proteins is essential for normal auxin signalling. Plant J. *21*, 553–562. 10.1046/j.1365-313X.2000.00703.x.

95. Ramos, J.A., Zenser, N., Leyser, O., and Callis, J. (2001). Rapid degradation of auxin/indoleacetic acid proteins requires conserved amino acids of domain II and is proteasome dependent. Plant Cell *13*, 2349–2360. 10.1105/tpc.13.10.2349.

96. Figueiredo, M.R.A. de, and Strader, L.C. (2022). Intrinsic and extrinsic regulators of Aux/IAA protein degradation dynamics. Trends Biochem. Sci. *47*, 865–874. 10.1016/j.tibs.2022.06.004.

97. Liao, C.Y., Smet, W., Brunoud, G., Yoshida, S., Vernoux, T., and Weijers, D. (2015). Reporters for sensitive and quantitative measurement of auxin response. Nat. Methods *12*, 207–210. 10.1038/nmeth.3279.

98. Mills, E.W., and Green, R. (2017). Ribosomopathies: There's strength in numbers. Science *358*, eaan2755. 10.1126/science.aan2755.

99. Warren, A.J. (2018). Molecular basis of the human ribosomopathy Shwachman-Diamond syndrome. Adv. Biol. Regul. *67*, 109–127. 10.1016/j.jbior.2017.09.002.

100. Hawer, H., Mendelsohn, B.A., Mayer, K., Kung, A., Malhotra, A., Tuupanen, S., Schleit, J., Brinkmann, U., and Schaffrath, R. (2020). Diphthamide-deficiency syndrome: a novel human developmental disorder and ribosomopathy. Eur. J. Hum. Genet. *28*, 1497–1508. 10.1038/s41431-020-0668-y.

101. Armistead, J., Patel, N., Wu, X., Hemming, R., Chowdhury, B., Basra, G.S., Del Bigio, M.R., Ding, H., and Triggs-Raine, B. (2015). Growth arrest in the ribosomopathy, bowen-

conradi syndrome, is due to dramatically reduced cell proliferation and a defect in mitotic progression. Biochim. Biophys. Acta - Mol. Basis Dis. *1852*, 1029–1037. 10.1016/j.bbadis.2015.02.007.

102. Zhou, C., Zang, D., Jin, Y., Wu, H., Liu, Z., Du, J., and Zhang, J. (2011). Mutation in ribosomal protein L21 underlies hereditary hypotrichosis simplex. Hum. Mutat. *32*, 710–714. 10.1002/humu.21503.

103. Dixon, M.J. (1995). Treacher Collins syndrome. J. Med. Genet. *32*, 806–808. 10.1136/jmg.32.10.806.

104. Gazda, H.T., Sheen, M.R., Vlachos, A., Choesmel, V., O'Donohue, M.F., Schneider, H., Darras, N., Hasman, C., Sieff, C.A., Newburger, P.E., et al. (2008). Ribosomal Protein L5 and L11 Mutations Are Associated with Cleft Palate and Abnormal Thumbs in Diamond-Blackfan Anemia Patients. Am. J. Hum. Genet. *83*, 769–780. 10.1016/j.ajhg.2008.11.004.

105. Oliver, E.R., Saunders, T.L., Tarlé, S.A., and Glaser, T. (2004). Ribosomal protein L24 defect in belly spot and tail (*Bst*), a mouse *Minute*. Development *131*, 3907–3920. 10.1242/dev.01268.

106. McGowan, K.A., Li, J.Z., Park, C.Y., Beaudry, V., Tabor, H.K., Sabnis, A.J., Zhang, W., Fuchs, H., De Angelis, M.H., Myers, R.M., et al. (2008). Ribosomal mutations cause p53-mediated dark skin and pleiotropic effects. Nat. Genet. *40*, 963–970. 10.1038/ng.188.

107. Oristian, D.S., Slooíman, L.G., Zhou, X., Wang, L., Farach-Carson, M.C., and Kirn-Safran, C.B. (2009). Ribosomal protein L29/HIP deficiency delays osteogenesis and increases fragility of adult bone in mice. J. Orthop. Res. *27*, 28–35. 10.1002/jor.20706.

108. Uechi, T., Nakajima, Y., Nakao, A., Torihara, H., Chakraborty, A., Inoue, K., and Kenmochi, N. (2006). Ribosomal protein gene knockdown causes developmental defects in zebrafish. PLoS One *1*, e37. 10.1371/journal.pone.0000037.

109. Marygold, S.J., Coelho, C.M.A., and Leevers, S.J. (2005). Genetic analysis of RpL38 and RpL5, two minute genes located in the centric heterochromatin of chromosome 2 of *Drosophila melanogaster*. Genetics *169*, 683–695. 10.1534/genetics.104.034124.

110. Lee, C.C., Tsai, Y.T., Kao, C.W., Lee, L.W., Lai, H.J., Ma, T.H., Chang, Y.S., Yeh, N.H., and Lo, S.J. (2014). Mutation of a Nopp140 gene *dao-5* alters rDNA transcription and increases germ cell apoptosis in *C. elegans*. Cell Death Dis. *5*, e1158. 10.1038/cddis.2014.114.

111. Ito, T., Kim, G.T., and Shinozaki, K. (2000). Disruption of an Arabidopsis cytoplasmic ribosomal protein S13-homologous gene by transposon-mediated mutagenesis causes aberrant growth and development. Plant J. *22*, 257–264. 10.1046/j.1365-313X.2000.00728.x.

112. Horiguchi, G., Mollá-Morales, A., Pérez-Pérez, J.M., Kojima, K., Robles, P., Ponce, M.R., Micol, J.L., and Tsukaya, H. (2011). Differential contributions of ribosomal protein genes to *Arabidopsis thaliana* leaf development. Plant J. *65*, 724–736. 10.1111/j.1365-313X.2010.04457.x.

113. Zhao, H., Lü, S., Li, R., Chen, T., Zhang, H., Cui, P., Ding, F., Liu, P., Wang, G., Xia, Y., et al. (2015). The Arabidopsis gene *DIG6* encodes a large 60S subunit nuclear export GTPase 1 that is involved in ribosome biogenesis and affects multiple auxin-regulated development processes. J. Exp. Bot. *66*, 6863–6875. 10.1093/jxb/erv391.

114. Takagi, M., Absalon, M.J., McLure, K.G., and Kastan, M.B. (2005). Regulation of p53 translation and induction after DNA damage by ribosomal protein L26 and nucleolin. Cell *123*, 49–63. 10.1016/j.cell.2005.07.034.

115. Deisenroth, C., and Zhang, Y. (2010). Ribosome biogenesis surveillance: Probing the ribosomal protein-Mdm2-p53 pathway. Oncogene *29*, 4253–4260. 10.1038/onc.2010.189.

116. Warner, J.R., and McIntosh, K.B. (2009). How Common Are Extraribosomal Functions of Ribosomal Proteins? Mol. Cell *34*, 3–11. 10.1016/j.molcel.2009.03.006.

117. Dutt, S., Narla, A., Lin, K., Mullally, A., Abayasekara, N., Megerdichian, C., Wilson, F.H., Currie, T., Khanna-Gupta, A., Berliner, N., et al. (2011). Haploinsufficiency for ribosomal protein genes causes selective activation of p53 in human erythroid progenitor cells. Blood *117*, 2567–2576. 10.1182/blood-2010-07-295238.

118. Danilova, N., Sakamoto, K.M., and Lin, S. (2008). Ribosomal protein S19 deficiency in zebrafish leads to developmental abnormalities and defective erythropoiesis through activation of p53 protein family. Blood *112*, 5228–5237. 10.1182/blood-2008-01-132290.

119. Girardi, T., Vereecke, S., Sulima, S.O., Khan, Y., Fancello, L., Briggs, J.W., Schwab, C., De Beeck, J.O., Verbeeck, J., Royaert, J., et al. (2018). The T-cell leukemia-associated ribosomal RPL10 R98S mutation enhances JAK-STAT signaling. Leukemia *32*, 809–819. 10.1038/leu.2017.225.

120. Ludwig, L.S., Gazda, H.T., Eng, J.C., Eichhorn, S.W., Thiru, P., Ghazvinian, R., George, T.I., Gotlib, J.R., Beggs, A.H., Sieff, C.A., et al. (2014). Altered translation of GATA1 in Diamond-Blackfan anemia. Nat. Med. *20*, 748–753. 10.1038/nm.3557.

121. Khajuria, R.K., Munschauer, M., Ulirsch, J.C., Fiorini, C., Ludwig, L.S., McFarland, S.K., Abdulhay, N.J., Specht, H., Keshishian, H., Mani, D.R., et al. (2018). Ribosome Levels Selectively Regulate Translation and Lineage Commitment in Human Hematopoiesis. Cell *173*, 90-103.e19. 10.1016/j.cell.2018.02.036.

122. In, K., Zaini, M.A., Müller, C., Warren, A.J., Von Lindern, M., and Calkhoven, C.F. (2016). Shwachman-Bodian-Diamond syndrome (SBDS) protein deficiency impairs translation re-initiation from C/EBPα and C/EBPβ mRNAs. Nucleic Acids Res. *44*, 4134–4146. 10.1093/nar/gkw005.

123. Kondrashov, N., Pusic, A., Stumpf, C.R., Shimizu, K., Hsieh, A.C., Xue, S., Ishijima, J., Shiroishi, T., and Barna, M. (2011). Ribosome-mediated specificity in Hox mRNA translation and vertebrate tissue patterning. Cell *145*, 383–397. 10.1016/j.cell.2011.03.028.

124. Deliu, L.P., Turingan, M., Jadir, D., Lee, B., Ghosh, A., and Grewal, S.S. (2022). Serotonergic neuron ribosomal proteins regulate the neuroendocrine control of Drosophila development. PLoS Genet. *18*, e1010371. 10.1371/journal.pgen.1010371.

125. Adams, K.W., and Cooper, G.M. (2007). Rapid turnover of Mcl-1 couples translation to cell survival and apoptosis. J. Biol. Chem. *282*, 6192–6200. 10.1074/jbc.M610643200.

126. Truckenbrodt, S., Viplav, A., Jähne, S., Vogts, A., Denker, A., Wildhagen, H., Fornasiero, E.F., and Rizzoli, S.O. (2018). Newly produced synaptic vesicle proteins are preferentially used in synaptic transmission. EMBO J. *37*, e98044. 10.15252/embj.201798044.

127. Mähönen, A.P., Bonke, M., Kauppinen, L., Riikonen, M., Benfey, P.N., and Helariutta, Y. (2000). A novel two-component hybrid molecule regulates vascular morphogenesis of the Arabidopsis root. Genes Dev. *14*, 2938–2943. 10.1101/gad.189200.

128. Sotta, N., Shantikumar, L., Sakamoto, T., Matsunaga, S., and Fujiwara, T. (2016). TPR5 is involved in directional cell division and is essential for the maintenance of meristem cell organization in *Arabidopsis thaliana*. J. Exp. Bot. *67*, 2401–2411. 10.1093/jxb/erw043.

129. Heisler, M.G., Ohno, C., Das, P., Sieber, P., Reddy, G. V., Long, J.A., and Meyerowitz, E.M. (2005). Patterns of auxin transport and gene expression during primordium development revealed by live imaging of the Arabidopsis inflorescence meristem. Curr. Biol. *15*, 1899–1911. 10.1016/j.cub.2005.09.052.

130. Müller, B., and Sheen, J. (2008). Cytokinin and auxin interaction in root stem-cell specification during early embryogenesis. Nature *453*, 1094–1097. 10.1038/nature06943.

131. Brackmann, K., Qi, J., Gebert, M., Jouannet, V., Schlamp, T., Grünwald, K., Wallner, E.S., Novikova, D.D., Levitsky, V.G., Agustí, J., et al. (2018). Spatial specificity of auxin responses coordinates wood formation. Nat. Commun. *9*, 875. 10.1038/s41467-018-03256-2.

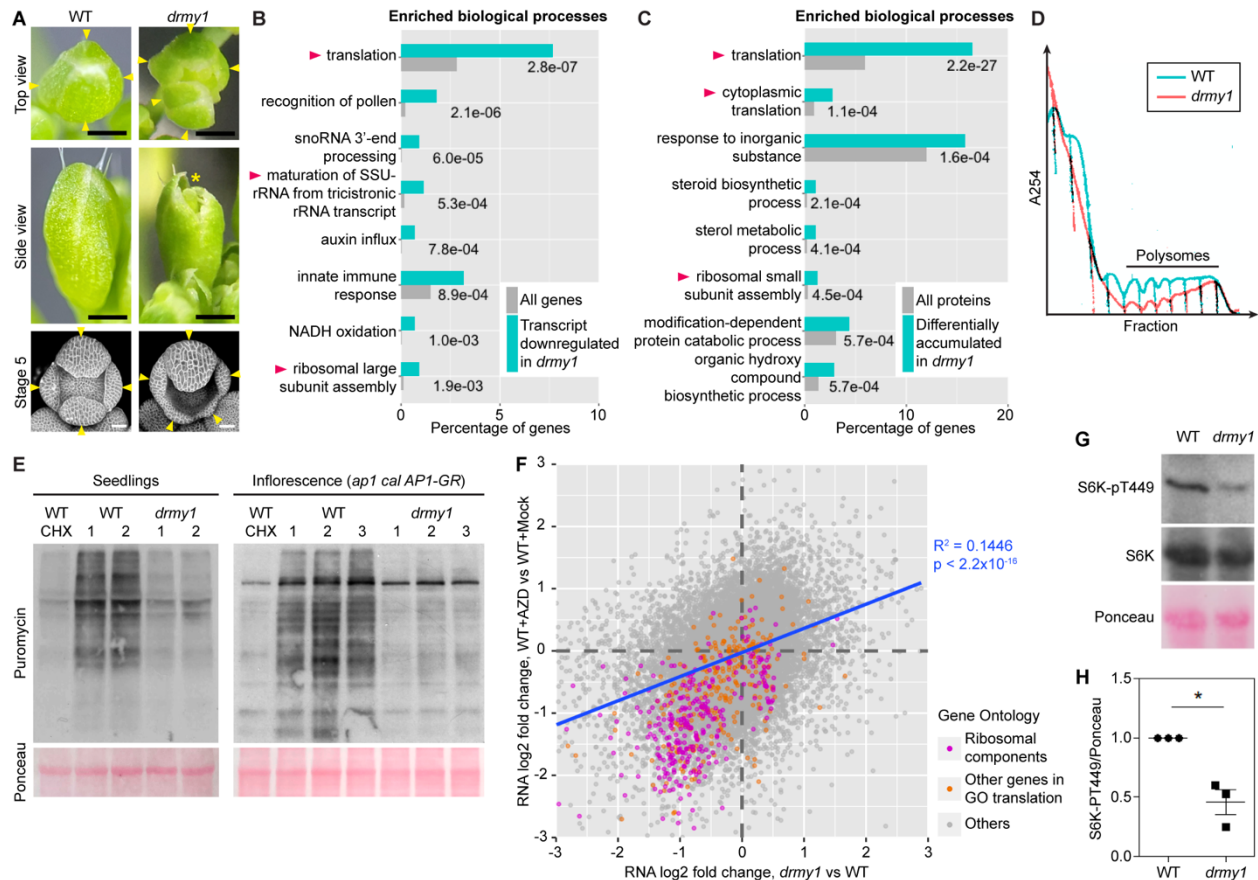132. Argyros, R.D., Mathews, D.E., Chiang, Y.H., Palmer, C.M., Thibault, D.M., Etheridge, N.,

Argyros, D.A., Mason, M.G., Kieber, J.J., and Schallera, G.E. (2008). Type B response regulators of Arabidopsis play key roles in cytokinin signaling and plant development. Plant Cell *20*, 2102–2116. 10.1105/tpc.108.059584.

133. Rademacher, E.H., Möller, B., Lokerse, A.S., Llavata-Peris, C.I., Van Den Berg, W., and Weijers, D. (2011). A cellular expression map of the *Arabidopsis AUXIN RESPONSE FACTOR* gene family. Plant J. *68*, 597–606. 10.1111/j.1365-313X.2011.04710.x.

134. Saerens, D., Pellis, M., Loris, R., Pardon, E., Dumoulin, M., Matagne, A., Wyns, L., Muyldermans, S., and Conrath, K. (2005). Identification of a universal VHH framework to graft non-canonical antigen-binding loops of camel single-domain antibodies. J. Mol. Biol. *352*, 597–607. 10.1016/j.jmb.2005.07.038.

135. Fujii, Y., and Kodama, Y. (2015). *In planta* comparative analysis of improved green fluorescent proteins with reference to fluorescence intensity and bimolecular fluorescence complementation ability. Plant Biotechnol. *32*, 81–87. 10.5511/plantbiotechnology.15.0120a.

136. Alamos, S., Reimer, A., Niyogi, K.K., and Garcia, H.G. (2021). Quantitative imaging of RNA polymerase II activity in plants reveals the single-cell basis of tissue-wide transcriptional dynamics. Nat. Plants *7*, 1037–1049. 10.1038/s41477-021-00976-0.

137. Alexa, A., Rahnenführer, J., and Lengauer, T. (2006). Improved scoring of functional groups from gene expression data by decorrelating GO graph structure. Bioinformatics *22*, 1600–1607. 10.1093/bioinformatics/btl140.

138. Mustroph, A., Juntawong, P., and Bailey-Serres, J. (2009). Isolation of Plant Polysomal mRNA by Differential Centrifugation and Ribosome Immunopurification Methods. In Methods in molecular biology (vol. 553) (Humana Press, a part of Springer Science+Business Media, LLC), pp. 109–126. 10.1007/978-1-60327-563-7_6.

139. Gao, X., Wan, J., Liu, B., Ma, M., Shen, B., and Qian, S.B. (2015). Quantitative profiling of initiating ribosomes *in vivo*. Nat. Methods *12*, 147–153. 10.1038/nmeth.3208.

140. Busche, M., Regina Scarpin, M., Hnasko, R., and Brunkard, J.O. (2021). TOR coordinates nucleotide availability with ribosome biogenesis in plants. Plant Cell *33*, 1615–1632. 10.1093/plcell/koab043.

141. Schindelin, J., Rueden, C.T., Hiner, M.C., and Eliceiri, K.W. (2015). The ImageJ ecosystem: An open platform for biomedical image analysis. Mol. Reprod. Dev. *82*, 518–529. 10.1002/mrd.22489.

142. Schindelin, J., Arganda-Carreras, I., Frise, E., Kaynig, V., Longair, M., Pietzsch, T., Preibisch, S., Rueden, C., Saalfeld, S., Schmid, B., et al. (2012). Fiji: An open-source platform for biological-image analysis. Nat. Methods *9*, 676–682. 10.1038/nmeth.2019.

143. de Reuille, P.B., Routier-Kierzkowska, A.L., Kierzkowski, D., Bassel, G.W., Schüpbach, T., Tauriello, G., Bajpai, N., Strauss, S., Weber, A., Kiss, A., et al. (2015). MorphoGraphX: A platform for quantifying morphogenesis in 4D. eLife *4*, 1–20. 10.7554/eLife.05864.

144. Schäfer, M., Brütting, C., Baldwin, I.T., and Kallenbach, M. (2016). High-throughput quantification of more than 100 primary- and secondary-metabolites, and phytohormones by a single solid-phase extraction based sample preparation with analysis by UHPLC-HESI-MS/MS. Plant Methods *12*, 30. 10.1186/s13007-016-0130-x.

145. Kojima, M., Kamada-Nobusada, T., Komatsu, H., Takei, K., Kuroha, T., Mizutani, M., Ashikari, M., Ueguchi-Tanaka, M., Matsuoka, M., Suzuki, K., et al. (2009). Highly sensitive and high-throughput analysis of plant hormones using ms-probe modification and liquid chromatographytandem mass spectrometry: An application for hormone profiling in oryza sativa. Plant Cell Physiol. *50*, 1201–1214. 10.1093/pcp/pcp057.

146. Novák, O., Antoniadi, I., and Ljung, K. (2017). High-resolution cell-type specific analysis of cytokinins in sorted root cell populations of *Arabidopsis thaliana*. Methods Mol. Biol. *1497*, 231–248. 10.1007/978-1-4939-6469-7_1.

1995   147.   R Core Team (2021). R: A language and environment for statistical computing. R
1996   Foundation for Statistical Computing, Vienna, Austria. URL https://www.R-project.org/.
1997   148.   Wickham, H. (2009). ggplot2: Elegant Graphics for Data Analysis R. Gentleman, K.
1998   Hornik, and G. Parmigiani, eds. (Springer) 10.1007/978-0-387-98141-3.
1999

Translation and developmental robustness

Figure 1. *drmy1* has reduced ribosome abundance, translation rate, and TOR activity.

(A) Top row, stage 12 buds of WT (left) and *drmy1* (right) viewed from the top. Arrowheads point to sepals. Note that the *drmy1* bud has 5 sepals of unequal size and unevenly spaced, exposing the stamens and carpels. Middle row, stage 12 buds of WT (left) and *drmy1* (right) viewed from the side. Asterisk shows the gap between sepals with petals and carpels exposed. Bottom row, stage 5 buds of WT (left) and *drmy1* (right) containing *35S::mCitrine-RCI2A* (plasma membrane marker). Arrowheads point to sepal primordia. Note that the *drmy1* bud has 5 sepal primordia of different sizes. Scale bars are 0.5 mm for stage 12 bud images and 25 μm for stage 5 bud images.

(B-C) Gene ontology (GO) enrichment of downregulated genes **(B)** and differentially accumulated proteins **(C)** in *drmy1* compared to WT, in the *ap1 cal AP1-GR* background. Shown are the top 8 GO terms and their enrichment p-values. A complete list can be found in Supplemental Dataset 1. Arrowheads highlight terms related to ribosome biogenesis or translation.

(D) Ribosome profiles of WT (blue) and *drmy1* (red) in the *ap1 cal AP1-GR* background, representative of 3 biological replicates each. Polysomal peaks are highlighted. All replicates can be found in Supplemental Dataset 2.

(E) Puromycin labeling of WT vs *drmy1*. Left, puromycin labeling in WT and *drmy1* seedlings. From left to right: WT pre-treated with CHX, two biological replicates of WT pre-treated with mock, and two biological replicates of *drmy1* pre-treated with mock. All groups were then treated with puromycin. For seedlings to match in size, WT seedlings were 8 days old and *drmy1* seedlings were 10 days old. Right, puromycin labeling in WT and *drmy1* inflorescences of induced *ap1 cal*
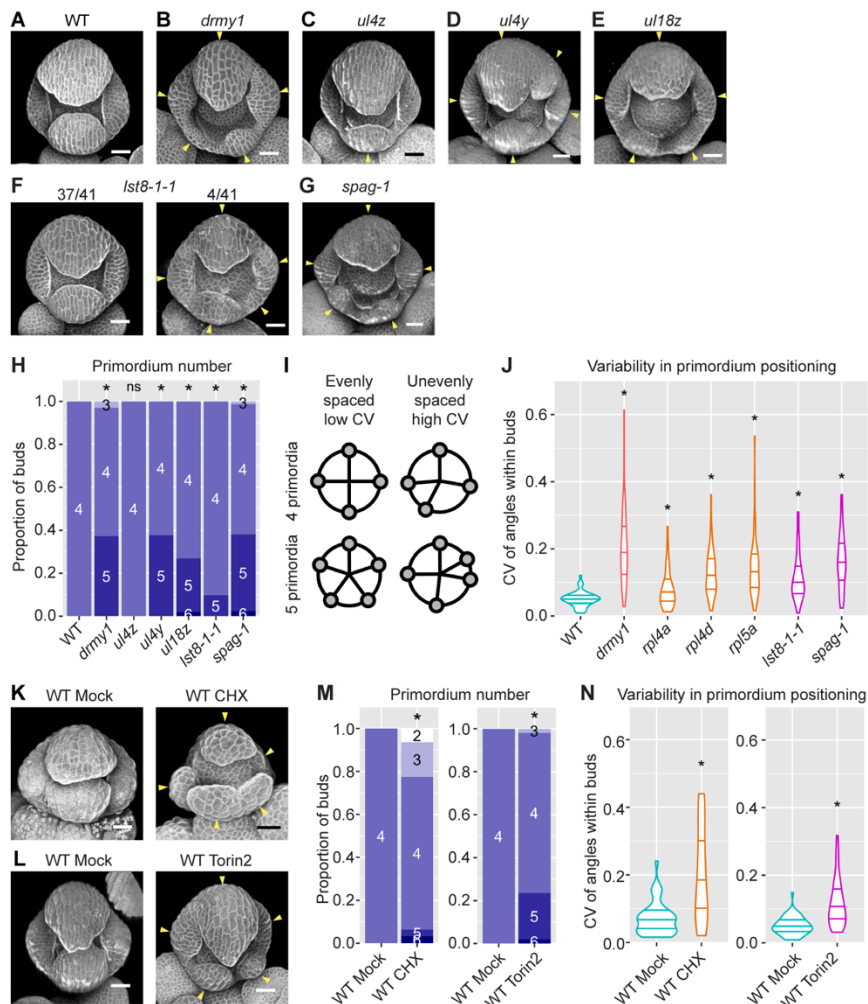
22   *AP1-GR* background. From left to right: WT co-treated with puromycin and CHX, three biological
23   replicates of WT treated with puromycin, and three biological replicates of *drmy1* treated with
24   puromycin. In both experiments, RuBisCO large subunit on Ponceau S-stained membrane is
25   shown as a loading control (bottom).
26   **(F)** Coherent alteration of gene expression by *drmy1* and AZD-8055 TOR inhibitor treatment.
27   Shown here is a scatterplot of RNA log 2 fold change in *drmy1* vs WT (x-axis), and WT+AZD vs
28   WT+Mock (y-axis), in 7-day-old seedlings. Genes are color-coded based on the following
29   categories: genes in "Structural constituents of the ribosome" (GO:0003735) and its offspring
30   terms (magenta); all other genes in "Translation" (GO:0006412) and its offspring terms (orange);
31   all other genes (gray). Blue line shows a linear regression of all points (R^2 = 0.1446, p < 2.2x10^{-16}
32   ). Note that the axes were trimmed to (-3,3) for ease of display.
33   **(G-H)** Phosphorylation of the direct TOR substrate, S6K-pT449, in WT and *drmy1*. Representative
34   images are shown in **(G)**. Top, Western blot against S6K-pT449. Middle, Western blot against
35   total S6K protein. Bottom, Ponceau S staining as a loading control. **(H)** Quantification of the
36   intensity of S6K-pT449 over Ponceau normalized by WT, in three experiments, shows that TOR
37   activity decreased by half in *drmy1*. (mean ± SD; *, p<0.05).
38

Translation and developmental robustness

39

Figure 2. Defects in TOR activity, ribosome integrity, and translation cause variable sepal initiation.

(A-G) Representative images of stage 5 buds in WT (A), *drmy1* (B), *ul4z* (C), *ul4y* (D), *ul18z* (E), *lst8-1-1* (F), and *spaghetti-1* (G). Tissue morphology is visualized by either propidium iodide (a cell wall-staining dye) or a plasma membrane marker. Arrowheads indicate sepal primordia that are variable in number, position, and size. Note that *ul4z* flowers always develop four sepal primordia, although of different sizes; *lst8-1-1* occasionally (4/41, 9.8%) develops buds with more than four sepal primordia. Scale bars, 25 μm.

(H) Quantification of sepal primordium number, comparing *drmy1* (n = 67 buds), *ul4z* (n = 52 buds), *ul4y* (n = 53 buds), *ul18z* (n = 52 buds), *lst8-1-1* (n = 41 buds), and *spaghetti-1* (n = 84 buds) with WT (n = 51 buds). Asterisks indicate statistically significant (p < 0.05) differences from WT in Fisher's contingency table tests.

(I) Illustration of robust versus variable positioning of sepal primordia. Primordia are considered robustly positioned if they are evenly distributed around the edge of the bud. Within each bud, angles between adjacent primordia with respect to the center of the bud are measured, and coefficient of variation (CV) is calculated. A bud with robustly positioned primordia would have

56 similar angular values and a low CV value. A bud with variably positioned primordia would have
57 very different angular values and a high CV value.
58 **(J)** Quantification of variability in primordium positioning (CV) in the same buds as in (H), following
59 illustration in (I). Asterisks indicate statistically significant ($p < 0.05$) differences from WT in
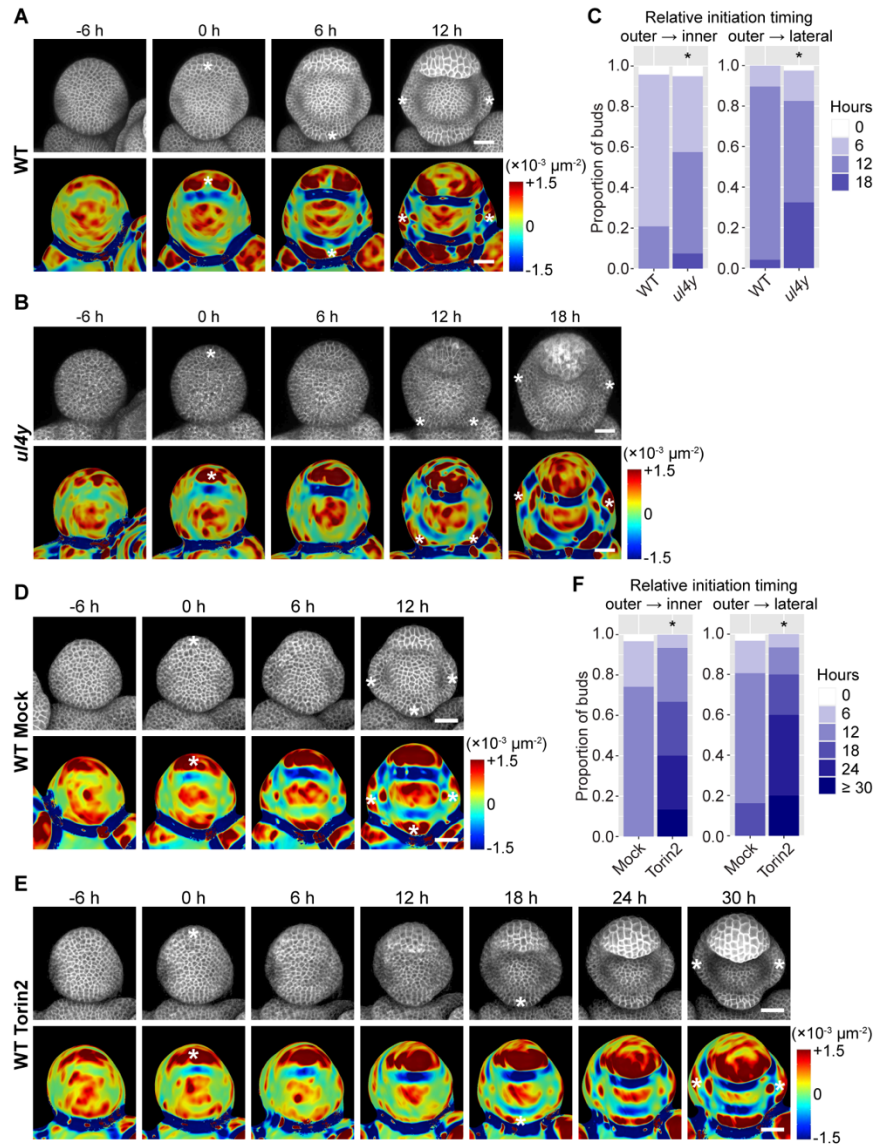60 Wilcoxon's rank sum tests.
61 **(K)** Representative images of buds from *in vitro*-cultured WT inflorescences treated with mock or
62 2 µM CHX for 9-10 days (see Material and Methods). Arrowheads indicate sepal primordia that
63 are variable in number, position, and size. Scale bars, 25 µm.
64 **(L)** Representative images of buds from WT plants treated with mock or 2 nmol Torin2 for 15 days
65 (see Material and Methods). Arrowheads indicate sepal primordia that are variable in number,
66 position, and size. Scale bars, 25 µm.
67 **(M-N)** Quantification of variability in primordium number (M) and positional variability (N) similar
68 to (H,J), comparing CHX-treated (n = 31 buds), CHX-mock (n = 42 buds), Torin2-treated (n = 51
69 buds) and Torin2-mock buds (n = 56 buds).
70

Translation and developmental robustness

Figure 3. TOR and ribosomal defects cause variability in the timing of sepal initiation.
(A-C) 6h-interval live imaging of the sepal initiation process in WT (A) and *ul4y* (B), which is quantified in (C). n = 48 buds for WT; n = 40 buds for *ul4y*.
(D-F) 6h-interval live imaging of the sepal initiation process in buds from WT plants treated with mock or 2 nmol Torin2 bi-daily for 15 days, which is quantified in (F). n = 31 buds for mock; n = 15 buds for Torin2.
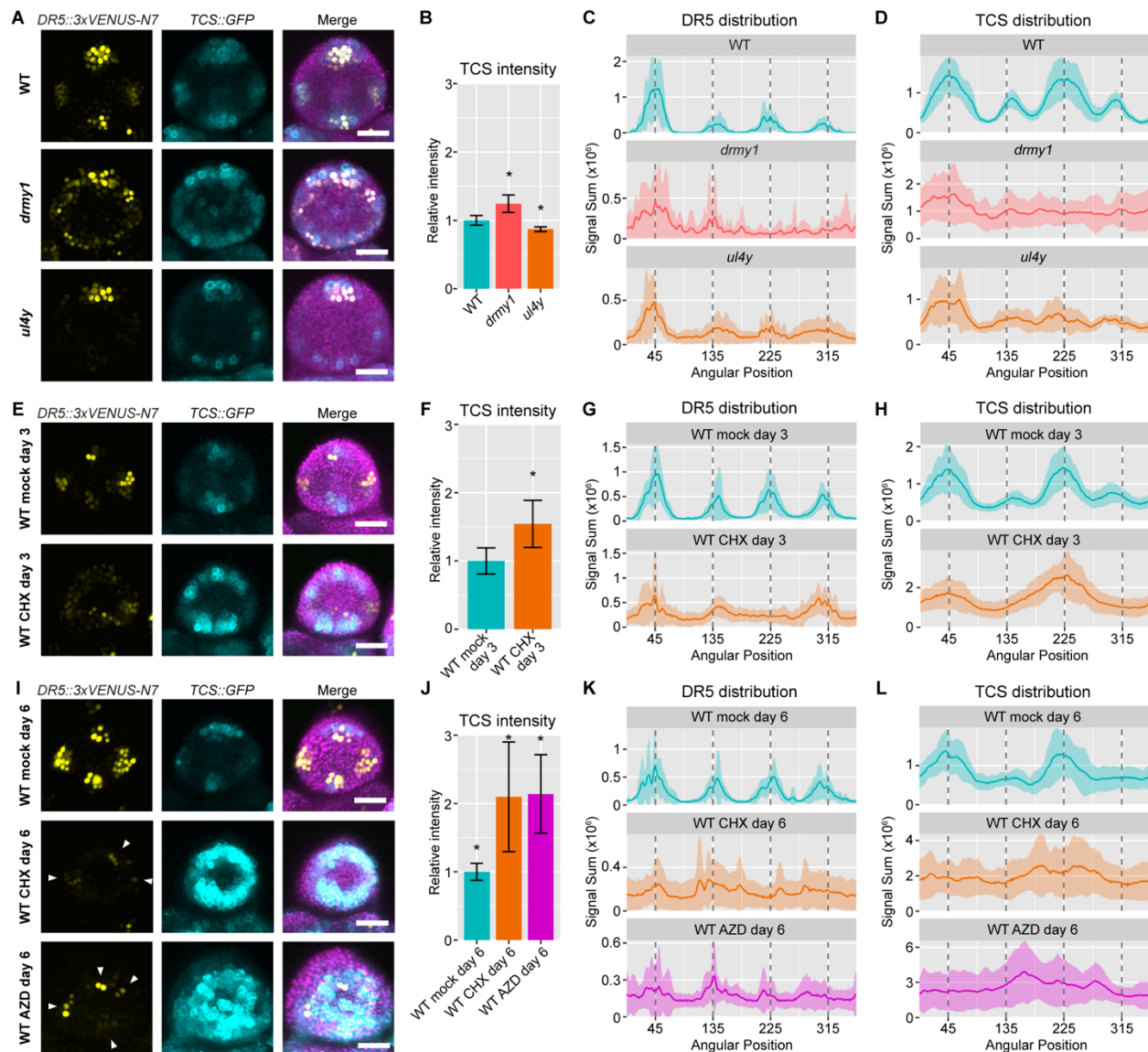In **(A,B,D,E)**, top rows show the *35S::mCitrine-RCI2A* membrane marker, and bottom rows show Gaussian curvature heatmaps calculated from the same image stacks. Asterisks indicate sepal initiation events, defined as a dark red band (primordium with positive curvature) separated from the floral meristem by a dark blue band (boundary with negative curvature) in the Gaussian curvature heatmap. Scale bars, 25 µm.
In **(C,F)**, the amount of time between outer and inner sepal initiation (left) and between outer and lateral sepal initiation (right) were calculated for each bud, and summarized over all the buds.

5

85 Asterisks indicate statistically significant ($p < 0.05$) differences in the distribution of relative
86 initiation timing in Fisher's contingency table tests.
87

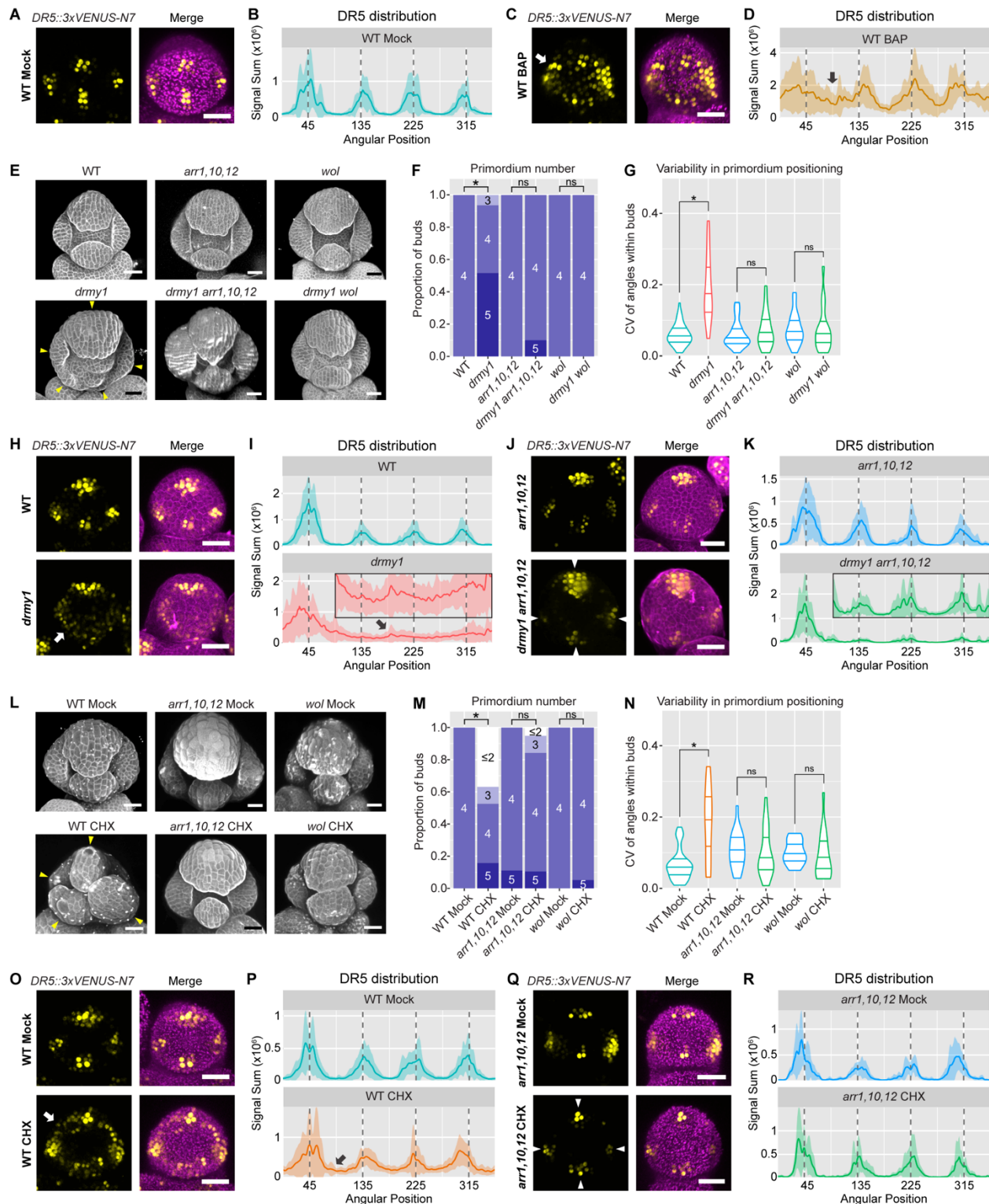Translation and developmental robustness

88

Figure 4. Defects in TOR activity, ribosome integrity, and translation cause variability in auxin and cytokinin signaling.

(A-D) The ribosomal mutant *ul4y* loses robustness in auxin and cytokinin signaling. (A) Representative images of late stage 2 buds of WT, *drmy1*, and *ul4y*, showing the auxin signaling reporter *DR5::3xVENUS-N7* in yellow, the cytokinin signaling reporter *TCS::GFP* in cyan, and both merged with Chlorophyll (in WT) or *UBQ10::mCherry-RCI2A* (in *drmy1* and *ul4y*) in magenta. (B) Quantification of TCS intensity (integrated density divided by area) from maximum intensity projection images, normalized to mean of WT. Shown are mean ± SD. Asterisks show statistically significant differences from WT in two-tailed Student's t-tests (*drmy1*, p = 2.1x10^{-6}; *ul4y*, p = 3.4x10^{-5}). (C) Circular histogram of DR5 distribution around the bud. Each bud was divided into 360 sectors of 1° each. Within each sector, DR5 signal measured in pixel intensity units (0-255 range) was summed. This sum was plotted along the x-axis starting from the sector at 1:30 position (between the incipient outer sepal and incipient lateral sepal on the right) going

7

102 counterclockwise. I.e. in WT, the outer sepal is near 45°, the inner sepal near 225°, and the lateral
103 sepals near 45° and 135° (vertical dotted lines). The mean was plotted as a solid line, and mean
104 ± SD was plotted as a shaded area. (D) Circular histogram of TCS distribution around the bud.
105 Sample size for (A-D): WT, n = 12 buds; *drmy1*, n = 15 buds; *ul4y*, n = 10 buds.
106 **(E-H)** 3 days of translation inhibition causes increased and diffuse cytokinin signaling, and diffuse
107 auxin signaling. (E) Representative images of late stage 2 buds from dissected and cultured WT
108 inflorescences treated with mock or 2 µM CHX for 3 days. Shown are *DR5::3xVENUS-N7* in
109 yellow, *TCS::GFP* in cyan, and both merged with Chlorophyll in magenta. (F) Quantification of
110 TCS intensity from maximum intensity projection images, normalized to mean of WT mock day 3.
111 Shown are mean ± SD. Asterisk shows statistically significant difference in a two-tailed Student's
112 t-test (p = $2.0x10^{-4}$). (G) Circular histogram of DR5 distribution around the bud. (H) Circular
113 histogram of TCS distribution around the bud. Sample size for (E-H): WT mock day 3, n = 10 buds;
114 WT CHX day 3, n = 12 buds.
115 **(I-L)** 6 days of TOR or translation inhibition causes increased and diffuse cytokinin signaling, and
116 randomly positioned auxin signaling maxima. (I) Representative images of late stage 2 buds from
117 dissected and cultured WT inflorescences treated with mock, 2 µM CHX, or 2 µM AZD for 6 days.
118 Shown are *DR5::3xVENUS-N7* in yellow, *TCS::GFP* in cyan, and both merged with Chlorophyll
119 in magenta. Arrowheads point to randomly positioned auxin maxima in buds of the CHX or AZD
120 group. (J) Quantification of TCS intensity from maximum intensity projection images, normalized
121 to mean of WT mock day 6. Shown are mean ± SD. Asterisks show statistically significant
122 differences from mock in two-tailed Student's t-tests (CHX, p = $1.0x10^{-3}$; AZD, p = $1.2x10^{-4}$). (K)
123 Circular histogram of DR5 distribution around the bud. (L) Circular histogram of TCS distribution
124 around the bud. Sample size for (I-L): WT mock day 6, n = 12 buds; WT CHX day 6, n = 11 buds;
125 WT AZD day 6, n = 10 buds. Scale bars in (A,E,I) represent 25 µm.
126

Translation and developmental robustness

Figure 5. Cytokinin signaling is required for variability in auxin signaling and sepal initiation under translation inhibition.

(A-D) Cytokinin treatment makes auxin signaling diffuse. Shown are late stage 2 WT buds under mock (A,B) or 5 µM cytokinin (BAP) treatment (C,D) for 4 days. (A,C) Representative images of

132   the auxin signaling reporter *DR5::3xVENUS-N7* in yellow, and *DR5* merged with Chlorophyll in
133   magenta. (B,D) Circular histograms of the *DR5::3xVENUS-N7* signal, showing mean (solid line)
134   and mean ± SD (shaded area). Arrows point to DR5 signal in variable positions. Sample size: WT
135   Mock n = 10, WT BAP n = 10. Also see Zhu et al. (2020), Extended Data Figure 7e.
136   **(E-G)** Cytokinin signaling is required for variable sepal initiation in *drmy1*. (E) Representative
137   images of stage 5 buds in WT, *drmy1*, *arr1,10,12*, *drmy1 arr1,10,12*, *wol*, and *drmy1 wol*.
138   Arrowheads indicate initiated sepal primordia that are variable in number, position, and size. (F,G)
139   Quantification of sepal primordium number (F) and positional variability (G), comparing WT (n =
140   58) with *drmy1* (n = 31), *arr1,10,12* (n = 24) with *drmy1 arr1,10,12* (n = 20), and *wol* (n = 36) with
141   *drmy1 wol* (n = 39). Asterisks indicate statistically significant (p < 0.05) differences in Fisher's
142   contingency table tests (F) and Wilcoxon's rank sum tests (G) respectively. ns indicates no
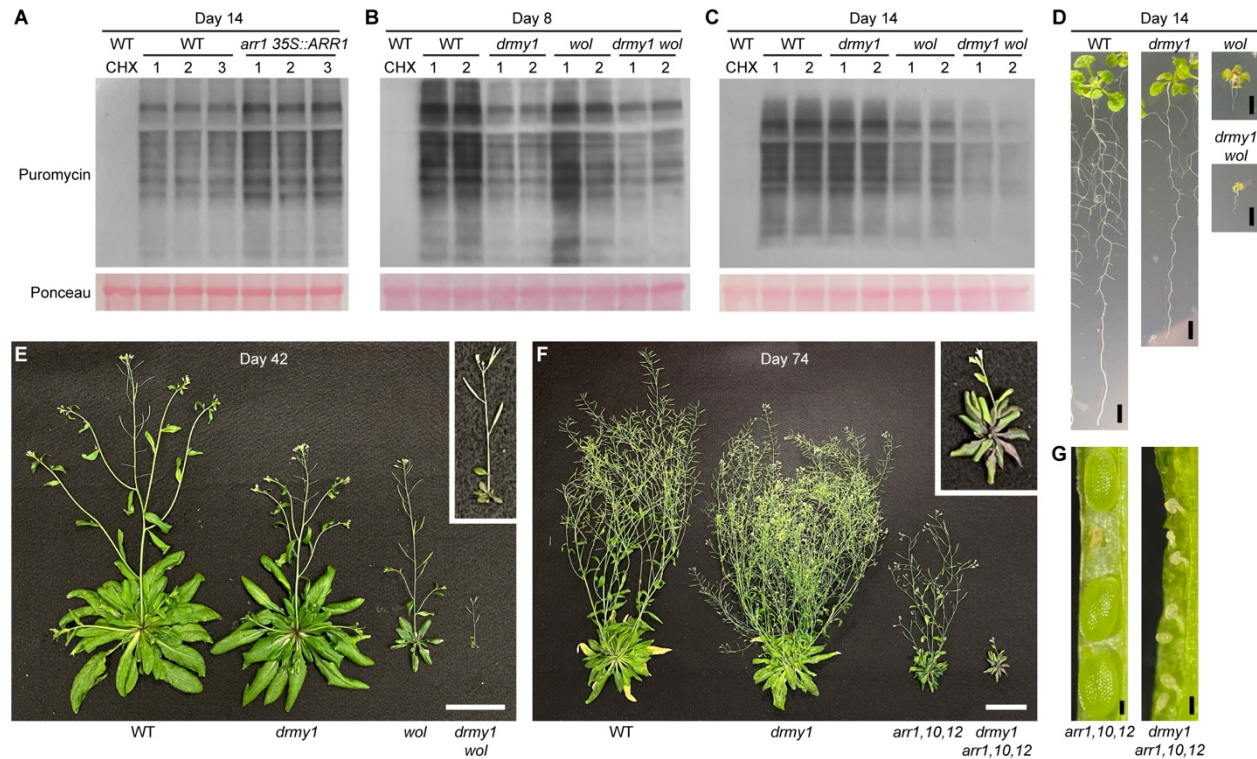143   significant difference.
144   **(H-K)** Cytokinin signaling is required for variable patterning of auxin signaling in *drmy1*. Shown
145   are late stage 2 buds of WT vs *drmy1* (H,I), and *arr1,10,12* vs *drmy1 arr1,10,12* (J,K). (H,J)
146   Representative images of the auxin signaling reporter *DR5::3xVENUS-N7* in yellow, and *DR5*
147   merged with propidium iodide in magenta. Arrows point to diffuse DR5 signal in variable positions
148   in the *drmy1* bud. Arrowheads show four robust DR5 maxima in *drmy1 arr1,10,12*. (I,K) Circular
149   histograms of the *DR5::3xVENUS-N7* signal, showing mean (solid line) and mean ± SD (shaded
150   area). For ease of visualization, circular histograms of *drmy1* and *drmy1 arr1,10,12* between 90
151   and 360 degrees are enlarged and shown as insets (y-axis range 0-0.4). Sample size: WT n = 19,
152   *drmy1* n = 16, *arr1,10,12* n = 13, *drmy1 arr1,10,12* n = 9.
153   **(L-N)** Cytokinin signaling is required for variable sepal initiation under translation inhibition. (L)
154   Representative images of stage 6 buds in WT, *arr1,10,12*, and *wol*, treated with Mock or 2 µM
155   CHX for 10 days. Arrowheads indicate variable initiation of sepal primordia. (M,N) Quantification
156   of sepal primordium number (M) and positional variability (N), comparing Mock and CHX within
157   each genotype. Sample size: WT Mock n = 29, WT CHX n = 19, *arr1,10,12* Mock n = 18,
158   *arr1,10,12* CHX n = 19, *wol* Mock n = 15, *wol* CHX n = 19. Asterisks indicate statistically significant
159   (p < 0.05) differences in Fisher's contingency table tests (M) and Wilcoxon's rank sum tests (N)
160   respectively. ns indicates no significant difference.
161   **(O-R)** Cytokinin signaling is required for diffuse auxin signaling under translation inhibition. Shown
162   are late stage 2 buds of WT (O,P) and *arr1,10,12* (Q,R), treated with Mock or 2 µM CHX for 3
163   days. (O,Q) Representative images of the auxin signaling reporter *DR5::3xVENUS-N7* in yellow,
164   and *DR5* merged with Chlorophyll in magenta. Arrows point to diffuse DR5 signal in variable
165   positions in CHX-treated WT. Arrowheads show four robust DR5 maxima in CHX-treated
166   *arr1,10,12*. (P,R) Circular histograms of the *DR5::3xVENUS-N7* signal, showing mean (solid line)
167   and mean ± SD (shaded area). Sample size: WT Mock n = 17, WT CHX n = 18, *arr1,10,12* Mock
168   n = 7, *arr1,10,12* CHX n = 7. Scale bars in (A,C,E,H,J,L,O,Q) represent 25 µm.
169

Figure 6. Upregulation of cytokinin signaling is required to maintain translation and fitness in *drmy1*.

(A) Puromycin labeling of WT seedlings with 4 h CHX pre-treatment (control), and three biological replicates each of WT and *arr1 35S::ARR1* seedlings with 4 h mock pre-treatment. All seedlings are 14 days old. RuBisCO large subunit in Ponceau S-stained membrane is shown as a loading control. Also see Karunadasa et al. (2020).

(B,C) Puromycin labeling of WT seedlings with 4 h CHX pre-treatment (control), and two biological replicates of WT, *drmy1*, *wol*, and *drmy1 wol* seedlings with 4 h mock pre-treatment. Seedlings are 8 days old in (B) and 14 days old in (C). RuBisCO large subunit in Ponceau S-stained membrane is shown as a loading control.

(D) Representative 14 days old seedling images of WT, *drmy1*, *wol*, and *drmy1 wol* used in (C). Notice that *drmy1 wol* is very small and pale. Scale bars, 5 mm.

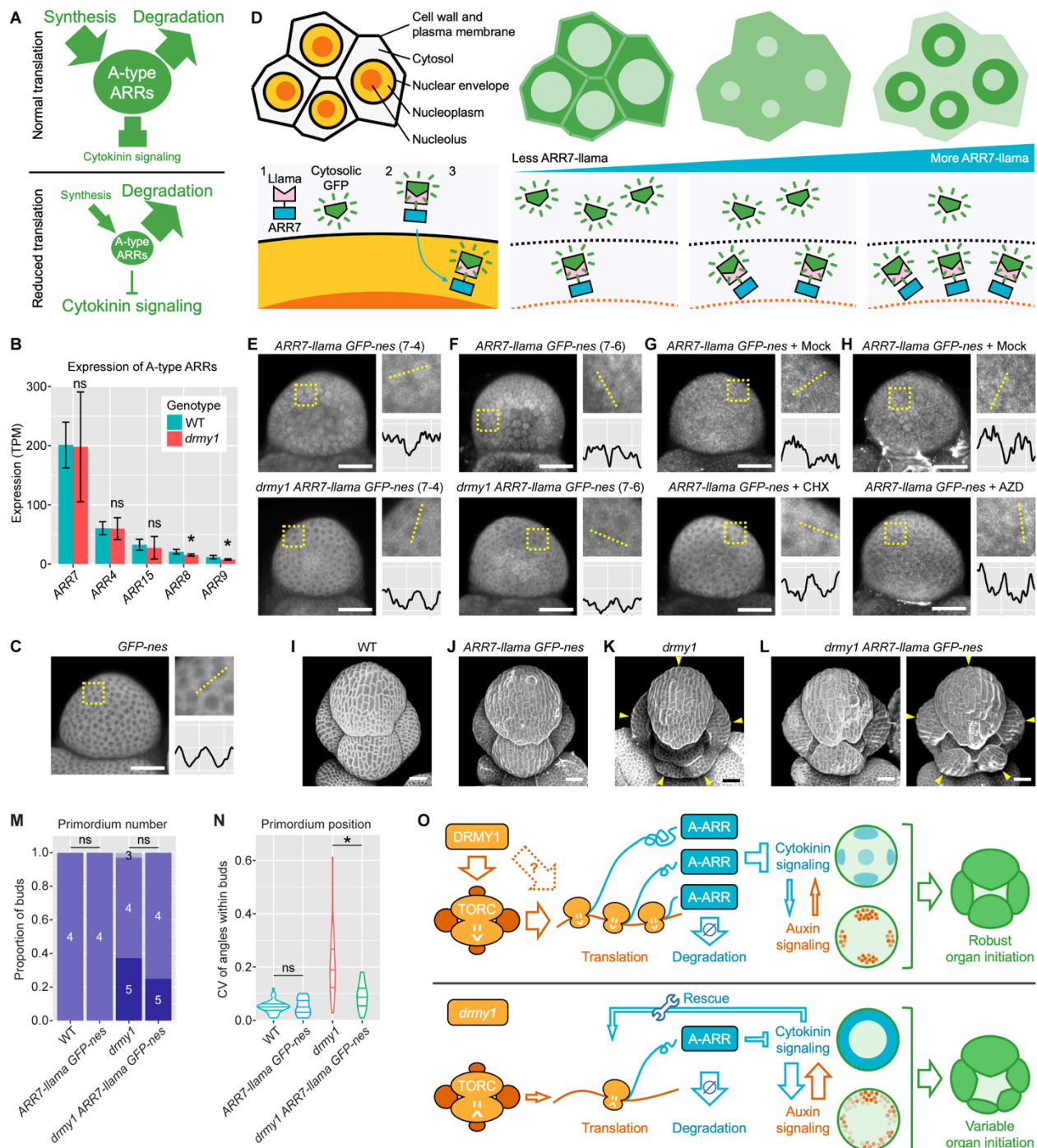**(E)** Representative aerial part images of 42 days old plants of WT, *drmy1*, *wol*, and *drmy1 wol*. Inset shows enlarged *drmy1 wol* plant; notice that it has a tiny rosette and inflorescence. Scale bars, 5 cm. See also Supplemental Figure 6F.

(F) Representative aerial part images of 74 days old plants of WT, *drmy1*, *arr1,10,12*, and *drmy1 arr1,10,12*. Inset shows enlarged *drmy1 arr1,10,12* plant; notice its pale leaves accumulating anthocyanin, and short inflorescence. Scale bars, 5 cm. See also Supplemental Figure 6E.

(G) Dissected siliques of *arr1,10,12* (left) and *drmy1 arr1,10,12* (right) showing developing seeds. Notice that while *arr1,10,12* occasionally have aborted seeds, all seeds in the *drmy1 arr1,10,12* silique were aborted. Scale bars, 0.2 mm.

11

Translation and developmental robustness

Figure 7. A-type ARR protein levels are sensitive to TOR and translation inhibition.

(A) The hypothesis. A-type ARRs are rapidly synthesized and degraded to dampen cytokinin signaling. Translation inhibition causes inability to rapidly synthesize these proteins in response to cytokinin signaling, resulting in an upregulation of cytokinin signaling.

(B) Expression of A-type ARR genes in WT vs *drmy1* inflorescences (*ap1 cal AP1-GR*) measured in RNA-seq. Shown are the five A-type ARR genes with the highest expression, ranked by mean expression level in WT. Asterisk indicates statistically significant difference, while ns means no

201   significant difference. P-values: ARR7, p = 0.807; ARR4, p = 0.611; ARR15, p = 0.532; ARR8, p
202   = 0.0115; ARR9, p = 0.0416.
203   **(C)** A GFP-channel image of a stage 2 bud of GFP-nes (*pUBQ10::sfGFP-nes-UBQ3ter*). For this
204   panel and (E-H), each image was brightened to reveal GFP distribution patterns. A square region
205   taken from the image containing 5-10 cells is enlarged and shown on the top right. Within the
206   enlargement, GFP intensity was quantified along the dotted line and plotted on the bottom right.
207   X-axis, pixels (range 0-238). Y-axis, GFP intensity in gray value (smoothened by taking the
208   average intensity of 11-pixel neighborhoods; range 90-210). Scale bars, 25 µm.
209   **(D)** Illustration of the Llama Tag system used in this study. Plants were co-transformed with *ARR7-*
210   *llama* (*pARR7::ARR7-linker-llama-ARR7ter*) and *GFP-nes* (*pUBQ10::sfGFP-nes-UBQ3ter*).
211   Without ARR7-llama, the GFP is localized in the cytosol. ARR7-llama is produced in the cytosol
212   and translocates into the nucleus. When this happens, the Llama Tag capable of binding GFP
213   drags GFP into the nucleus (note that from our observation it is excluded from the nucleolus).
214   Therefore, at low ARR7-llama levels, GFP signal is mainly seen in the cytosol. At intermediate
215   ARR7-llama levels, GFP is at comparable intensities between the cytosol and the nucleus, and
216   no clear pattern can be seen. At high ARR7-llama levels, GFP is mainly seen in the nucleus.
217   **(E,F)** GFP channel images of stage 2 buds from two independent transgenic lines of *ARR7-llama*
218   *GFP-nes*, 7-4 (E) and 7-6 (F), in WT (top) vs *drmy1* (bottom). Images are representative of n =
219   17 (line 7-4, WT), n = 40 (line 7-4, *drmy1*), n = 9 (line 7-6, WT), and n = 6 (line 7-6, *drmy1*) buds.
220   **(G)** GFP channel images of WT *ARR7-llama GFP-nes* buds treated with mock (top) or 2 µM CHX
221   (bottom) for 24 hours. The mock image is representative of n = 20 buds (12 from line 7-4, 5 from
222   line 7-6, and 3 from line 7-12). The CHX image is representative of n = 19 buds (11 from line 7-4,
223   5 from line 7-6, and 3 from line 7-12).
224   **(H)** GFP channel images of WT *ARR7-llama GFP-nes* buds treated with mock (top) or 2 µM AZD-
225   8055 (bottom) for 72 hours. The mock image is representative of n = 13 buds (8 from line 7-4 and
226   5 from line 7-6). The AZD-8055 image is representative of n = 11 buds (8 from line 7-4 and 3 from
227   line 7-6).
228   **(I-N)** *ARR7-llama* partially restores robustness in *drmy1* sepal primordia. (I-L) Representative
229   stage 5 or 6 buds from WT (I), WT with the *ARR7-llama* and *GFP-nes* constructs (J), *drmy1* (K),
230   and *drmy1* with these constructs (L). (M) Quantification of sepal primordium number. ns indicates
231   no significance difference in a Fisher's exact test (WT vs *ARR7-llama*, p = 1; *drmy1* vs *drmy1*
232   *ARR7-llama*, p = 0.44). (N) Quantification of variability in sepal primordium position. Asterisk
233   indicates statistically significant difference (p = 5.7×10^{-6}), while ns indicates no statistically
234   significant difference (p = 0.91). Data for WT and *drmy1* were reused from Figure 2H, 2J. Data
235   for *ARR7-llama GFP-nes* and *drmy1 ARR7-llama GFP-nes* were pooled from line 7-4 and 7-6.
236   Sample size: WT n = 51, *ARR7-llama GFP-nes* n = 16, *drmy1* n = 67, *drmy1 ARR7-llama GFP-*
237   *nes* n = 20. Scale bars, 25 µm.
238   **(O)** Working model. In WT, DRMY1 maintains TOR activity and translation, which sustains the
239   rapid translation of A-type ARRs in response to cytokinin signaling. This suppresses excessive
240   cytokinin signaling, allowing auxin and cytokinin signaling to interact and form robust spatial
241   patterns. Robust patterning of auxin and cytokinin signaling gives rise to robustly numbered,
242   positioned, and sized sepal primordia. In *drmy1*, A-type ARR protein levels are reduced due to

243   insufficient TOR activity, ribosome content, and translation rate. Cytokinin signaling is upregulated,

244   which rescues the translation rate reduction in a homeostatic mechanism. This upregulation of

245   cytokinin signaling disrupts the robust spatial pattern of both cytokinin and auxin signaling, which

246   in turn causes variable sepal initiation.

247